

Extratropical Sea Surface Temperature Impacts on Large-Scale Atmospheric Circulation



Guidi Zhou

GEOMAR Helmholtz Centre for Ocean Research Kiel

Dissertation

in fulfillment of the requirements for the degree “Dr. rer. nat.”
of the Faculty of Mathematics and Natural Sciences at
Kiel University

Kiel

19.01.2016

First Referee: Prof. Dr. Mojib Latif
Second Referee: Prof. Dr. Richard Greatbatch
Date of Examination: 18.01.2016
Approved for Publication: 18.01.2016

Signed: Prof. Dr. Wolfgang J. Duschl, Dean

This thesis is dedicated to Zhuhua, my beloved wife, who made this journey worthwhile...

Abstract

The atmospheric response to large-scale extratropical North Pacific sea surface temperature (SST) anomalies associated with the Pacific Decadal Oscillation (PDO) is assessed using observational data, coupled ocean-atmosphere general circulation model (CGCM) simulations, and forced high-resolution atmospheric general circulation model (AGCM) experiments. The characteristics of the atmospheric response as well as its sensitivity to daily to decadal variability in the background SST, on which the SST anomalies are superimposed, are inspected. Here, only the boreal winter (DJF) season is considered.

The analysis of the observational data reveals that the PDO exhibits significant variability on interannual, decadal and multidecadal timescales, and is highly correlated with the El Niño/Southern Oscillation (ENSO). In the atmosphere, significant spectral peaks at similar frequencies as those identified in the PDO are found in the observed sea level pressure over the North Pacific, suggesting potential links between the ocean and the atmosphere. This link is further supported by a number of regression and correlation analyses. It is proposed that SST anomalies associated with the PDO can persist for several winters through the “reemergence” mechanism, repeatedly exerting anomalous SST forcing on the atmosphere and causing the latter to respond. The atmospheric response is of the “cold SST-low pressure”-type, also known as the “cold-trough” (or “warm-ridge”) response.

Exactly the same analyses as those described above are repeated on the output of a coarse-resolution CGCM, the Kiel Climate Model (KCM). Results show that the KCM depicts the reemergence mechanism but does not simulate an atmospheric response consistent with that suggested by the observations. It is conjectured that too coarse horizontal resolution in the atmospheric component of the KCM inhibits a realistic representation of the atmospheric response to extratropical North Pacific SST anomalies.

To further investigate the mechanism of the atmospheric response and to examine the reason for the failure of the KCM to simulate such a response, a high-(horizontal) resolution version of the ECHAM5 AGCM is integrated in stand-alone mode forced by prescribed SSTs. The SST forcing consists of the observed daily SSTs of 1981–1990, which serve as the background SSTs, on which a fixed PDO-like SST anomaly, which as been derived from

observations, is superimposed. Results show that the winter-mean atmospheric response to the SST anomaly (averaged over all 10 winters) is equivalent barotropic, with a significant low pressure anomaly over the eastern North Pacific and a northeast-southwest shift in the storm track. It is further pointed out that the response is established and maintained by anomalous eddy vorticity and momentum flux convergence. Noticeable changes in zonal and vertical winds are also found. In terms of surface pressure, the model results compare reasonably well with the observations.

In order to further investigate the role of the background SSTs in the atmospheric response, a set of sensitivity experiments with the ECHAM5 AGCM is designed employing identical SST anomalies but different background SSTs. It is found that daily background SST variability plays a key role in the atmospheric response, whereas interannual variability of the background SST is only of minor importance. It is thus proposed that sufficient daily extratropical SST variability must be simulated by the ocean components and resolved by the atmospheric components of CGCMs to enable realistic simulation of decadal climate variability in the North Pacific sector.

Identical AGCM integrations were conducted for the subsequent 10 winters of 1991–2000. Together, the two sets of integrations reveal a remarkable decadal transition with sign reversal in terms of the area-averaged 500 hPa height anomalies over the North Pacific. Although the response is characterized by an equivalent barotropic, circumglobal Rossby wave train in both periods, the primary wave source switches from baroclinic eddy vorticity forcing over the eastern North Pacific in 1981–1990 to mean-flow divergence over the western North Pacific in 1991–2000. By examining the decadal changes of the background SSTs, it is then proposed that the wave source transition can be linked to the decadal reduction of daily SST variability in the eastern North Pacific and the decadal strengthening of the Oyashio Extension front over the western North Pacific. In this view, the decadal variations of small-scale features of the background SSTs, temporal and spatial, are emphasized.

Zusammenfassung

Die atmosphärische Antwort auf großskalige Anomalien der Meeresoberflächentemperatur (engl. "sea surface temperature", SST) im extratropischen Nordpazifik wurden anhand von Beobachtungsdaten sowie von Modellsimulationen mit gekoppelten Ozean-Atmosphärenmodellen (engl. "coupled ocean-atmosphere general circulation model", CGCM) und Experimenten mit hochauflösenden Atmosphärenmodellen (engl. "atmospheric general circulation model", AGCM) mit vorgeschriebenen Randbedingungen untersucht. Es wurden die Charakteristik der atmosphärischen Reaktion betrachtet, sowie deren Sensitivität gegenüber täglicher bis dekadischer Variabilität der Hintergrund-SST, der SST-Anomalien überlagert wurden. Hierbei wurde ausschließlich der boreale Winter (DJF) berücksichtigt.

Die Analyse der Beobachtungsdaten ergab, dass die PDO signifikante Variabilität auf interannualen, dekadischen und multidekadischen Zeitskalen aufweist, und in hohem Maße mit dem El Niño/Southern Oscillation-Phänomen (ENSO) korreliert ist. In der Atmosphäre können spektrale Peaks auf ähnlichen Frequenzen wie sie in der PDO auftreten im beobachteten Luftdruck auf Meeressniveau über dem Nordpazifik identifiziert. Dies weist auf einen Zusammenhang zwischen dem Ozean und der Atmosphäre hin. Diese Verknüpfung wird ferner durch eine Reihe von Regressions- und Korrelationsanalysen untermauert. Es wird vorgeschlagen, dass mit der PDO verknüpfte SST-Anomalien durch den sog. "reemergence"-Mechanismus mehrere Winter überdauern können, indem sie wiederholt einen anomalen SST-Antrieb der Atmosphäre darstellen und eine Antwort derselben verursachen. Die atmosphärische Antwort ist von der Art dass kalte SST mit verringertem Luftdruck einhergehen, auch bekannt als Kaltlufttrog/Warmlufttrücken.

Die oben beschriebenen Analysen wurden für Experimente mit dem niedrigauflösenden CGCM, dem "Kiel Climate Model (KCM)" wiederholt. Die Ergebnisse zeigen, dass das KCM den reemergence-Mechanismus aufweist, jedoch nicht die atmosphärische Antwort zu den Beobachtungen konsistent wiedergibt. Es kann vermutet werden, dass die zu niedrige Auflösung in der atmosphärischen Komponente des KCM eine realistische Antwort der Atmosphäre auf die SST-Anomalien im tropischen Pazifik verhindert.

Zur weiteren Untersuchung des Mechanismus der atmosphärischen Antwort und um herauszufinden, warum das KCM nicht in der Lage ist, diese wiederzugeben, wurden Experimente mit der (horizontal) hochauflösenden Version des ECHAM5 Atmosphärenmodells im alleinstehenden Modus mit vorgeschriebenen SSTs durchgeführt. Der SST-Antrieb besteht aus den beobachteten täglichen SSTs des Zeitraums 1981–1990 als Hintergrund-SST. Dieser wurde eine feste PDO-artige SST-Anomalie überlagert, die aus Beobachtungen abgeleitet wurde. Die Ergebnisse zeigen, dass die gemittelte Antwort der Atmosphäre im Winter zu dieser SST-Anomalie (gemittelt über alle zehn Winter) äquivalent-barotropisch ist, mit einer signifikanten negativen Luftdruckanomalie über dem östlichen Nordpazifik und einer Nordost-Südwest-Verschiebung des Storm-Tracks einhergeht. Ferner ist hervorzuheben, dass die in der Atmosphäre hervorgerufenen Veränderungen durch die anomale Konvergenz von Vortizität und Impulsfluss transienter Störungen entstehen und erhalten werden. Ebenfalls wurden erkennbare Veränderungen in den zonalen und vertikalen Winden gefunden. Bezüglich des Luftdrucks auf Meeresoberflächenniveau entsprechen sich Modellergebnisse und Beobachtungen in annehmbarer Genauigkeit.

Um die Rolle der Hintergrund-SST für die atmosphärische Antwort eingehender zu untersuchen, wurde eine Reihe von Sensitivitätsexperimenten mit dem ECHAM5 Atmosphärenmodell durchgeführt, bei denen identische SST-Anomalien unterschiedlichen Hintergrund-SSTs überlagert wurden. Es wurde herausgefunden, dass der täglichen Variabilität der Hintergrund-SST eine Schlüsselrolle zukommt, wohingegen die interannuale Variabilität der Hintergrund-SST nur von untergeordneter Bedeutung ist. Deshalb wird vorgeschlagen, dass es zur realistischen Wiedergabe der dekadischen Klimavariabilität im Nordpazifiksektor notwendig ist, dass die Ozeankomponente des gekoppelten Klimamodells die tägliche Variabilität der extratropischen SSTs hinreichend simulieren können muss und die atmosphärische Komponente diese zufriedenstellend auflösen muss.

Identische Atmosphärenmodellläufe wurden für die zehn aufeinanderfolgenden Winter von 1991 bis 2000 durchgeführt. Zusammen weisen die zwei Gruppen Läufe auf der dekadischen Zeitskala eine bemerkenswerte Vorzeichenumkehr bezüglich der flächengewichteten Anomalie der 500 hPa-Höhe auf. Obwohl der Einfluss in beiden Dekaden durch einen äquivalent-barotropischen, weltumspannenden Rossby-Wellenzug charakterisiert ist, wechselt die primäre Quelle für Wellenaktivität vom Antrieb durch Änderungen der Wirbelhaftigkeit barokliner (transienter) Störungen über dem Ostpazifik im Zeitraum 1981–1990 hin zu Divergenz des Grundstroms über dem westlichen Nordpazifik im Zeitraum 1991–2000. Durch Untersuchung der dekadischen Änderungen der Hintergrund-SST ergeben sich Hinweise darauf, dass der Wechsel der Quelle für Wellenaktivität auf dekadischen Zeitskalen mit der Abnahme der täglichen SST-Variabilität im östlichen Nordpazifik und der

Verstärkung der Verlängerung der Oyashio-Front im westlichen Nordpazifik auf diesen Zeitskalen in Verbindung steht. Aus diesem Blickwinkel seien die dekadischen Variationen der klein-skaligen Merkmale der Hintergrund-SST, sowohl räumlich als auch zeitlich, hervorgehoben.

摘要

本文研究大尺度大气环流对于与太平洋年代际振荡 (PDO) 相关的中纬度北太平洋海温异常的响应。通过观测数据分析、耦合的大气—海洋环流模型 (CGCM) 数值模拟, 以及大气环流模型 (AGCM) 的强迫实验, 本文研究了上述大气响应的特征及其对于背景海温场的日变化及年代际变化的敏感性。这里仅关注北半球冬季。

观测数据分析显示 PDO 具有显著的年际、年代际和多年代际变化, 且与厄尔尼诺/南方涛动现象密切相关。研究发现观测到的北太平洋海面气压具有与 PDO 一致的谱峰频率, 因此揭示出大气与海洋之间的潜在联系。进一步的回归和相关分析确认了这一联系的存在。我们认为与 PDO 相关的海温异常因为“再现”现象而在海面上持续多个冬季, 藉此不断地向大气施加异常的海温驱动并引起大气的响应。此大气响应遵从“冷海温—低气压”的模式, 又称“冷—槽”或“热—脊”响应。

我们使用一个低分辨率的 CGCM, 即基尔气候模型 (KCM) 的模拟结果并重复上述分析。结果显示 KCM 能够模拟再现现象, 但不能模拟出与观测一致的大气响应。因此我们假定是 KCM 的大气模块的分辨率过低导致其无法真实地模拟大气对中纬度北太平洋海温异常的响应。

为了进一步研究大气响应的机制并探索 KCM 失败的原因, 我们使用一个高分辨率的 AGCM 即 ECHAM5 来进行强迫模拟实验。使用的边界强迫是以逐日观测的全球海温数据作为背景, 并在其上叠加一个同样由观测数据计算得到的类似 PDO 的北太平洋海温异常。模拟的时间范围为 1981 年到 1990 年。模拟结果显示, 对于该海温异常, 10 年冬季平均的大气响应呈现等效正压的特征, 且伴随有东北太平洋上空的低气压异常, 以及风暴轨迹区从东北向西南方向的移动。本文接下来进一步指出大气的响应是由异常的涡旋涡量和动量辐聚建立和维持的。此外模拟的大气响应还表现出显著的水平 and 垂直风速变化。就海面气压来讲, 模拟结果与观测结果较为一致。

接下来, 为了研究背景海温场对大气响应的影响, 我们使用 ECHAM5 模型设计并进行了一系列的敏感性实验。这些实验使用相同的海温异常, 但海温异常叠加在不同的背景海温场之上。结果显示, 背景海温场的日变化对于大气响应非常重要, 而年际变化对大气响应影响不大。在此基础上我们提出为了正确地模拟大气对于中纬度北太平洋海温异常的响应, CGCM 的海洋模块必须能够模拟背景海温场的日变化, 而大气模块必须能够分辨它。

我们将1981年到1990年的AGCM实验扩展到1991至2000年。此20年的模拟结果揭示出北太平洋上空的500百帕高度值呈现出显著的年代际差异和符号翻转。在这20年里，尽管大气响应一直表现为等效正压且环绕地球传播的罗斯贝波列，其主要的波源却由前一年代在东北太平洋上空的斜压涡旋驱动变为后一年代在西北太平洋上空的平均流辐散驱动。基于对于背景海温场的进一步分析，我们认为主要波源的变化可以解释为两方面的原因：东北太平洋海温日变化幅度的递减，以及西北太平洋亲潮延伸体锋面强度的递增。于是本文研究重点强调了背景海温场的时/空小尺度变化所呈现出的年代际变迁。

Table of contents

List of figures	xv
1 General Introduction	1
2 Atmospheric Response to an Extratropical North Pacific SST Anomaly Pattern: Observations and CGCM Results	5
2.1 Introduction	6
2.2 Data and Methods	11
2.2.1 Observational Data	11
2.2.2 Kiel Climate Model	12
2.2.3 Statistical Analyses	12
2.3 Removing Tropical Effects	14
2.4 Observed Ocean-Atmosphere Linkage	16
2.4.1 Fundamental Oceanic Variability	16
2.4.2 Fundamental Atmospheric Variability	18
2.4.3 Reemergence	20
2.4.4 Ocean-Atmosphere Relation	21
2.5 Simulated Ocean-Atmosphere Linkage	24
2.5.1 Fundamental Oceanic Variability	24
2.5.2 Fundamental Atmospheric Variability	25
2.5.3 Reemergence	27
2.5.4 Ocean-Atmosphere Relation	29
2.6 Summary and Discussions	32
3 Atmospheric Response to the North Pacific Enabled by Daily Sea Surface Temperature Variability	35
3.1 Introduction	36
3.2 Observational Evidence	37

3.3	Experimental Design	38
3.4	Response Characteristics	40
3.5	Importance of Daily SST Variability	41
3.6	Summary and Discussion	45
	Appendix 3.A Supplementary Figures	46
4	State-Dependence of Atmospheric Response to Extratropical North Pacific SST	
	Anomalies	51
4.1	Introduction	52
4.2	Model, Experimental Setup, Data	53
4.3	Response	55
4.3.1	Linear Trend	55
4.3.2	Decadal-Mean Response 1981–1990	55
4.3.3	Decadal-Mean Response 1991–2000	57
4.4	Relation to Background SST Changes	59
4.4.1	Deep Convection Associated with Sharp SST Fronts	59
4.4.2	Decadal SST Changes in the North Pacific	60
4.4.3	The WNP Divergence-Driven Wave Source	60
4.4.4	The ENP Eddy-Driven Wave Source	60
4.5	Summary and Discussion	62
	Appendix 4.A Significance Tests	63
4.A.1	Decadal Means	63
4.A.2	Linear Trends	64
5	Summary and Discussion	65
5.1	Summary	65
5.2	Discussion	66
5.2.1	Role of Model Resolution	66
5.2.2	Role of the Arch of Warm SST Anomaly	68
5.3	Outlook	70
	References	71

List of figures

2.1	(ERSST) Patterns of the leading EOFs [$^{\circ}\text{C}$] of SST variability based on winter mean (DJF) anomalies over (a) North Pacific, (b) Tropical Pacific. The percentage of explained variance is shown in the sub-captions. (c) The PDO and ENSO time series corresponding to the above EOF patterns. The thick curves indicate the 11-year running mean.	16
2.2	(ERSST) Power spectra of the (a) PDO index, (b) ENSO index. The horizontal line and the red curve indicate the white and red spectral fits, respectively, at the 95% significance level. (c) Cross-correlation between the above two indices. Positive lag means the PDO index leads. The 95% significance level is shown by the red horizontal lines.	17
2.3	(ERSST) The leading mode of North Pacific SST variability with ENSO removed (PDO [*]). (a) The EOF [$^{\circ}\text{C}$]. The percentage of explained variance is shown in the sub-caption. (b) The PC, with the thick curve indicating the 11-year running mean. (c) The power spectrum. The horizontal line and the red curve indicate the white and red spectral fits, respectively, at the 95% significance level. (d) Cross-correlation with the ENSO index. Positive lag means the PDO [*] index leads. The 95% significance level is shown by the red horizontal lines.	18
2.4	(ERSLP) The leading mode of North Pacific SLP variability. (a) The EOF [hPa]. The percentage of explained variance is shown in the sub-caption. (b) The PC, with the thick curve indicating the 11-year running mean. (c) The power spectrum. The horizontal line and the red curve indicate the white and red spectral fits, respectively, at the 95% significance level.	19
2.5	(SODA) Cross-correlation of the winter PDO [*] index with monthly temperature anomalies averaged over 140 $^{\circ}\text{E}$ –180 $^{\circ}\text{E}$, 35 $^{\circ}\text{N}$ –50 $^{\circ}\text{N}$ as a function of depth and time lag for five years.	20

-
- 2.6 (ERSST) Regression coefficients (shading) of North Pacific winter SST [$^{\circ}\text{C}$] on to the PDO* Index when the index leads the SST by (a) 0, (b) 1, (c) 2, (d) 3 year(s). Contours indicate the ratio of variance explained by regression. Contour interval is 0.1. 21
- 2.7 (ERSST/SLP) Cross-correlation between the leading PC of North Pacific SLP and the PDO* index. Positive lag means the PDO* index leads. The PCs and correlations are based on monthly data. Time lags being multiples of 12 months are denoted by dots. The 95% significance level is shown by the red horizontal lines. 23
- 2.8 (ERSLP) Regression coefficients (shading) of North Pacific wintertime SLP [hPa] on to the PDO* Index when the index leads the SLP by (a) 0, (b) 1, (c) 2, (d) 3 year(s). Contours indicate the ratio of variance explained by regression. Contour interval is 0.1. 24
- 2.9 (OAFlux) Regression coefficients (shading) of North Pacific wintertime turbulent heat flux (THFX, downward is positive) [W m^{-2}] on to the PDO* Index when the index leads the THFX by (a) 0, (b) 1, (c) 2, (d) 3 year(s). Turbulent heat flux is defined as the sum of sensible and latent heat fluxes. Contours indicate the ratio of variance explained by regression. Contour interval is 0.1. Hatching denotes area with positive SST-heat flux feedback. 25
- 2.10 (KCM) Patterns of the leading EOFs [$^{\circ}\text{C}$] of SST variability based on winter mean (DJF) anomalies over (a) North Pacific, (b) Tropical Pacific. The percentage of explained variance is shown in the sub-captions. (c) The PDO and ENSO time series corresponding to the above EOF patterns only showing the first 88 model years. The thick curves indicate the 11-year running mean. 26
- 2.11 (KCM) Power spectra of the (a) PDO index, (b) ENSO index. The horizontal line and the red curve indicate the white and red spectral fits, respectively, at the 95% significance level. (c) Cross-correlation between the above two indices. Positive lag means the PDO index leads. The 95% significance level is shown by the red horizontal lines. 26

- 2.12 (KCM) The leading mode of North Pacific SST variability with ENSO removed (PDO^{*}). (a) The EOF [°C]. The percentage of explained variance is shown in the sub-caption. (b) The first 88 years of the PC, with the thick curve indicating the 11-year running mean. (c) The power spectrum. The horizontal line and the red curve indicate the white and red spectral fits, respectively, at the 95% significance level. (d) Cross-correlation with the ENSO index. Positive lag means the PDO^{*} index leads. The 95% significance level is shown by the red horizontal lines. 27
- 2.13 (KCM) The leading mode of North Pacific SLP variability. (a) The EOF [hPa]. The percentage of explained variance is shown in the sub-caption. (b) The first 88 years of the PC, with the thick curve indicating the 11-year running mean. (c) The power spectrum. The horizontal line and the red curve indicate the white and red spectral fits, respectively, at the 95% significance level. 28
- 2.14 (KCM) Cross-correlation of the winter PDO^{*} index with monthly temperature anomalies averaged over 140°E–180°E, 35°N–50°N as a function of depth and time lag for five years. Only the first 100 years of monthly temperature anomalies are used for the sake of computational efficiency. 28
- 2.15 (KCM) Regression coefficients (shading) of North Pacific winter SST [°C] on to the PDO^{*} Index when the index leads the SST by (a) 0, (b) 1, (c) 2, (d) 3 year(s). Contours indicate the ratio of variance explained by regression. Contour interval is 0.1. 29
- 2.16 (KCM) Cross-correlation between the leading PC of North Pacific SLP and the PDO^{*} index. Positive lag means the PDO^{*} index leads. The PCs and correlations are based on monthly data. Only the first 100 years of monthly temperature anomalies are used for the sake of computational efficiency. Time lags being multiples of 12 months are denoted by dots. The 95% significance level is shown by the red horizontal lines. 30
- 2.17 (KCM) Regression coefficients (shading) of North Pacific winter SLP [hPa] on to the PDO^{*} Index when the index leads the SLP by (a) 0, (b) 1, (c) 2, (d) 3 year(s). Contours indicate the ratio of variance explained by regression. Contour interval is 0.1. 31

2.18 (KCM) Regression coefficients (shading) of North Pacific winter THFX [W m^{-2}] on to the PDO* Index when the index leads the THFX by (a) 0, (b) 1, (c) 2, (d) 3 year(s). Turbulent heat flux is defined as the sum of sensible and latent heat fluxes. Contours indicate the ratio of variance explained by regression. Contour interval is 0.1. Hatching denotes area with positive SST-heat flux feedback.	31
3.1 Regression patterns of (a, c) observed SST [$^{\circ}\text{C}$], (b, d) SLP [hPa] anomalies on the ENSO-removed PDO index. Figs. 3.1a and 3.1b show simultaneous regressions (lag 0). Figs. 3.1c and 3.1d show regressions when the PDO index leads by one year (lag 1 year). Long-term linear trends are removed before computing regression. Color shading indicates the amplitudes (regression coefficients), while contours show the explained variances (contour interval 0.1). According to an F test, the 0.1 contour in Figs. 3.1b and 3.1d is significant at the 99% significance level.	38
3.2 Ten year mean winter (DJF) response of (a) sea level pressure [hPa], (b) 500 hPa geopotential height [m], (c) 500 hPa eastward zonal velocity [m s^{-1}], (d) surface latent heat flux (downward positive) [W m^{-2}], (e) 500 hPa storm track defined as the standard deviation of band-pass (2–8 days) filtered geopotential heights [m], (f) vertical velocity (downward positive) [Pa s^{-1}] simulated by the experiment DAGL. Statistical significance at the 90% level is indicated by hatching.	41
3.3 Vertical sections of the 10 year mean winter (DJF) response simulated by the experiment DAGL, zonally averaged over the Pacific sector for (a) geopotential height [m], (b) divergence of eddy vorticity flux [d^{-2}], (c) downward vertical velocity [Pa s^{-1}], (d) divergence of eddy momentum flux [$\text{m s}^{-1} \text{d}^{-1}$], (e) zonal wind velocity [m s^{-1}]. Statistical significance at the 90% level is indicated by hatching.	42
3.4 Vertical sections of the 10 year mean winter (DJF) response zonally averaged over the Pacific sector for geopotential height [m] simulated in the experiments (a) DAGL, (b) DANP, (c) CLIM, (d) FILT, (e) HFCL, (f) the T31-experiment. Statistical significance at the 90% level is indicated by hatching.	43
3.5 Bar chart showing the mean absolute value of the storm track [m] response at 500 hPa spatially averaged over the eastern North Pacific (180°E – 100°W , 10°N – 60°N). Storm track is defined as the standard deviation of band-pass (2–8 days) filtered geopotential heights.	44
3.S1 Same as Fig. 3.1 but for further lags at (a, b) 2, (c, d) 3 years.	46

- 3.S2 Cross-correlation between the leading PC of North Pacific SLP and the ENSO-removed PDO index. Positive lag means the PDO index leads. The PCs and correlations are based on monthly data. Time lags being multiples of 12 months are denoted by dots. The 95% significance level is shown by the red horizontal lines. 46
- 3.S3 Positive phase of the winter (DJF) mean pattern of the daily SST anomaly forcing in the North Pacific [$^{\circ}\text{C}$]. No SST anomaly is present in other basins. 47
- 3.S4 NOAA-OI-SST observation at 1 January, 1984 (red solid contours; DAGL/DANP), the 11-day filtered SST (red dashed contours; FILT), the “high-frequency-plus-climatological” SST (black dashed contours; HFCL), and the 1981–1990 daily climatology (black solid contours; CLIM) for the same calendar day [m]. 47
- 3.S5 Time series of wintertime (DJF) SST [$^{\circ}\text{C}$] averaged over 145°E – 150°E , 35°N – 42.5°N (indicated by the box in the inset) from the NOAA-OI-SST daily observations. The red and blue dotted curves represent the 1984–85 and 1990–91 winters (DAGL/DANP) respectively, whereas the smooth red and blue curves are the 11-day running means of the same winters (FILT). The black dotted curve shows the “high-frequency-plus-climatological” SST (HFCL), and the smooth black curve is the 10-year daily climatology (CLIM). 47
- 3.S6 10-year time series of (a) winter mean field STD [$^{\circ}\text{C}$] indicating the level of spatially small-scale variability. It is the spatial STD of SST difference from the 10-year daily climatology computed using every ocean grid point in the North Pacific (120°E – 100°W , 10°N – 60°N). (b) winter-mean sub-monthly STD [$^{\circ}\text{C}$] indicating the level of temporally high-frequency variability computed after subtracting the linear trend within each month. The variability in CLIM and HFCL is due to leap years. 48
- 3.S7 Ten year mean winter (DJF) storm track [m] response at 500 hPa simulated in (a) DANP, (b) CLIM, (c) FILT, (d) HFCL. Storm track is defined as the standard deviation of band-pass (2–8 days) filtered geopotential heights. Statistical significance at the 90% level is indicated by hatching. 48
- 3.S8 Probability density function (PDF) of the magnitude of 2-dimensional SST gradients over (a) the whole gradient range, (b) the high gradient range ($\geq 1^{\circ}\text{C } 100\text{ km}^{-1}$). Note that in (b), bars within each group have the same gradient value. Gradients are computed by comparing adjacent grid points. The PDF is computed over all grid points in the North Pacific and at all time steps during the 10 winters. 49

- 3.S9 Vertical profiles of the 10 year mean winter (DJF) response of (a) Eady growth rate [10^6 s^{-1}], (b) Brunt-Väisälä frequency [10^3 s^{-1}], (c) vertical wind shear [10^4 s^{-1}], (d) divergence of eddy heat flux [$^{\circ}\text{C d}^{-1}$] averaged over the area 30°N – 40°N , 120°E – 180°E 49
- 3.S10 Ten year mean winter (DJF) surface latent heat flux [W m^{-2}] response (downward positive) simulated in (a) DANP, (b) CLIM, (c) FILT, (d) HFCL, (e) the T31-experiment. Statistical significance at the 90% level is indicated by hatching. 50
- 4.1 (a) Positive phase of the winter-mean (DJF) SST anomaly forcing in the North Pacific [$^{\circ}\text{C}$]. No SST anomaly is present in other basins. (b) 1981–2000 mean winter (DJF) convective precipitation [mm d^{-1}] from the control run showing the climatological deep convection zone south the Oyashio Extension front, whose climatological mean position is indicated by the black line. 54
- 4.2 Time series of 500 hPa geopotential height [m] responses during winter (DJF) averaged over the western (120°E – 180°E , blue dotted curves) and eastern (180°W – 100°W , red dotted curves) North Pacific (10°N – 60°N). The thick horizontal lines denote the two separate decadal means, and the thin lines are the decadal trends for the two decades. The trends for the western and eastern North Pacific are both statistically significant at the 90% level. 55
- 4.3 1981–1990 decadal-mean winter (DJF) responses of (a) sea level pressure [hPa], (b) 500 hPa geopotential height [m], (c) 500 hPa zonal wind velocity [m s^{-1}]. In (c), contours show the decadal mean zonal velocity from the negative SST anomaly polarity case, where solid and dashed contours indicate positive and negative values, and the zero contours are highlighted by bold lines. Contour interval is 5 m s^{-1} . (d) Response of winter (DJF) 500 hPa storm track [m] defined as the standard deviation of 2–8 day filtered geopotential height. (e) Winter (DJF) responses of 500 hPa downward velocity [Pa s^{-1}] and (f) convective precipitation [mm d^{-1}]. Statistical significance at the 90% level is indicated by hatching. 57

- 4.4 1991–2000 decadal-mean winter (DJF) responses of (a) sea level pressure [hPa], (b) 500 hPa geopotential height [m], (c) 500 hPa zonal wind velocity [m s^{-1}]. In (c), contours show the decadal mean zonal velocity from the negative SST anomaly polarity case, where solid and dashed contours indicate positive and negative values, and the zero contours are highlighted by bold lines. Contour interval is 5 m s^{-1} . (d) Response of winter (DJF) 500 hPa storm track [m] defined as the standard deviation of 2–8 day filtered geopotential height. (e) Winter (DJF) responses of 500 hPa downward velocity [Pa s^{-1}] and (f) convective precipitation [mm d^{-1}]. Statistical significance at the 90% level is indicated by hatching. 58
- 4.5 (left) Difference (Dec9100-Dec8190) of decadal-mean (a) SST [$^{\circ}\text{C}$], (c) (contours) Meridional SST gradient [$^{\circ}\text{C } 100 \text{ km}^{-1}$] with black and blue respectively stand for positive and negative values. Contours start at ± 0.4 with interval 0.2. Color coding shows Dec8190 mean. (e) standard deviation of daily SST variability [$^{\circ}\text{C}$]. (right) Time series averaged over the boxes indicated in the respective left panels. Solid lines show the linear trends. All trends pass the t test at the 95% level. 61
- 5.1 10-year mean winter (DJF) response simulated by the T31-experiment averaged over the (left) 1981–1990 and (right) 1991–2000 decade for (a, b) sea level pressure [hPa], (c, d) 500 hPa geopotential height [m], (e, f) surface latent heat flux (downward positive) [W m^{-2}]. Statistical significance at the 90% level is indicated by hatching. 68
- 5.2 1981–1990 mean winter (DJF) response simulated by the “PDO-cold”-experiment in which only the cold SST anomaly shown in Figs. 3.S3 and 4.1a drives the AGCM for (a) sea level pressure [hPa], (b) 500 hPa geopotential height [m], (c) surface latent heat flux (downward positive) [W m^{-2}], (d) 500 hPa storm track [m]. Statistical significance at the 90% level is indicated by hatching. 69

Chapter 1

General Introduction

Climate, as defined by the World Meteorological Organization, is the statistical description of weather in terms of the mean and variability of relevant quantities over a period of time long enough to allow the statistics to be determined. A typical time period is 30 years. Over longer time periods, climate defined in such a manner also varies due to internal and external factors.

Regarding external forcing, the Earth's climate is modulated, for example, by changes in the orbital parameters such as ecliptic and obliquity which vary on millennial timescales and primarily lead to regional variation in solar forcing. Changes in the solar constant, volcanic eruptions, and changes in the composition of the atmosphere (forced by e.g. rising greenhouse gas concentrations such as CO₂) also lead to radiative forcing and are among other important external factors that can drive climate variability on a wide range of timescales.

The Earth's climate system consists of six components ([Latif, 2009](#)): the atmosphere (gases including water vapor), the hydrosphere (liquid water including the ocean), the cryosphere (solid water), the biosphere (ecosystems), the pedosphere (soil), and the lithosphere (crust and uppermost solid mantle), each exhibiting different heat conductivity and capacity, and fluctuating on different timescales ranging from hours to millennia. The lower atmosphere, for instance, adjusts to perturbations in hours. The ocean is commonly divided into two parts, the upper few hundred meters, which comes into seasonal contact with the atmosphere, and the deep ocean interior, which fluctuates over periods of decades to centuries, respectively. The cryosphere too is characterized by distinctive components, e.g., sea ice which changes over seasons and years, glaciers which change over decades to centuries, and ice sheets which take many millennia to adjust to forcing. Lithospheric movements (i.e., tectonics) generally occur on timescales of millions of years ([Marshall and Plumb, 2008](#)).

Changes in the climate system cannot only emerge from fluctuations of a single component, but also from interactions among the individual climate system components. Regarding the water cycle, the atmosphere, hydrosphere and the cryosphere interact in an obvious way through phase changes of water. The atmosphere and the biosphere influence each other by means of photosynthesis, cellular respiration, and other processes. Interactions between the biosphere and the pedosphere are also conceptually straightforward. Lithosphere-atmosphere-hydrosphere interactions mostly take the form of physical and chemical weathering, as well as the feedback of weathering on the atmosphere and the ocean, an example of which can be found in [Gislason et al. \(2009\)](#). On very long timescales of millions of years, the pedosphere and lithosphere also interact via weathering and lithification. Each and every of these interactions have attracted extensive research interest over the recent decades.

Atmosphere-ocean interactions are of particular importance in generating climate variability on seasonal to decadal timescales. Due to its relatively small density, viscosity and heat capacity, the atmosphere reacts to dynamical and thermodynamical perturbations rather quickly, generating a variety of weather conditions. On the contrary, the ocean, the largest component of the hydrosphere, is characterized by enormous heat capacity and large density, and as a result much slower variations compared to the atmosphere. The large thermal and dynamical inertia of the ocean provides long-term memory to the climate system and drives the atmosphere on seasonal to decadal timescales and possibly beyond. Furthermore, both the atmosphere and the ocean exhibit movements over long distances, hence they both play a great role in mass and heat transports which contribute to shaping the Earth's climate. The atmosphere and the ocean form the most fundamental part of the global water cycle, with the hydrological processes such as evaporation, condensation, cloud formation and precipitation closely coupled to atmospheric dynamics (e.g., convection) and thermodynamics. Finally, it is important to note that with respect to global warming, the atmosphere-ocean system is also crucial, which is due to air-sea heat, freshwater and greenhouse gas exchange, and variability in these exchanges which occur on timescales up to millennial. This variability is one important reason for surface climate variability that superimposes the long-term anthropogenic warming trend.

Atmosphere-ocean interactions are quite complex and involve a large range of temporal and spatial scales. Surface exchanges of momentum, heat and freshwater drive oceanic movements on scales from as small as surface gravity waves to scales as large as the global ocean circulation. On the other hand, oceanic processes can feed back on the atmosphere. Ocean surface waves alter surface roughness and may thus modify wind flow and momentum transfer in the marine atmospheric boundary layer ([Chalikov and Rainchik, 2011](#); [Hara and Belcher, 2004](#); [Kihara and Hirakuchi, 2008](#)). Besides the atmospheric meridional heat

transport, the ocean currents carry a great amount of heat accumulated in the tropics and released in the mid- and high-latitudes, thereby effectively mitigating the equator-to-pole temperature contrast. Furthermore, the ocean supplies a large amount of moisture to the atmosphere through evaporation. The water vapor carries enormous latent heat that is released by condensation, an important heat source for the atmosphere. The latent heat is also a major energy source for tropical and mid-latitudinal storms (Chang et al., 2002).

Because of the great importance of atmosphere-ocean interactions in climate variability, this topic has received extensive scientific attention ever since the 1950s (e.g., Bjerknes, 1959; Namias, 1959). By the 1990s, a reasonable understanding had already been established regarding atmosphere-ocean interactions in the tropics associated with El Niño/Southern Oscillation (ENSO; Philander, 1989), the largest interannual climate signal with far-reaching global impacts (e.g., Diaz and Markgraf, 2000; Iizumi et al., 2014; Lyon and Barnston, 2005; Newman et al., 2003; Wilkinson et al., 1999). The tropical atmosphere drives sea surface temperature (SST) anomalies through non-local, delayed changes in ocean heat transport, and the SST anomalies are damped by surface heat fluxes. The atmospheric response to SST anomalies, on the other hand, is “local” and thermally direct, associated with deep convection, upward-shifted latent heat release, anomalous large-scale surface convergence and upper-level divergence (Neelin et al., 1998).

Regarding ocean-atmosphere interaction in the extratropics, Bjerknes (1964) conjectured that extratropical SST anomalies are largely forced by the atmosphere on interannual to decadal timescales, while the ocean significantly contributes to the extratropical SST variability on longer timescales. This conjecture has been supported by many succeeding studies (e.g., Cayan, 1992a,b,c; Deser and Blackmon, 1993; Gulev et al., 2013; Kushnir, 1994; Nakamura et al., 1997). For decadal climate variability controlled by the ocean to be possible, however, the atmosphere must respond to SST anomalies. Thus, understanding the atmospheric response to extratropical SST perturbations is of great importance when it comes to the origin of extratropical climate variability. Due to the short adjustment time of the atmosphere (e.g., Ferreira and Frankignoul, 2005), such response takes the form of fast atmospheric adjustments to SST perturbations, even when considering decadal timescales.

Due to the generally much smaller and shallower latent heat release through convection in the extratropics compared to that in the tropics, the atmospheric response to anomalous extratropical SSTs is expected to be weak. Indeed, several studies have suggested that the amplitude of such response is smaller than the intrinsic atmospheric variability (e.g., Ferranti et al., 1994; Kushnir et al., 2002), drastically reducing the signal-to-noise ratio and thus increasing the difficulty of detecting the response. However, the problem of the atmospheric response to extratropical SST anomalies is still under debate (for a comprehensive review

see [Kushnir et al., 2002](#)). Observational studies are only useful in detecting the response and are subject to statistical and dynamical uncertainties (see [Section 2.1](#)). Numerical modeling studies during the past decades, on the other hand, have contributed significantly to the understanding of the possible mechanisms of the atmospheric response and its sensitivity to atmospheric and oceanic background states (see [Sections 3.1](#) and [4.1](#)), but they have produced controversial and perplexing results, rendering the problem largely unresolved.

This study attempts to deepen the understanding regarding the mechanism and sensitivity of the atmospheric response to large-scale extratropical SST anomalies in the North Pacific by means of observational analyses, coupled ocean-atmospheric general circulation model (CGCM) simulations, and forced atmospheric general circulation model (AGCM) experiments. The characteristics of the response detected by these three approaches are compared, and the sensitivity of the response to both high-frequency (daily) and low-frequency (decadal) background SST variability is assessed. [Chapter 2](#) presents results of statistical analyses on observational data and CGCM output. [Chapter 3](#) describes the atmospheric response of an AGCM forced by prescribed PDO-like SST anomalies, and the role of daily variability in the background SST on which the SST anomalies are superimposed. In [Chapter 4](#), the state-dependence of the response is discussed by investigating the response to identical SST anomalies which are superimposed on the observed SSTs during two adjacent decades. A decadal transition of the response is presented, from which the role of the decadal variability of small-scale features in the background SSTs is identified. [Chapters 3](#) and [4](#) are each based on a journal article. Summary and discussions are given in [Chapter 5](#).

Chapter 2

Atmospheric Response to an Extratropical North Pacific SST Anomaly Pattern: Observations and CGCM Results

Abstract

By analyzing high-resolution sea surface temperature (SST) observations, the most salient features of SST variability in the North Pacific are presented. It is shown that the Pacific Decadal Oscillation (PDO) exhibits significant interannual, bi-decadal and multidecadal variations, and is highly correlated with the El Niño/Southern Oscillation (ENSO). Sea level pressure (SLP) observations over the North Pacific depict significant spectral peaks at similar frequencies as the PDO, suggesting potential dynamical links between the ocean and the atmosphere. This link is confirmed by regression and correlation analyses. It is proposed that North Pacific SST anomalies can persist for several winters through the “reemergence” mechanism, repeatedly exerting anomalous SST to the atmosphere which responds in a characteristic manner. The response style is of the cold SST-low pressure type, also known as the “warm-ridge” (or “cold-trough”) response.

Exactly the same analyses as those described above are repeated using the output of a coarse-resolution coupled ocean-atmospheric general circulation model. Results show that the model does not simulate an atmospheric response consistent with observations, which stimulated uncoupled high-resolution atmospheric general circulation model experiments forced by prescribed extratropical North Pacific SST anomalies, the results of which are described below in Chapters 3 and 4.

2.1 Introduction

It is both tempting and challenging to study the problem of ocean-atmosphere interaction from observational data. Compared to theoretical and numerical models, observations are the most accurate representation of the climate system, since they are the direct measurement which do not rely on any assumptions and are only subject to random sampling error, in case of perfect instruments. Therefore observations are the yardstick of climate research. On the other hand, when studying ocean-atmosphere interaction, it is often necessary to distinguish the two directions of the mutual relationship between the ocean and the atmosphere, i.e., the ocean's impacts on the atmosphere and the atmosphere's impacts on the ocean. However, in nature any observable oceanic or atmospheric state is the final product of the coupled feedbacks, hence specialized statistical techniques must be developed and employed in order to untangle the causes from the effects. Such techniques, though, may be subject to statistical and dynamical constraints. Another complexity to be further tackled, especially in the extratropics, is the presence of strong external forcing, a typical example of which is the El Niño/Southern Oscillation (ENSO; [Philander, 1989](#)) in the equatorial Indo-Pacific region which considerably modulates the climate system over the entire globe (see, e.g., [Compo and Sardeshmukh, 2010](#); [Newman et al., 2003](#)). To remove external forcing such as ENSO, statistical approaches are required, which can also introduce additional errors. Moreover, coupled ocean-atmospheric general circulation models (CGCMs) form another type of commonly used tools that seek to realistically simulate the climate system and are thus subject to the same constraints as the observations, while also limited by additional errors resulting from unrealistic physical representation and numerical parameterization. They are nevertheless useful in filling the gap due to spatially and temporally sparse observations and in conducting experiments which are otherwise impossible in the real world.

The statistical methods used in the literature on the problem of ocean-atmosphere interaction are commonly based on linear correlation or regression, both of which are classic statistical methods measuring the potential quasi-equilibrium linear relation between two given variables. When applied on two time series with a time lag, the correlation or regression might then be able to indicate a potential cause and effect relationship. A significantly high value of correlation or regression is indicative of a forcing of the time series that leads on the one that lags, or, in other words, a response of the delaying one to the leading one. It must be noted that the correlation and regression methods can merely indicate potential statistical relationships which are possibly driven by external forcing. Thus these methods do not imply causality in any sense. Nevertheless, on the basis of current knowledge, ENSO is the most powerful external forcing to the extratropical ocean-atmosphere system. There-

fore by applying a skillful ENSO-removing technique, one can improve confidence about the causality implied by lead-lag correlation or regression. Previous researchers have made extensive use of this perspective to assess the causal link between the ocean and the atmosphere at the midlatitudes. Ever since the mid-1970s, many of these studies have found high correlations when the extratropical atmosphere leads the underlying ocean by about a month, which indicates an atmospheric forcing on the ocean (Davis, 1976, 1978; Deser and Timlin, 1997). The dynamical and thermodynamical oceanic responses to the atmospheric forcing in the midlatitudes have already been thoroughly examined, showing that changes in surface heat flux due to anomalous advection of heat and moisture, changes in wind stress and hence Ekman currents are the fundamental contributors of extratropical sea surface temperature (SST) anomalies (Cayan, 1992a,b,c; Seager et al., 2000).

Studies on the other direction, i.e., the atmospheric response to anomalous SST as identified with the SST leading the atmosphere, date back to the 1970s (Palmer and Sun, 1985; Pitcher et al., 1988; Ratcliffe and Murray, 1970; Rowntree, 1972). Particularly, Frankignoul et al. (1998) found that the cross-correlation between surface heat flux and SST anomalies indicates a damping of the SST anomalies and thus a plausible atmospheric response when the ocean leads the atmosphere, although not necessarily a dynamical response. A whole range of statistical methods have been developed since then and applied to investigate the atmospheric response to extratropical SST anomalies, including maximum covariance analysis (MCA; Czaja and Frankignoul, 1999, 2002; Frankignoul and Sennéchaël, 2007; Rodwell and Folland, 2002) which rests on singular value decomposition (SVD; Bretherton et al., 1992), canonical correlation analysis (CCA; Friederichs and Hense, 2003), generalized equilibrium feedback analysis (GEFA; Liu and Wen, 2008; Liu et al., 2008; Wen et al., 2010), combined GEFA and SVD (GEFA-SVD; Liu and Wen, 2008), linear inverse model (LIM; Newman et al., 2009; Penland and Sardeshmukh, 1995a,b), fluctuation-dissipation theorem (FDT; Bell, 1980; Leith, 1975), and maximum response estimation (MRE; Frankignoul et al., 2011a). Frankignoul et al. (2011a) and Liu et al. (2012a,b) offered systematic cross validations for some of these methods. The MCA has been proven to be a robust technique that maximizes the (possibly delayed) atmospheric response to a given SST anomaly field, and is widely used to study the influences of the ocean on the atmosphere in the midlatitudes from a variety of perspectives (e.g., Gan and Wu, 2013; Gastineau and Frankignoul, 2012; Zhang et al., 2015).

By applying statistical analyses to observational data, some insights into the problem have been achieved by previous researchers. It has been argued that SST anomalies in the North Atlantic markedly influence the overlying large-scale atmospheric circulation, especially during the cold season (Czaja and Frankignoul, 1999, 2002). Similarly, Rodwell and

Folland (2002) performed the lagged SVD analysis and found a significant mid-tropospheric response that strongly projects onto the North Atlantic Oscillation and with the SST anomalies leading by a few months. The reason for a response at such long delay is attributed to the persistence of the SST anomalies, which is called by the authors the “ocean bridge”. More recently, Gastineau and Frankignoul (2015) presented similar results in winter but different in summer.

Over the North Pacific, however, the problem seems more difficult, probably due to the extremely influential ENSO phenomenon which effectively masks the signal. Nevertheless, it was proposed that the oceanic reemergence phenomenon, namely the annual re-occurrence of SST anomalies of the same sign at the surface, may cause the atmosphere to respond, although the extent to which the atmosphere responds was not answered (Alexander et al., 1999). Nonaka and Xie (2003) found a robust covariance in SST and surface wind speed over the Kuroshio and its extension region by analyzing satellite measurements, indicating a local response through the vertical shear adjustment mechanism, although only within the atmospheric boundary layer. Lau et al. (2002) noticed that potential predictability of precipitation over the United States seems to depend on SST anomalies over the North Pacific. Recent findings of Zhong et al. (2011) confirmed the impact of North Pacific SST variability on precipitation in the United States, also pointing out that the impact is very small comparing to the modulations by other ocean basins. Wang et al. (2013) offered more in-depth investigation into this issue. Further evidence of potentially large-scale imprints of SST anomalies was reported by Liu and Wu (2004). By means of lead-lag correlation analyses on both observations, they suggested a possible yet only marginally significant atmospheric response to SST anomalies during fall. Wu et al. (2005) showed that the ocean-atmosphere interaction over the North Pacific may have a remote influence on the tropical Indian Ocean, the western subtropical South Pacific, and the tropical and North Atlantic.

More specific research by Liu et al. (2006) who performed the MCA on reanalysis and observational data suggested a significant local summertime atmospheric response to SST anomalies in the previous winter which resembles the leading mode of North Pacific SST variability, i.e., the well-known Pacific Decadal Oscillation (PDO; Mantua and Hare, 2002; Mantua et al., 1997) mode. It is argued that the atmospheric response is characterized by a high wave number wave train across the North Pacific, as reflected by the 500 hPa geopotential height anomaly. A similar study by Frankignoul and Sennéchaël (2007) detected a large-scale atmospheric response to negative PDO SST anomaly over the North Pacific both during late summer and late full-early winter, both significantly related to SST anomalies up to at least 4 or 5 months before. Such long lead time, they argued, does not imply that it takes the atmosphere that much time to adjust but is due to the large persistence of the

SST anomalies, a view in general accordance with the “ocean bridge” hypothesis (Kushnir et al., 2002; Rodwell and Folland, 2002). However, they also argued that it might indeed imply a somewhat longer atmospheric response time than usually assumed, in line with the modeling study of Ferreira and Frankignoul (2005). The response is shown to closely resemble the Pacific-North America pattern, the dominant winter mode in the North Pacific, with an equivalent barotropic high over the western-central Pacific, a low over the eastern Pacific-western North America, and again a high over the eastern North America.

An important paper by Liu et al. (2007) presented clear seasonal atmospheric response to reemergent SST anomalies over the North Pacific, by analyzing both observations and CGCM experiments. It is shown that in winter when the reemergent SST anomalies are strongly forcing the atmosphere, the atmosphere exhibits a local equivalent barotropic ridge response to warm SST anomalies over the Aleutian Low region together with a downstream wave train response over North America and the North Atlantic. The barotropic ridge response over the Aleutian Low region is known as the “warm-ridge”, or equivalently “cold-trough”, response style meaning that the atmospheric response is a ridge (trough) in response to warm (cold) SST anomalies. During summer, on the other hand, the reemergent SST anomalies disappear at the surface and the atmospheric response becomes very weak. They concluded that the significance of the atmospheric response relative to natural atmospheric variability increases dramatically on annual and longer timescales, due to the fast reduction of atmospheric internal variability and slow reduction of the response, which is related to the slow reduction (large persistence) of the reemergent SST anomalies. Their study thus attempted to answer the question of the extent of atmospheric imprints of reemergence raised by Alexander et al. (1999). Zhao and Li (2010, 2012a,b) further noticed winter-to-winter recurrence of North Pacific atmospheric anomalies which arise from anomalous eddy forcing associated with storm track changes, with remote forcing by ENSO and the Arctic Oscillation shown to be unimportant.

By using the GEFA, Wen et al. (2010) performed a comprehensive assessment of the global atmospheric response to selected modes of SST variability. Their results showed that in response to PDO-like SST anomalies, the atmosphere exhibits a local low over the Aleutian Low region, confirming the so-called warm-ridge (cold-trough) response pattern suggested by many modeling studies (see Kushnir et al., 2002, and Chapter 3). There is also a downstream response over the North Atlantic which is suggestive of the winter atmospheric teleconnection pattern known as the Aleutian-Icelandic seesaw (Honda et al., 2005; Honda and Nakamura, 2001). More recently, a similar response pattern that is commonly found by the GEFA, LIM, and FDT analyses is reported by Liu et al. (2012a), whose second part (Liu et al., 2012b) reported a dramatic seasonality of the response, with the winter season response

being the strongest. Moreover, recently there is increasing interest on frontal scale air-sea interaction focusing on the sharp SST fronts at midlatitudes, e.g., the Kuroshio Extension front in North Pacific and the Gulf Stream front in North Atlantic, which are found capable of exerting significant large-scale impacts on the overlying atmosphere extending over the entire troposphere (e.g., [Minobe et al., 2008](#); [Xu et al., 2011](#)). Since the emphasis of this study is the atmospheric response to large basin scale SST anomalies, frontal scale air-sea interaction is not central here, but the importance of the fronts should anyway be kept in mind.

On the other hand, CGCMs have been widely used as well, but mostly by comparing the midlatitude atmospheric variability with the results of forced atmospheric general circulation models (AGCMs), in order to assess the role of coupling. As this perspective is not directly relevant to this study, summarized here are the few dynamical and/or statistical studies on the mechanism of the atmospheric response to anomalous SST in the extratropical North Pacific, treating the coupled model results in the same way as the observations. [Liu and Wu \(2004\)](#) performed an ensemble experiment with a fully coupled model, with each ensemble member starting from a different atmosphere-ocean climatological initial condition plus a warm mixed layer (upper 200 m) temperature anomaly in the western North Pacific, an approach similar to the breeding method ([Toth and Kalnay, 1993](#)). Such coupled model setup simulates an atmospheric response favoring the warm-ridge response style, with an equivalent barotropic high downstream of the warm surface and subsurface temperature anomalies. The same approach was employed by [Liu et al. \(2007\)](#) but the temperature anomaly was applied to the upper 560 m, well into the permanent thermocline. The findings are rather similar to that presented above when discussing the observational part of their work, featuring highly seasonal responses with a significant warm-ridge response in winter and a very weak response in summer. The winter response and the seasonality are attributed to the oceanic reemergence mechanism. [Kwon and Deser \(2007\)](#) analyzed the output of a 650-year control integration of the Community Climate System Model (CCSM; [Kiehl and Gent, 2004](#)) version 2 and statistically detected a wind stress curl response to North Pacific SST anomalies that is to the opposite sign of the atmospheric forcing, favoring a warm-trough (as opposed to warm-ridge) style response. Further, [Zhong and Liu \(2008\)](#) assessed the atmospheric response in an updated version of the model, CCSM3 ([Collins et al., 2006](#)), by means of the GEFA, the original equilibrium feedback assessment (EFA), and the same dynamical approach of [Liu and Wu \(2004\)](#) except that the temperature anomaly was applied to the upper 400 m. All of the three methods identify a warm-trough response to SST anomalies over the Kuroshio Extension region. The warm-trough response style which is contradicting to many observational and modeling studies discussed above is attributed to the CCSM's model

physics. Recently, by analyzing the results of multiple CGCMs in the Coupled Model Intercomparison Project Phase 5 (Taylor et al., 2012; Yim et al., 2015) demonstrated that a significant atmospheric response to PDO-like SST anomalies is detected in models in which the PDO-related Aleutian Low is more to the south, implying a two-way ocean-atmosphere feedback. The strength of the two-way feedback, however, shows large discrepancies among the CGCMs.

To summarize, much progress has been made by observational and modeling studies on the existence, characteristics, and mechanism of the atmospheric response to SST anomalies in the extratropical North Pacific. It is now generally acknowledged that extratropical SST anomalies do have significant large-scale atmospheric imprints, either locally or remotely, and that the response exhibits remarkable seasonality. The oceanic reemergence mechanism is mostly responsible for the response itself and its seasonality. However, the response style is still under debate, and the mechanism is still poorly understood. In this chapter the problem is revisited by performing canonical lead-lag correlation and regression analyses on the basis of observations and a coupled model integration.

The chapter is organized as follows: first the observational datasets, the model, and the statistical methodology are described in Section 2.2. Thereafter in Section 2.3 a simple statistical approach to remove tropical impacts from the extratropical SST anomalies is introduced. Sections 2.4 and 2.5 form the main content of this chapter by presenting results of statistical analyses on the observed and simulated ocean-atmosphere system, respectively. In each of the two sections, the fundamental SST and atmospheric variability is examined, then the SST reemergence mechanism is studied, and finally the relationship between the ocean and atmosphere is inspected. Summary and discussions are presented in Section 2.6.

2.2 Data and Methods

2.2.1 Observational Data

The nature of air-sea interactions over the North Pacific is studied by analyzing observed monthly mean SST, sea level pressure (SLP) and net surface turbulent heat flux (THFX). SST and SLP data are from the Extended Reconstruction SST (ERSST; Smith et al., 2008) version 2 product¹ and the Extended Reconstruction SLP (Smith and Reynolds, 2004, ERS-
SLP;) data², respectively. The horizontal resolution of both ERSST and ERS-
SLP is $2^\circ \times 2^\circ$.

¹Data source: <http://www.esrl.noaa.gov/psd/data/gridded/data.noaa.ersst.html>

²Data source: <http://www.esrl.noaa.gov/psd/data/gridded/data.noaa.erslp.html>

Only a sub-period (1910–1997) of the ERSLP data is used, due to the poor data quality before 1910. The SST records are also truncated to the same period for consistency. THFX data are provided by the Objectively Analyzed Air-Sea Heat Fluxes (OAFlux; Yu and Weller, 2007) version 3 dataset¹ on a global $1^\circ \times 1^\circ$ grid for the period of 1958–2013. The Simple Ocean Data Assimilation (SODA; Carton et al., 2000a,b) version 2.1.6 reanalysis product² with a half-degree horizontal resolution covering 1958–2008 is also employed to examine the reemergence mechanism by exploring the upper 1000 m temperature. Monthly anomalies are computed, after detrending, by subtracting a monthly mean seasonal cycle averaged over the whole period from the respective time series. Winter mean anomalies are then derived by averaging over boreal winter (December–February, DJF).

2.2.2 Kiel Climate Model

The Kiel Climate Model (KCM; Park et al., 2009) is a coupled ocean-atmosphere-sea ice climate system model developed at the Helmholtz Centre for Ocean Research Kiel. It consists of the European Centre for Medium-Range Weather Forecasts Hamburg version 5 (ECHAM5; Roeckner et al., 2003) AGCM coupled to the Nucleus for European Modeling of the Ocean (Madec, 2008; Madec et al., 1998) ocean-sea ice general circulation model, coupled with the Ocean Atmosphere Sea Ice Soil version 3 (Valcke, 2013) coupler. No form of flux correction or anomaly coupling, either in freshwater, heat, or wind stress is used.

Here a 4700-year integration of the KCM that assumes “present day” values for greenhouse gases ($\text{CO}_2=348$ ppm) is analyzed. The initial condition is from the Levitus et al. (1998) climatology and the first 500 years are eliminated as spin-up period. The atmospheric component is on the T31 horizontal grid ($\sim 3.75^\circ$) and has 19 vertical levels extending up to 20 hPa. The oceanic model runs on a 2° Mercator grid with an enhanced meridional resolution of 0.5° near the equator, and with 31 vertical levels. The 4200-year model output is processed in the same manner as is done for the observations to obtain monthly and winter anomalies.

2.2.3 Statistical Analyses

Empirical Orthogonal Function

The Empirical Orthogonal Function (EOF) analysis is a multivariate statistical technique also known as Principal Component Analysis in statistics. With the eigenvectors of the spa-

¹Data source: <http://oaflux.who.edu/data.html>

²Data source: http://icdc.zmaw.de/easy_init_ocean.html?&L=1

tially weighted covariance matrix of anomalies, the anomaly field is partitioned into mathematically orthogonal modes, or EOFs. The time series of the amplitude associated with each mode is then determined by projecting the EOFs onto the anomalies and is known as the Principal Component (PC). The level of explained variance is measured by the ratio of each mode's corresponding eigenvalue to the trace of the covariance matrix (von Storch and Zwiers, 1999).

A spatial weight defined by the area of each grid cell is applied to the winter mean SST anomalies both in observations and in KCM, after removing their respective linear trend. The leading EOFs and PCs of winter (DJF) mean SST anomalies in the North Pacific (120°E–80°W, 20°N–60°N) and Tropical Pacific (120°E–80°W, 30°S–20°N) are then computed. The PCs are normalized by dividing by their standard deviations (STDs) and are thus dimensionless, while the EOFs are multiplied by the STDs of their corresponding PCs, hence having the dimension of temperature. It will be shown that the leading mode of North Pacific SST variability has a decadal-to-multidecadal spectral peak associated with the PDO. The EOF and PC of this mode are referred to as the PDO pattern and index hereafter, although sometimes in the literature the term “PDO Index” may also indicate the low-pass filtered version of the index. Likewise, the first mode of Tropical Pacific SST variability represents ENSO, therefore the EOF and PC are denoted the “ENSO pattern” and “index” in this study.

Spectral Analyses

In signal processing, the power spectrum of a time series describes the distribution of variance over its sinusoidal component waves spanning the frequency domain. Under the assumption that the original time series may be decomposed into the linear sum of component waves with various frequencies and amplitudes, the Fourier transform solves for the amplitudes of the individual components, hence producing the power spectrum. For computational efficiency, the Discrete Fourier Transform (DFT) algorithm is often used. The significance of the spectrum is usually tested against the null hypothesis that the signal is virtually white or red noise, thus a spectral peak exceeding the spectrum of white or red noise may be considered statistically significant under a certain confidence level (von Storch and Zwiers, 1999). Here the power spectra of the observed and simulated PDO and ENSO indices are computed using the DFT algorithm.

Linear Regression

Linear regression is a statistical approach to model the relationship between a dependent variable and one or more independent variables. It assumes that the dependent variable may

be expressed as the linear combination of the independent variables, each multiplied by a coefficient, plus a residual term. Given a set of observations of the dependent and independent variables, the objective of the linear regression analysis is to find an optimal solution of the coefficients so that the linear combination of the independent variables explains the most of the variance of the dependent variable, in the meantime minimizing the variance of the residual (von Storch and Zwiers, 1999). The optimal coefficients are then referred to as the regression coefficients, indicating the variability associated with the independent variables and leaving out the effects from other potential contributors. In the context of climate data, the analysis is usually repeated for each grid point, and the observations are most commonly a time series. By shifting the dependent and independent time series for a certain time lag, the lead-lag regression may also be informative to demonstrate the delayed effect of a variable on another.

Linear Correlation

The linear correlation coefficient, or more strictly the Pearson product-moment correlation coefficient, is a measure of the statistical relationship between two random variables or two sets of data. It is defined as the covariance of the two variables divided by the product of their STDs, with the value 1 meaning total positive correlation, 0 no correlation, and -1 total negative correlation. As for regression, lead-lag correlations may also be used to examine the delayed relationship between two variables. In case of two different variables, the term “cross-correlation” is used, whereas the term “auto-correlation” is for the lead-lag correlation of a variable with itself. Correlations are useful as they indicate potential casual relationships that can be exploited in practice. However, one should note that the existence of casual relationships cannot be inferred from correlations. The causes underlying a high correlation, if any, might be indirect, external, and unknown. It is also plausible that the relationship is nonlinear, in which case the linear correlation coefficient, although exists, may not be adequate (von Storch and Zwiers, 1999).

2.3 Removing Tropical Effects

As is going to be shown in Section 2.4, the PDO index comprises significant spectral peaks on interannual timescales which mostly arise from teleconnections of tropical processes such as ENSO. In order to inspect ocean-atmosphere interactions within the extratropical North Pacific using linear regression, one needs to define a modified version of the PDO index which excludes tropical impacts. Here such an index is defined by the leading PC of North

Pacific SST variability from which tropical impacts are properly removed beforehand. The index is denoted the “PDO^{*}” index hereafter.

A variety of methods have been proposed by previous studies to remove the ENSO signature from climate records. Many of these methods involve linear regression on a certain predefined ENSO index, for instance the leading PC of tropical SST, the leading Principal Oscillation Component (POP; Hasselmann, 1988; von Storch et al., 1988) time-coefficient, or canonical indices such as the Niño 3.4 index¹ (e.g., Angell, 2000; Baquero-Bernal et al., 2002; Robock and Mao, 1995; Thompson et al., 2008). Frankignoul and Sennéchael (2007) removed ENSO impacts by linear regressions on the leading two PCs of Tropical Pacific SST, applying a running window of three months to get smoothly varying estimates. They also took into account the phase asymmetry of ENSO by performing the regression separately for the positive and negative values of the tropical PC. Compo and Sardeshmukh (2010) reviewed the pros and cons of the commonly employed ENSO removing techniques, and proposed a much more sophisticated approach based on a LIM technique themselves.

In this chapter an approach following the canonical multivariate regression model but on objectively selected tropical indices are employed. First, the North Pacific winter SST anomalies (1910–1997) are regressed onto a certain selected set of indices representing tropical SST variability, and take the residual as the ENSO-unrelated part whose first PC is defined as the PDO^{*} index. The correlation coefficients between the Niño 3+4 index² and the resultant PDO^{*} index within ± 8 year lags are computed and their average absolute value is used as a crude indicator of the ENSO-removing skill. Apparently the smaller value of the averaged correlation suggests the better skill. Five sets of tropical SST indices have been tested for their ENSO-removing skills: the first PC of Tropical Pacific SST, the first two PCs of Tropical Pacific SST, the first three PCs of Tropical Indo-Pacific SST, the first POP time-coefficient of Tropical Pacific SST, and the Niño 3.4 index. The test was performed for both ERSST and KCM data. It was found that for both datasets removing the first two PCs of Tropical Pacific offers the best skill, therefore hereafter the PDO^{*} index is defined as the first PC of North Pacific SST from which the leading two PCs of Tropical Pacific are removed by linear regression. In the end this is rather similar to the technique used by Frankignoul and Sennéchael (2007) but somewhat simpler. The corresponding EOF of the PDO^{*} index is named the PDO^{*} pattern.

¹Defined as SST averaged over 120°W–170°W, 5°S–5°N.

²Defined as SST averaged over 160°E–90°W, 5°S–5°N.

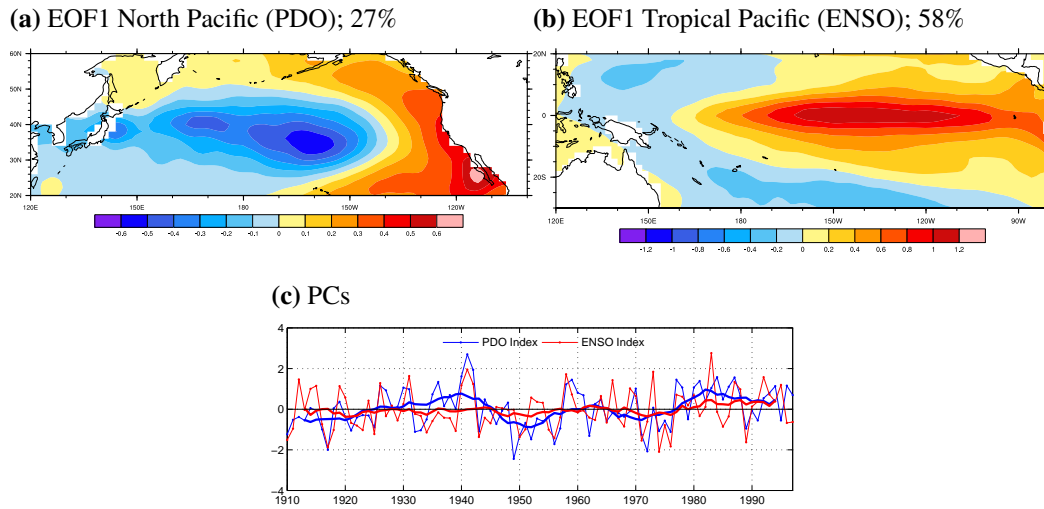


Fig. 2.1: (ERSST) Patterns of the leading EOFs [$^{\circ}\text{C}$] of SST variability based on winter mean (DJF) anomalies over (a) North Pacific, (b) Tropical Pacific. The percentage of explained variance is shown in the sub-captions. (c) The PDO and ENSO time series corresponding to the above EOF patterns. The thick curves indicate the 11-year running mean.

2.4 Observed Ocean-Atmosphere Linkage

2.4.1 Fundamental Oceanic Variability

The leading mode, i.e. the PDO mode (Mantua and Hare, 2002; Mantua et al., 1997), of the observed North Pacific SST variability is shown in Figs. 2.1a and 2.1c. The pattern (positive phase) depicts a long band of cooling over the western to middle North Pacific along 40°N , surrounded by an arch of warming to the north, east and south. This pattern is also known as the “horseshoe” pattern. The largest amplitude of cooling appears over the central North Pacific, while maximum warming is observed to the southeast of the depicted area. The most energetic mode of SST variability in Tropical Pacific shown in Figs. 2.1b and 2.1c represents the ENSO mode (Philander, 1989).

It can be noticed from the time series that both the PDO and ENSO indices exhibit substantial interannual variability, whilst fluctuations on decadal timescales are considerable only in the PDO index, although the ENSO index also show some decadal modulation (Fig. 2.1c). The power spectra of the indices provide a more lucid view with regard to the distribution of variance across the frequency components (Figs. 2.2a and 2.2b). The PDO index consists of significant spectral peaks at 3–4, 5–6, 20, and 50 year periods, whereas the ENSO index has components at 3–4 and 5–6 year periods. The 20- and 50-year components of PDO are known as the bi-decadal and penta-decadal oscillations which interact with each

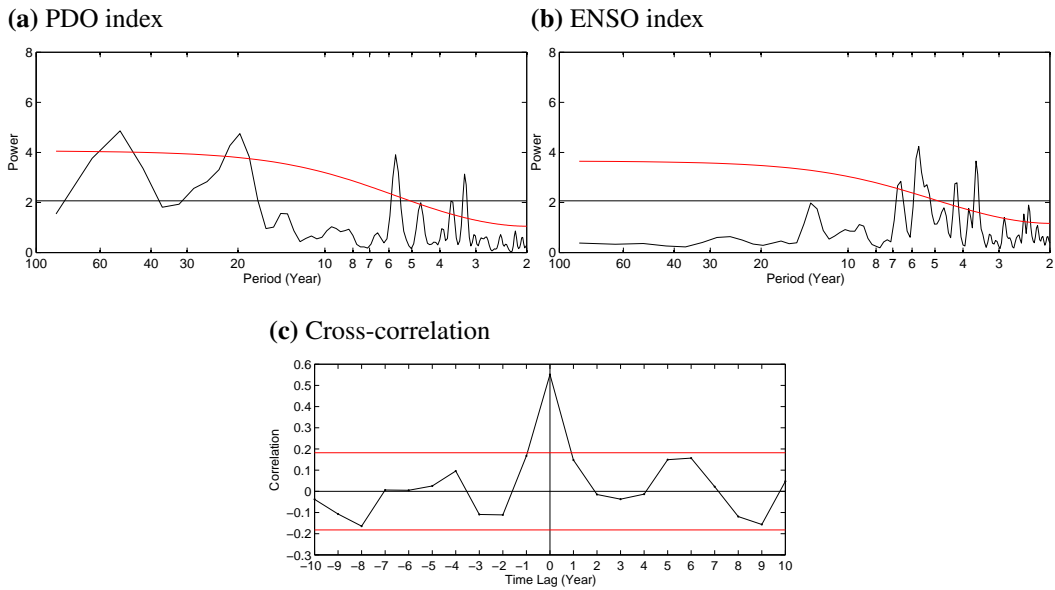


Fig. 2.2: (ERSST) Power spectra of the (a) PDO index, (b) ENSO index. The horizontal line and the red curve indicate the white and red spectral fits, respectively, at the 95% significance level. (c) Cross-correlation between the above two indices. Positive lag means the PDO index leads. The 95% significance level is shown by the red horizontal lines.

other (Minobe, 2000). On interannual timescales, the presence of significant spectral peaks in both indices suggests potential linkage between the two, which is in agreement with many previous studies (e.g., Newman et al., 2003) and is also confirmed by the significantly high instantaneous correlation shown in Fig. 2.2c. Other tropical modes may also affect the PDO index, although presumably to a lesser extent (Wu et al., 2003).

Since the main interest of this study is ocean-atmosphere interaction internal to the North Pacific sector, it is desirable to define a new PDO index from which ENSO signatures are properly removed. This is accomplished by linearly regressing out the North Pacific SST variability associated with the leading two tropical modes and take the leading PC of the resultant North Pacific SST variability. More detail was presented in Section 2.3. The leading EOF and PC of the ENSO-removed PDO mode, or the PDO* mode, are shown in Fig. 2.3. The power spectrum of the PDO* index as well as its correlation with the ENSO index are also shown. The PDO* pattern is in principle similar to the PDO pattern consisting of tropical signatures, but some differences are still noticeable: the magnitude is in general smaller, and the maximum cooling moves from the middle Pacific to the western boundary immediately off Japan. From the PC time series and power spectrum, it can be inferred that while the bi-decadal and penta-decadal oscillations are largely kept, the interannual variability is dramatically suppressed. Significant reductions in the cross-correlation with the ENSO in-

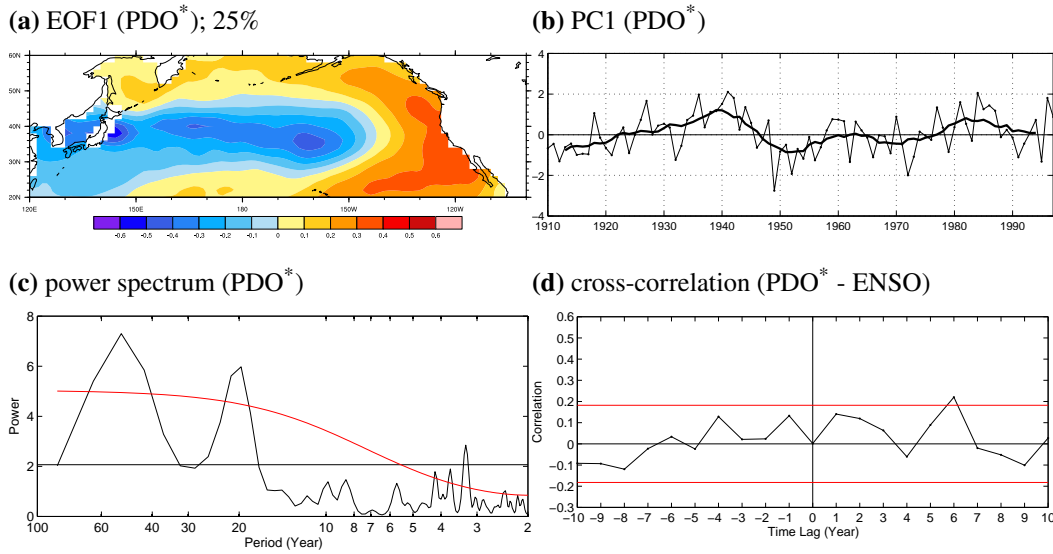


Fig. 2.3: (ERSST) The leading mode of North Pacific SST variability with ENSO removed (PDO^*). (a) The EOF [$^{\circ}\text{C}$]. The percentage of explained variance is shown in the sub-caption. (b) The PC, with the thick curve indicating the 11-year running mean. (c) The power spectrum. The horizontal line and the red curve indicate the white and red spectral fits, respectively, at the 95% significance level. (d) Cross-correlation with the ENSO index. Positive lag means the PDO^* index leads. The 95% significance level is shown by the red horizontal lines.

dex are also found, suggesting the success of the ENSO-removing technique. Therefore it can be argued that the PDO^* index demonstrates essentially long-term SST variability that is internal to the North Pacific.

2.4.2 Fundamental Atmospheric Variability

In order to investigate the most salient feature of North Pacific atmospheric variability, EOF and spectral analyses are also performed on observed wintertime SLP data. The primary mode of extratropical North Pacific atmospheric variability, which is responsible for 55% of the total variance, displays (in its positive phase) a basin scale low pressure center located over the Gulf of Alaska and the Aleutian Islands (Fig. 2.4a). This mode essentially describes the deepening/shallowing fluctuations of the Aleutian Low, the persistent feature of planetary-scale extratropical atmospheric circulation. It is noteworthy that the Aleutian Low is a statistical feature having its source in the atmospheric synoptic low pressure systems originated off the Asian continent, propagating while intensifying eastwards (e.g., Rodionov et al., 2007). Since climatologically the Aleutian Low is believed to drive the counterclock-

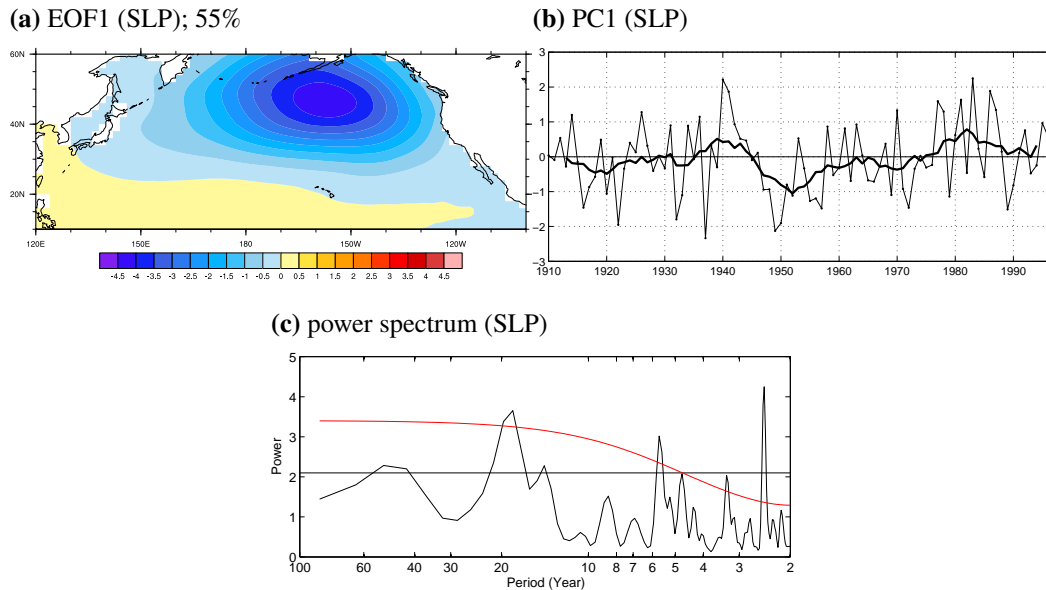


Fig. 2.4: (ERSLP) The leading mode of North Pacific SLP variability. (a) The EOF [hPa]. The percentage of explained variance is shown in the sub-caption. (b) The PC, with the thick curve indicating the 11-year running mean. (c) The power spectrum. The horizontal line and the red curve indicate the white and red spectral fits, respectively, at the 95% significance level.

wise oceanic subpolar gyre circulation (Pickart et al., 2009), its oscillations associated with the leading mode have the ability to force anomalous extratropical SSTs, through changes in surface heat flux due to abnormal wind speed, horizontal advection of heat and moisture, as well as Ekman currents (Cayan, 1992a,b,c; Seager et al., 2000). It is obvious from the PC time series and the power spectrum (Figs. 2.4b and 2.4c) that the extratropical atmospheric variability comprises significant components on interannual and decadal-to-multidecadal timescales, which is also found by e.g. Overland et al. (1999) and Minobe (2000). The spectrum is in fact very similar to that of the PDO index (Fig. 2.2a), both featuring significant peaks at 3–4, 5–6, 20, and 50 year periods, except that the penta-decadal peak of SLP is only significant above the white spectrum level. Therefore it seems plausible that potential connections between the extratropical atmosphere and ocean exist, especially on timescales longer than decadal where modulation by ENSO is absent. Moreover, it is obvious that the SLP spectrum has a remarkably powerful 2–3-year component which is very likely a surface manifestation of the Quasi-Biennial Oscillation (QBO; Baldwin et al., 2001), yet this is not relevant to this study and thus omitted.

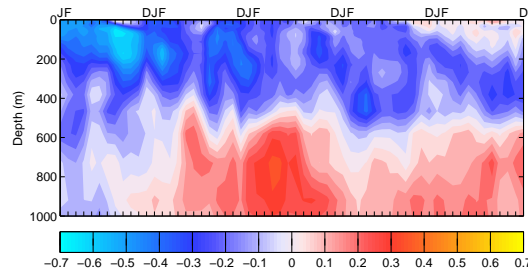


Fig. 2.5: (SODA) Cross-correlation of the winter PDO* index with monthly temperature anomalies averaged over 140°E–180°E, 35°N–50°N as a function of depth and time lag for five years.

2.4.3 Reemergence

Previous studies (e.g., Alexander and Deser, 1995; Alexander et al., 1999; Alexander and Penland, 1996; Bhatt et al., 1998; Namias and Born, 1970, 1974) have found that in the midlatitude North Pacific, winter SST anomaly signals tend to recur through the subsequent winters and disappear in the intervening summers. Such a mechanism is known as the “reemergence mechanism”. Following Alexander and Deser (1995), Fig. 2.5 shows the lead-lag correlations between the PDO* index defined above and the upper 1000 m ocean temperature anomalies. It is evident that anomalous temperature signal appearing at the surface is transmitted into the ocean interior and is decoupled from the surface during summer. In subsequent winters, however, the signal stored in the deeper ocean repeatedly reappears at the surface. The driving force of the reemerging anomalies is attributed to the strong wind mixing during winter which stores the surface signal into the deep seasonal mixed layer, and releases it by stirring it into the mixed layer in subsequent winters. The wintertime mixed layer depth is around 100 m–150 m, according to de Boyer Montégut et al. (2004). During summer when the mixed layer is shallow, the signal is hidden beneath and thus isolated from surface anomalies. Obviously, the large thermal capacity of the deep extratropical oceanic mixed layer is vitally important for the reemergence mechanism.

The reemergence mechanism can also be observed from the regression coefficients of the North Pacific winter SST anomalies on to the PDO* index, as depicted in Fig. 2.6. The instantaneous regression pattern is by definition very similar to the PDO* pattern, since they both represent the variabilities associated with the PDO* index. At higher lags the cold and warm SST anomalies recur with reduced size and strength for as long as 6 years. This persistent annual recurrence of temperature anomalies at the ocean surface is believed to provide extra predictability to the climate system (Liu and Wu, 2004). It also imposes abnormal lower boundary conditions to the atmosphere, causing the latter to respond by altering surface sensible and latent heat fluxes (Kushnir et al., 2002).

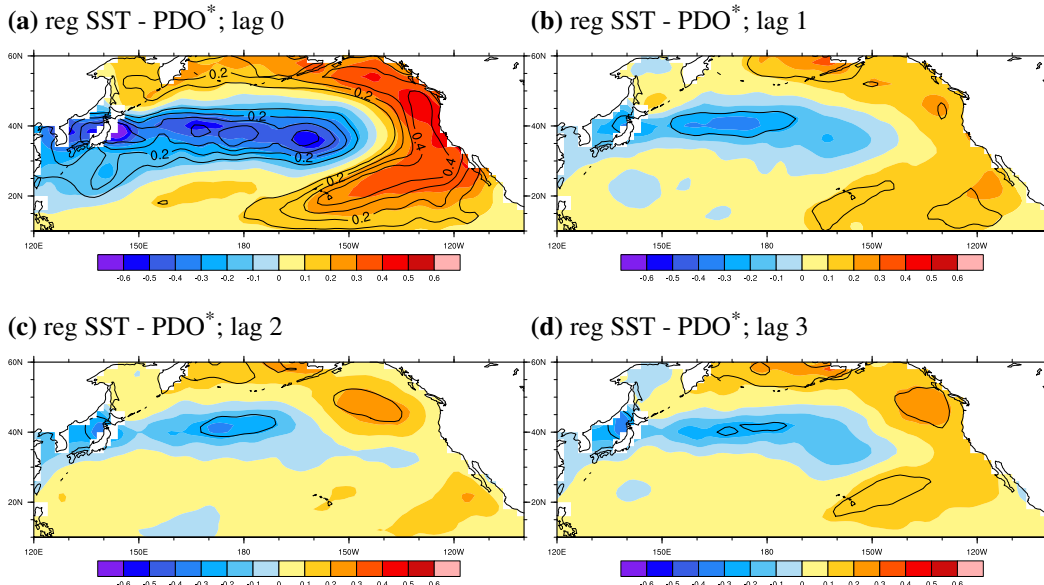


Fig. 2.6: (ERSST) Regression coefficients (shading) of North Pacific winter SST [$^{\circ}\text{C}$] on to the PDO* Index when the index leads the SST by (a) 0, (b) 1, (c) 2, (d) 3 year(s). Contours indicate the ratio of variance explained by regression. Contour interval is 0.1.

2.4.4 Ocean-Atmosphere Relation

Thus far it has been shown that the coexistence of atmospheric and oceanic spectral peaks on both interannual and decadal-to-multidecadal timescales suggests potential linkage between the two, and that North Pacific SST anomalies associated with the long-term PDO* index tend to persistently recur for several years. On interannual timescales, it has been proposed by Bjerknes (1964) and confirmed by many succeeding studies that extratropical SST anomalies are primarily generated by the atmosphere (Cayan, 1992a,b,c). The main interest of this study is then on the long-term linkage between the extratropical ocean and atmosphere.

Linear correlations between the PC1 of North Pacific winter SLP variability and the PDO* index are computed and depicted in Fig. 2.7. Note that in contrast to most analyses in this study, here monthly data are used in order to display the seasonal difference. When the PDO* index leads (positive lags), significant albeit weak correlations are found only in winters, persisting for as long as six years. Previously, Zhao and Li (2010, 2012a,b) noticed high correlations at one year lag and named the phenomenon the “winter-to-winter recurrence (WWR) of atmospheric circulation anomalies”, yet annually recurring high correlations up to lags as long as 6 years are presented in this study for the first time. Given that the positive lags indicate the precedence of SST anomalies, the significant correlations at these lags actually suggest an atmospheric response to the SST anomalies, as long as the causality between

the two exists in the first place. As argued before, if prior to the analyses the linear trend and the external forcing from ENSO are properly removed, the causality is most likely real. This view was originally proposed by Frankignoul et al. (1998) and has been the keystone in developing statistical techniques to detect the atmospheric response to anomalous SSTs in observations (e.g., Frankignoul et al., 2011a; Frankignoul and Sennéchaël, 2007; Liu et al., 2012a,b; Wen et al., 2010). Moreover, the annual recurrence of significant correlations is remarkably suggestive of the oceanic reemergence mechanism, therefore it seems perfectly plausible that the reemergent SST anomalies repeatedly impose lower boundary heat flux forcing to the atmosphere, exciting the latter to respond somehow. According to Marotzke and Pierce (1997), the adjustment time of the atmosphere to surface heat flux changes is on the scale of days, hence anomalous SLP is expected in each winter in response to the annually exerted boundary forcing. The WWR is thus explained. It is also evident that the link from the ocean to the atmosphere at such long lags must not be direct, owing to the atmosphere's rapid adjustment timescale. Rather, the link arises from reemergence and the associated large thermal inertia of the ocean mixed layer. Such a pathway through reemergence is an example of the "ocean bridge" of Rodwell and Folland (2002). Considering the fact that the SLP index used here is the first PC of North Pacific SLP variability associated with a basin-scale spatial pattern, the significant albeit weak correlations may additionally indicate the large-scale character of the response. This finding is consistent with the observational and modeling results of Liu et al. (2007) who discussed the seasonal atmospheric response to reemergent North Pacific SST anomalies only in winter. One step further, since the reemergent SST anomalies are associated with the PDO* featuring profound bi-decadal and penta-decadal variations, the immediate atmospheric response, or the WWR, may then explain the long-term spectra peaks of SLP at the same frequencies. Furthermore, although not central to this study, the very noticeable high correlation at -1 month lag is in agreement with literature studies (e.g., Davis, 1976, 1978; Wallace and Jiang, 1987) indicating that the ocean needs about one month to adjust to atmospheric wind stress and heat flux forcing.

Fig. 2.8 shows regression coefficients of North Pacific SLP with regard to the PDO* index at various time lags when the SST leads. The instantaneous regression representing the pattern of SLP variability associated with the dominate SST variability, as depicted in Fig. 2.8a, closely resembles the primary mode of atmospheric internal variability, i.e., the Aleutian Low (Fig. 2.4a). It is difficult to isolate the forcing and response from the highly significant in-phase regression (and correlation), since both directions are present. The problem becomes easier when the atmosphere lags behind the ocean by one or more years and thus the regression coefficients depict the delayed atmospheric response to PDO* SST perturbations some years ago. In this view, Figs. 2.8b–2.8d portray an interesting picture that

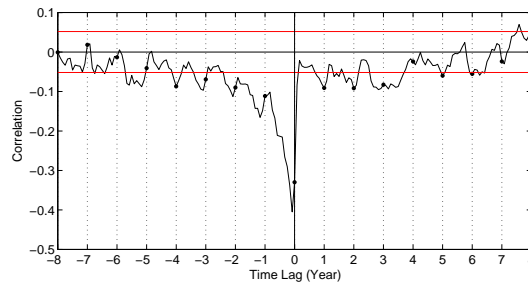


Fig. 2.7: (ERSST/SLP) Cross-correlation between the leading PC of North Pacific SLP and the PDO* index. Positive lag means the PDO* index leads. The PCs and correlations are based on monthly data. Time lags being multiples of 12 months are denoted by dots. The 95% significance level is shown by the red horizontal lines.

is in favor of the results of the correlation analyses, that is, the SST anomalies retain a large-scale impact on the overlying atmosphere for several winters, with a pattern resembling the atmospheric internal variability. The impact is not only persistent but also significant, since after as long as three years, it still explains over 10% of the total SLP variance over a fairly large area, which is already considerable given that the typical signal-to-noise ratio of the extratropical atmosphere lies in the range of 5–15% (Harzallah and Sadourny, 1995). This finding is in accordance with previous observational studies, e.g., Wen et al. (2010), Liu et al. (2012a,b), favoring the warm-ridge (or cold-trough) response style. We do not analyze the response at upper levels in this chapter, yet the surface response is already informative since the response has been shown to be equivalent barotropic (Kushnir et al., 2002).

To get more insights into the problem, the same regression analyses are performed over the period of 1958–2013 on surface turbulent heat flux, the interface of ocean-atmosphere interaction (Fig. 2.9). The patterns are mostly patchy, yet a few persistent features can still be noticed: First, the instantaneous regression pattern largely resembles the PDO* SST anomalies with upward heat transfer over colder than normal SST, indicating an atmospheric forcing on the SST. Second, at higher lags, there seems to be a persistent region with upward heat flux along the Kuroshio Extension, giving hint to a robust positive heat flux-SST feedback that tends to reinforce the SST anomalies. Third, positive feedback is found over large areas over the North Pacific, in agreement with Palmer and Sun (1985) and Latif and Barnett (1994) but not Park and Latif (2005) and Frankignoul and Sennéchael (2007).

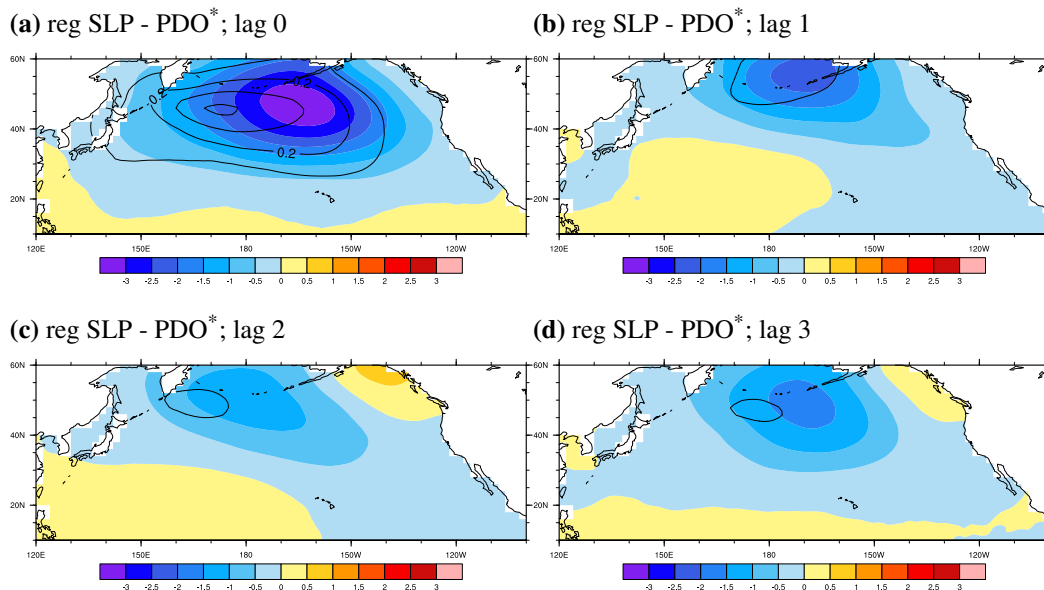


Fig. 2.8: (ERSLP) Regression coefficients (shading) of North Pacific wintertime SLP [hPa] onto the PDO^* Index when the index leads the SLP by (a) 0, (b) 1, (c) 2, (d) 3 year(s). Contours indicate the ratio of variance explained by regression. Contour interval is 0.1.

2.5 Simulated Ocean-Atmosphere Linkage

So far the analyses have been based on observations. Here in this section the same procedures are repeated on a 4200-year coupled simulation using KCM, in order to investigate the potential ocean-atmosphere linkage in the model.

2.5.1 Fundamental Oceanic Variability

The PDO and ENSO modes of North and Tropical Pacific SST variability simulated by KCM (Fig. 2.10) are rather similar to those observed (Fig. 2.1), except that the simulated PDO mode is more powerful and that the pattern is closer to the observed PDO^* mode (Fig. 2.3a), with the maximum near the western boundary off Japan. By comparing the spectra displayed in Fig. 2.11a with Fig. 2.2a, it could be inferred that the model reasonably simulates the dominate components of the PDO index, i.e. the interannual, bi-decadal, and penta-decadal variabilities, although in the model the 3–4-year and the 5–6-year spectral peaks are missing, instead a 7–9-year component stands out. As reported by Park et al. (2009), the ENSO variability simulated by KCM is in good agreement with observations (Figs. 2.2b and 2.11b). The PDO and ENSO indices are highly correlated both simultaneously and when the ENSO

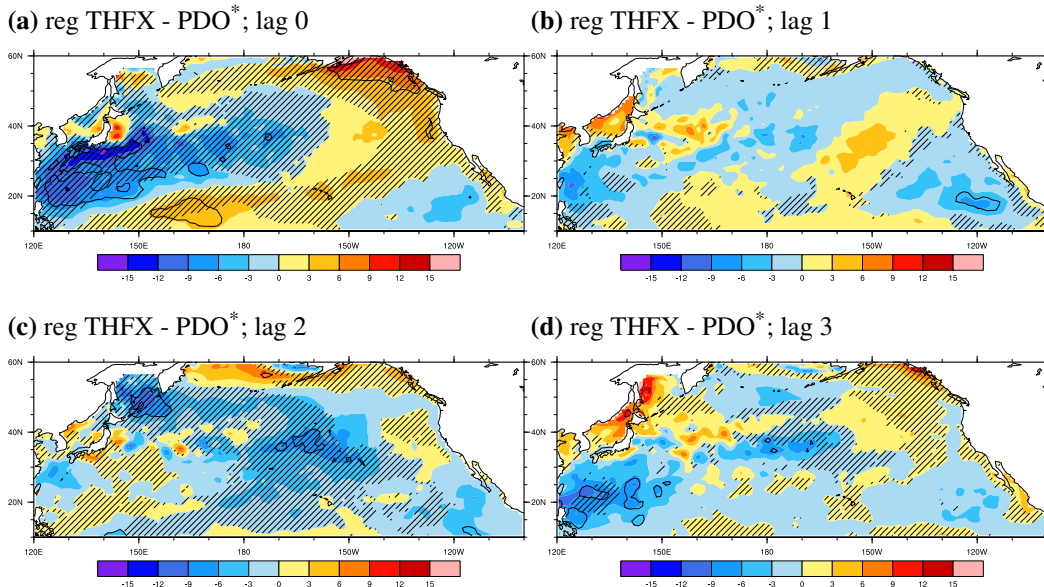


Fig. 2.9: (OAFIux) Regression coefficients (shading) of North Pacific wintertime turbulent heat flux (THFX, downward is positive) [W m^{-2}] on to the PDO^* Index when the index leads the THFX by (a) 0, (b) 1, (c) 2, (d) 3 year(s). Turbulent heat flux is defined as the sum of sensible and latent heat fluxes. Contours indicate the ratio of variance explained by regression. Contour interval is 0.1. Hatching denotes area with positive SST-heat flux feedback.

leads by one year (Fig. 2.11c), the former case of which is consistent with observations whereas the latter is not (Fig. 2.2c).

Applying the same ENSO-removing technique as described in Section 2.3, the resultant PDO^* mode of simulated North Pacific SST variability (Figs. 2.12a and 2.12b) shows a close resemblance with that observed (Figs. 2.3a and 2.3b), in spite of some discrepancies. The power spectrum of the PDO^* index (Fig. 2.12c) suggests acceptable ENSO-removing skill, since the interannual components are substantially suppressed while the decadal-to-multidecadal peaks are almost untouched. Fig. 2.12d further confirms this by showing that the correlations between the PDO^* and ENSO indices are dramatically reduced.

2.5.2 Fundamental Atmospheric Variability

In terms of the atmospheric variability in the North Pacific, KCM does a relatively good job too, as shown in Figs. 2.13a and 2.13b. The pattern of the primary SLP mode matches the observed version (Figs. 2.4a and 2.4b) extremely well, except that the amplitude is overly strong. There are manifest discrepancies between the simulated power spectrum of the lead-

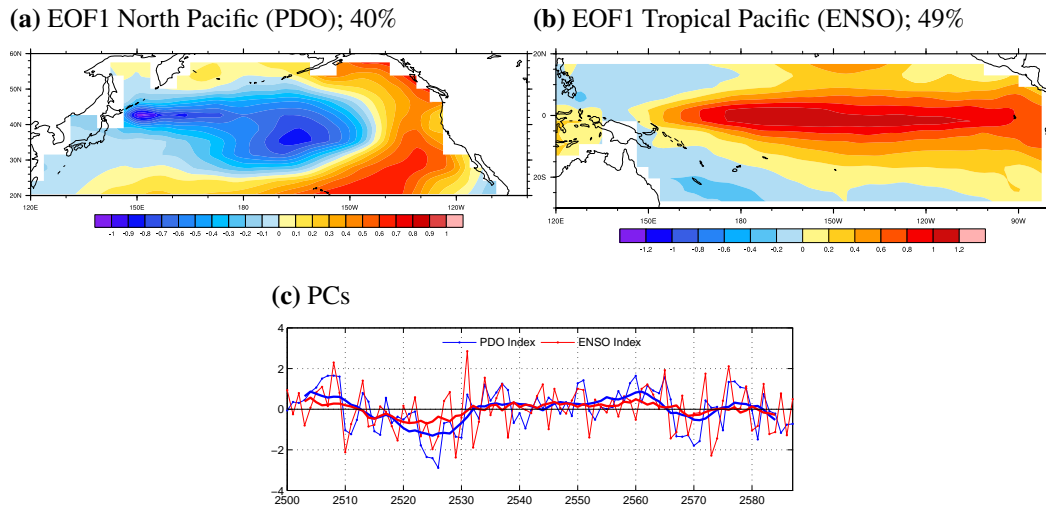


Fig. 2.10: (KCM) Patterns of the leading EOFs [$^{\circ}\text{C}$] of SST variability based on winter mean (DJF) anomalies over (a) North Pacific, (b) Tropical Pacific. The percentage of explained variance is shown in the sub-captions. (c) The PDO and ENSO time series corresponding to the above EOF patterns only showing the first 88 model years. The thick curves indicate the 11-year running mean.

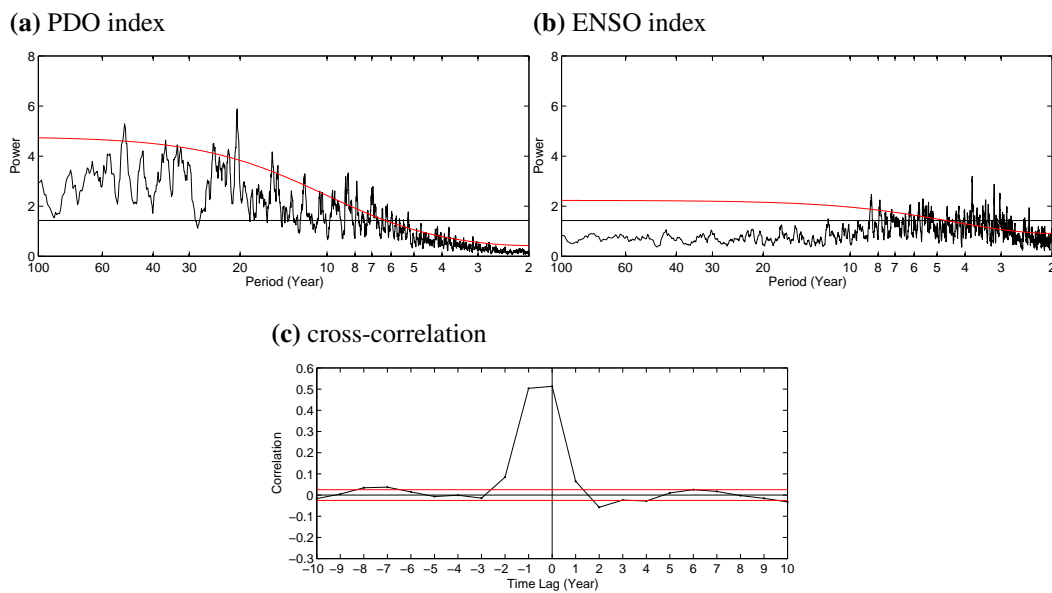


Fig. 2.11: (KCM) Power spectra of the (a) PDO index, (b) ENSO index. The horizontal line and the red curve indicate the white and red spectral fits, respectively, at the 95% significance level. (c) Cross-correlation between the above two indices. Positive lag means the PDO index leads. The 95% significance level is shown by the red horizontal lines.

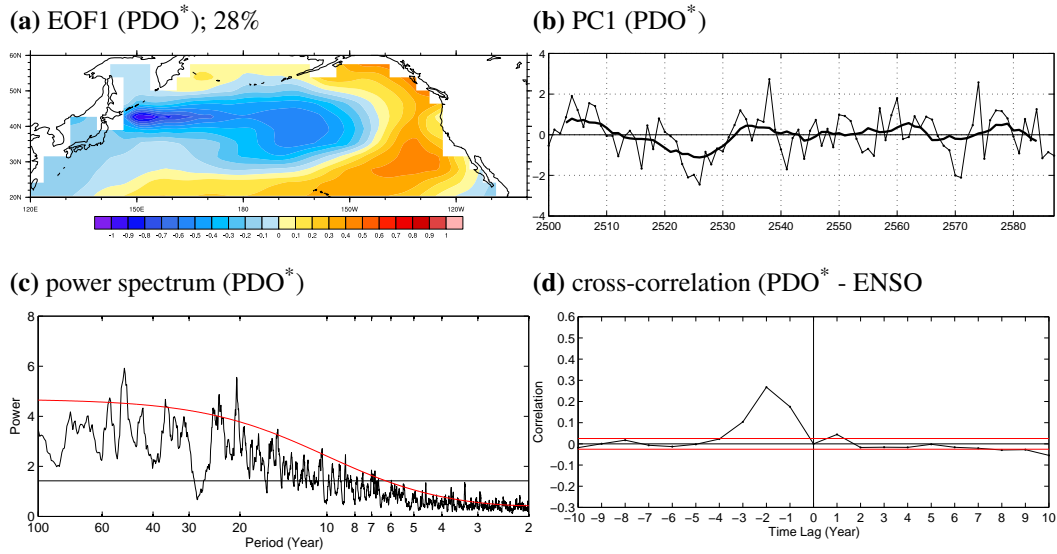


Fig. 2.12: (KCM) The leading mode of North Pacific SST variability with ENSO removed (PDO^*). (a) The EOF [$^{\circ}\text{C}$]. The percentage of explained variance is shown in the sub-caption. (b) The first 88 years of the PC, with the thick curve indicating the 11-year running mean. (c) The power spectrum. The horizontal line and the red curve indicate the white and red spectral fits, respectively, at the 95% significance level. (d) Cross-correlation with the ENSO index. Positive lag means the PDO^* index leads. The 95% significance level is shown by the red horizontal lines.

ing PC and its observational counterpart as well (Figs. 2.4c and 2.13c), namely the absence of significant peaks near the high frequency end of the spectrum. Particularly, the model does not reproduce the 2–3-year peak likely associated with the QBO which originates from the lower stratosphere, presumably due to the low top of the model atmosphere (20 hPa). The bi-decadal component is still evident but only marginally significant, whilst a hint of the penta-decadal oscillation is also noticeable. There is also a component at the 8-year period, which corresponds to the component of the PDO index at the same frequency.

2.5.3 Reemergence

As for the observations, correlations between the PDO^* index and extratropical sub-surface temperature are calculated and displayed as a function of depth and time lag (Fig. 2.14). Although the structure of the correlation in the ocean interior is different from the observations, it is quite clear that the anomalous surface signal is stored beneath the surface and reappear during following winters (Fig. 2.5). The explanation of the discrepancies with the SODA reanalysis in the deep ocean is beyond the scope of this study, but as the majority of

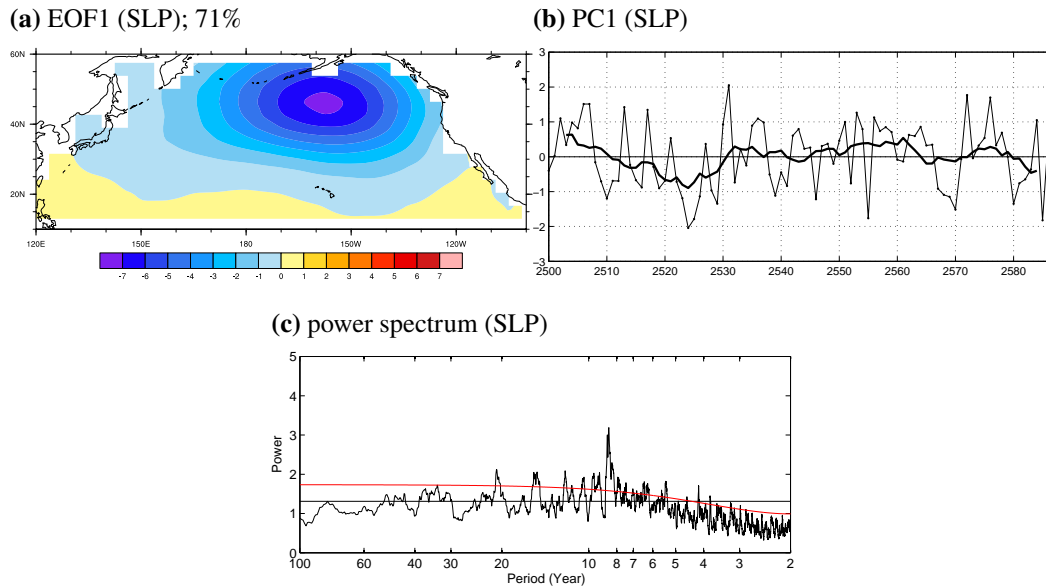


Fig. 2.13: (KCM) The leading mode of North Pacific SLP variability. (a) The EOF [hPa]. The percentage of explained variance is shown in the sub-caption. (b) The first 88 years of the PC, with the thick curve indicating the 11-year running mean. (c) The power spectrum. The horizontal line and the red curve indicate the white and red spectral fits, respectively, at the 95% significance level.

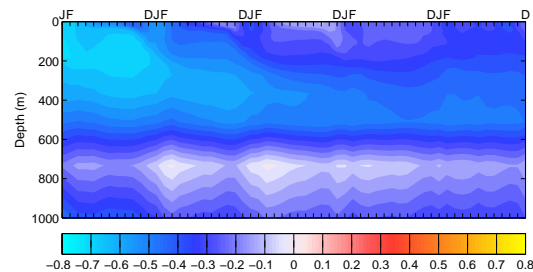


Fig. 2.14: (KCM) Cross-correlation of the winter PDO* index with monthly temperature anomalies averaged over 140°E–180°E, 35°N–50°N as a function of depth and time lag for five years. Only the first 100 years of monthly temperature anomalies are used for the sake of computational efficiency.

the ocean's heat content is contained in the surface mixed layer which controls the oceanic thermal inertia and thus the interaction with the atmosphere, we note here that the climatology of wintertime mixed layer depth in extratropical North Pacific simulated by KCM is reasonably similar to, although slightly smaller than, observational results (100 m–150 m) shown by [de Boyer Montégut et al. \(2004\)](#).

Patterns of North Pacific SST variability associated with the PDO* index when the index leads 0–3 years are shown in Fig. 2.15. Akin to the observational evidences (Fig. 2.6), the

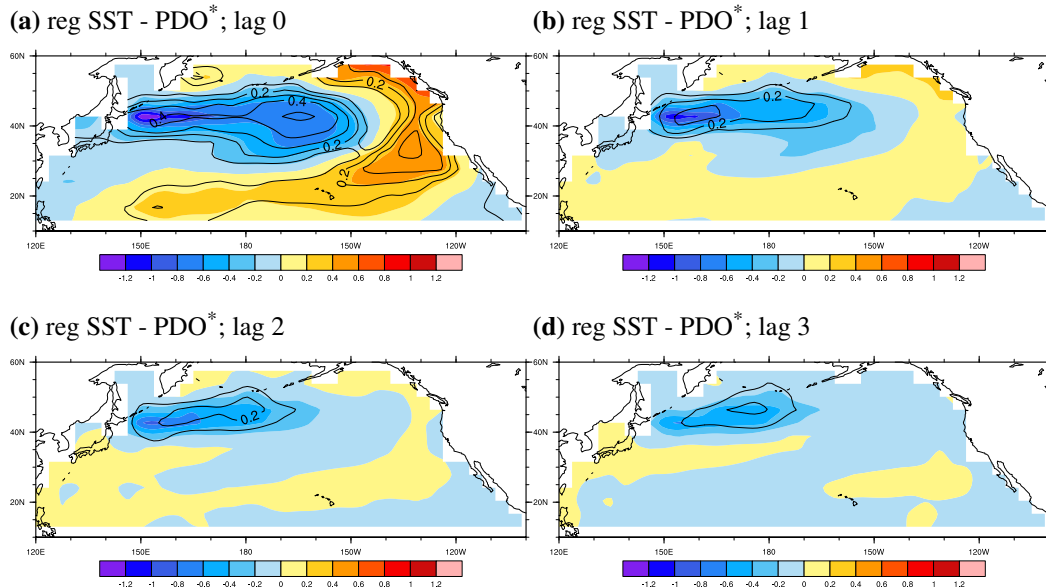


Fig. 2.15: (KCM) Regression coefficients (shading) of North Pacific winter SST [$^{\circ}\text{C}$] on to the PDO^* Index when the index leads the SST by (a) 0, (b) 1, (c) 2, (d) 3 year(s). Contours indicate the ratio of variance explained by regression. Contour interval is 0.1.

reemergence mechanism in North Pacific appears as the most salient feature in those plots, yet differences in several aspects are noticed. First, although over most parts of the basin the amplitudes of the instantaneous regression in ERSST and KCM are alike, the maximum amplitude in KCM is roughly twice that in ERSST. Second, the KCM patterns are shifted northward by $\sim 5^{\circ}$ comparing to ERSST. Third, the reemergent cold SST anomalies at higher lags are much stronger and more persistent in the model than in observations. Last of all, in the model the arch of warm SST anomalies almost vanishes after a lag of one year, in contrast with the observations where both the cold and warm SST anomalies take part in the reemergence mechanism. Efforts are not paid in this study to address the reason for the above differences in the ocean, yet the potential influence of the presence of the warm SST anomalies in the eastern North Pacific on the atmosphere are briefly discussed in Chapter 5.

2.5.4 Ocean-Atmosphere Relation

Now that the general agreement as well as the discrepancies between the observed and simulated fundamental ocean-atmosphere variabilities have been discussed, it is of interest how the ocean-atmosphere relation differs. Fig. 2.16, which is the KCM counterpart of Fig. 2.7, shows the lagged cross-correlation between the leading PC of North Pacific SLP and the PDO^* index. While it is true that the two figures are similar in general, in the model the an-

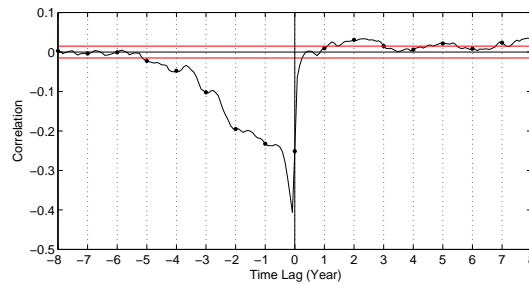


Fig. 2.16: (KCM) Cross-correlation between the leading PC of North Pacific SLP and the PDO* index. Positive lag means the PDO* index leads. The PCs and correlations are based on monthly data. Only the first 100 years of monthly temperature anomalies are used for the sake of computational efficiency. Time lags being multiples of 12 months are denoted by dots. The 95% significance level is shown by the red horizontal lines.

nually recurring significant correlations at positive lags are missing, which were attributed to the fast atmospheric response to reemergent anomalous SSTs in Section 2.4.4. SLP regressions on the PDO* index supply further confirmation to the correlation results, as illustrated in Fig. 2.17. The instantaneous regression pattern is again in general accordance with the observed version (Fig. 2.8) except for the slight northeastwards shift, the somewhat higher amplitude, and the smaller percentage of explained variance. Regressions when SST leads by one or more years, nevertheless, contrast sharply with observational results, exhibiting barely any signal. Therefore it is concluded that KCM does not simulate the observed atmospheric response to reemergent SST anomalies.

Lastly, the surface turbulent heat flux regression patterns depicted by Fig. 2.18 invariably show a small center of highly significant downward heat flux co-located with the maximum cold SST anomaly off Hokkaido. These results indicate a thermal damping, or a negative feedback, of the anomalous SSTs. This negative feedback center is actually rather strong, with the magnitude of the damping rate (defined as heat flux divided by SST anomalies) comparable to the maximum climatological value ($28 \text{ W m}^{-2} \text{ K}^{-1}$) over the entire North Pacific (Park and Latif, 2005). Over other parts of the basin the heat flux-SST feedback is vastly negative, yet patches of positive feedback are also found over some areas. The negative feedback is in general accordance with Frankignoul et al. (2004) and Wen et al. (2013), but here it is more spatially confined to the Kuroshio Extension region.

When trying to interpret the model results, the same two-step picture suggested by the observational analyses is assumed: the ocean imposes PDO*-associated boundary conditions to the overlying atmosphere on a yearly basis through reemergence, and the atmospheric large-scale circulation responds instantly. Such a response, however, does not seem to be

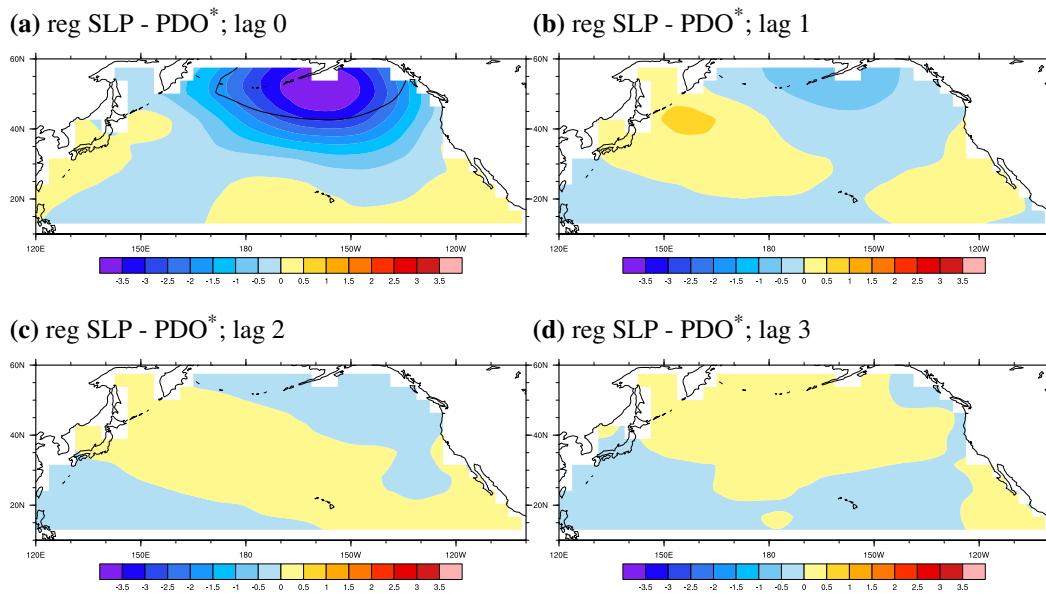


Fig. 2.17: (KCM) Regression coefficients (shading) of North Pacific winter SLP [hPa] on to the PDO* Index when the index leads the SLP by (a) 0, (b) 1, (c) 2, (d) 3 year(s). Contours indicate the ratio of variance explained by regression. Contour interval is 0.1.

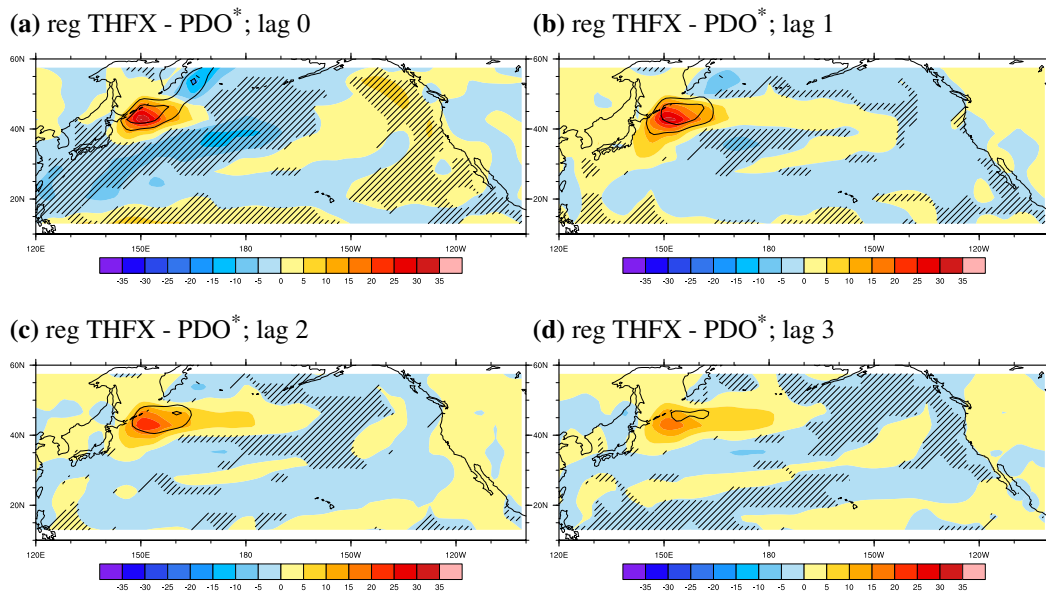


Fig. 2.18: (KCM) Regression coefficients (shading) of North Pacific winter THFX [W m^{-2}] on to the PDO* Index when the index leads the THFX by (a) 0, (b) 1, (c) 2, (d) 3 year(s). Turbulent heat flux is defined as the sum of sensible and latent heat fluxes. Contours indicate the ratio of variance explained by regression. Contour interval is 0.1. Hatching denotes area with positive SST-heat flux feedback.

detectable in the model, even though reemergence is actually stronger and more persistent. Possible reasons are discussed in the next section.

2.6 Summary and Discussions

In this chapter, statistical analyses were conducted on both observational data and a coupled model integration using the Kiel Climate Model (KCM), in order to examine the fundamental elements of atmospheric and oceanic variability as well as their relationship. It has been shown that in both observations and the KCM, the primary mode of North Pacific sea surface temperature (SST) variability is associated with the PDO which consists of significant interannual, bi-decadal and penta-decadal components. After removing tropical influences by linear regression, the leading mode of North Pacific SST variability is denoted the “PDO*” mode whose interannual spectral components are substantially suppressed. It is also found that the variability of Aleutian Low explains much of the atmospheric variance in terms of sea level pressure (SLP), comprising significant spectral components at similar frequencies as SST. This gives a hint to potential relations between the ocean and the atmosphere. An important phenomenon, the reemergence mechanism, is then presented by showing the annual reappearance of anomalous wintertime SSTs emanated from the previous years. Although reemergence is found both in observations and in the model, the warm SST anomalies in the eastern North Pacific do not exhibit annual recurrence in the model. Lead-lag correlations between the PDO* index and the leading mode of observed SLP in the extratropical North Pacific repeatedly show significant correlations when the SST leads the SLP by one or more winters. It is then proposed that due to the fast adjustment nature of the atmosphere, the high correlations at such long lags are indicative of an instantaneous atmospheric response to the reemergent anomalous SSTs. Further regression analyses show that the atmospheric response is rather large-scale with a spatial pattern resembling the atmospheric internal variability, i.e. the Aleutian Low. These results are in general agreement with literature studies. However, no response is found in the KCM simulation.

The reason for the failure of KCM to simulate an ocean-atmosphere relationship that agrees with the observations, from the author’s perspective, may stem from the insufficient model resolution and the absence of reemergent SST anomalies in the eastern North Pacific. First of all, since the atmospheric response virtually represents a modification of the Aleutian Low, which is essentially a mean flow statistic of the individual atmospheric storm systems, i.e. eddies, that propagate across the North Pacific along the storm track (e.g., [Rodionov et al., 2007](#)). Thus atmospheric eddy dynamics must be crucial in the response, an argu-

ment proven by many model studies (see, e.g., [Kushnir et al., 2002](#)) and also suggested by observational studies ([Zhao and Li, 2012a](#)). The typical spatial scale of midlatitude atmospheric storms is $O(1000 \text{ km})$ ([Chang et al., 2002](#)), while the model resolution of the KCM integration (T31, $\sim 3.75^\circ$) equals to roughly 300 km at midlatitude. Although already eddy-permitting, such a relatively coarse resolution is not expected to adequately resolve eddy dynamics and hence the atmospheric mean flow response. Horizontal model resolution has yet another role to play. It has been suggested by previous observational and model studies that the sharp midlatitude oceanic fronts associated with western boundary currents are important in generating and anchoring the atmospheric storm track and are thus crucial in simulating a realistic atmospheric basic state ([Nakamura et al., 2008, 2004](#); [Ogawa et al., 2012](#); [Taguchi et al., 2009](#)). The typical spatial scale of these sharp fronts are as small as $1^\circ\text{--}2^\circ$ ([Chen, 2008](#); [Qiu and Chen, 2005](#)), which is beyond the ability of a T31 grid to resolve. In both senses the horizontal resolution employed by the KCM simulation appears overly crude, and a finer model resolution is desirable. Furthermore, for an unknown reason the positive SST anomalies surrounding the cold band do not reemerge in the model, which might well be responsible for the absence of the observed ocean-atmosphere relation, if the positive SST anomalies are important in driving an instantaneous atmospheric response. This, however, cannot be easily tackled by analyzing observational data or coupled model simulations but requires properly designed numerical experiments. In Chapter 5 the roles of the model resolution and the eastern North Pacific positive SST anomalies are discussed by means of forced atmospheric general circulation model (AGCM) experiments.

Statistical analyses have been employed in this chapter to investigate the linkage between the ocean and the atmosphere in observational data and a coupled model simulation. However, since in these coupled climate systems the two directions of mutual interaction are already tangled up, it is always challenging to separate the forcing and the response. The statistical approaches used here and by previous studies are subject to statistical and dynamical constraints, sampling errors, as well as the skill of removing external forcing such as the El Niño/Southern Oscillation. It is also impossible to examine the effects of a single factor while suppressing those of others. To that end, dedicated AGCM experiments forced by systematically designed SST anomalies, whose results indisputably represent the atmospheric response to the prescribed SST anomalies, are conducted and presented in the succeeding chapters.

Chapter 3

Atmospheric Response to the North Pacific Enabled by Daily Sea Surface Temperature Variability¹

Abstract

Ocean-atmosphere interactions play a key role in climate variability on a wide range of timescales from seasonal to decadal and longer. The extratropical oceans are thought to exert noticeable feedbacks on the atmosphere especially on decadal and longer timescales, yet the large-scale atmospheric response to anomalous extratropical sea surface temperature (SST) is still under debate. Here we show, by means of dedicated high-resolution atmospheric model experiments, that sufficient daily variability in the extratropical background SST needs to be resolved to force a statistically significant large-scale atmospheric response to decadal North Pacific SST anomalies associated with the Pacific Decadal Oscillation, which is consistent with observations. The large-scale response is mediated by atmospheric eddies. This implies that daily extratropical SST fluctuations must be simulated by the ocean components and resolved by the atmospheric components of coupled ocean-atmospheric general circulation models to enable realistic simulation of decadal North Pacific sector climate variability.

¹Reformatted based on [Zhou et al. \(2015\)](#)

3.1 Introduction

The North Pacific exhibits sea surface temperature (SST) variability on a variety of timescales. An example is the Pacific Decadal Oscillation (PDO), the leading mode of North Pacific SST variability, which strongly impacts the land surface climate around and ecosystems in the North Pacific (Deser et al., 2004; Mantua et al., 1997). Atmospheric forcing and a number of oceanic processes such as the reemergence mechanism (Alexander et al., 1999) have been proposed as influences on the North Pacific SST. Independent of their origin, changes in SST alter the lower boundary condition for the atmosphere and have the potential to drive large-scale atmospheric circulation changes (Czaja and Frankignoul, 2002; Rodwell and Folland, 2002). Whereas the atmospheric response to equatorial Pacific SST anomalies is well understood, that to midlatitude SST anomalies is still highly controversial (Kushnir et al., 2002; Peng and Whitaker, 1999). Disentangling the extratropical ocean's impact on the atmosphere using observations is difficult due to the fact that any observable ocean-atmospheric state is the final product of the mutual interaction between the atmosphere and the ocean and that the methods employed are subject to statistical and dynamical constraints. Until now, many observational (Frankignoul and Sennéchaël, 2007; Liu et al., 2006, 2012b; Wen et al., 2010), theoretical (e.g., Frankignoul, 1985), forced atmospheric general circulation model (AGCM) (Kushnir and Held, 1996; Latif and Barnett, 1994; Liu and Wu, 2004; Palmer and Sun, 1985; Peng et al., 1997), and coupled climate model (Kwon and Deser, 2007; Lee et al., 2008; Liu et al., 2007; Liu and Wu, 2004; Saravanan, 1998; Zhong and Liu, 2008) studies presented complex and sometimes controversial results regarding the vertical structure and sign of the atmospheric response to midlatitude SST anomalies. Nevertheless, a shallow (baroclinic) linear response and a deep (barotropic) response driven by atmospheric eddies are commonly suggested (Kushnir et al., 2002).

Although the feedback by baroclinic eddies has been recognized as being important in shaping the atmospheric response to extratropical SST anomalies (Kushnir et al., 2002; Peng and Whitaker, 1999; Ting and Peng, 1995), the sensitivity to potential factors affecting the generation and evolution of atmospheric eddies has been poorly understood. Recent studies suggest that the presence and variability of sharp SST fronts associated with the Gulf Stream and Kuroshio/Oyashio extensions are important factors influencing the storm track and thus for large-scale air-sea interactions (Kelly et al., 2010; Kwon et al., 2010; Minobe et al., 2008; Nakamura et al., 2004; Ogawa et al., 2012; Small et al., 2014; Smirnov et al., 2015; Taguchi et al., 2009). Small-scale ocean surface structures such as ocean mesoscale eddies can impact the atmospheric boundary layer (Frenger et al., 2013), yet whether the influence extends to the large-scale atmospheric circulation outside the boundary layer remains unclear. Here

by means of statistical analyses and dedicated numerical experiments, we investigate the impact of daily variability in the extratropical background SST on the large-scale atmospheric response to PDO-like extratropical SST anomalies.

This paper is organized as follows: observational evidence of a midlatitude atmospheric response to a North Pacific SST anomaly is presented in Section 3.2. The experimental setup is described in Section 3.3. Section 3.4 addresses the characteristics of the response. In Section 3.6, the importance of daily SST variability for the response is demonstrated by discussing a number of sensitivity experiments. Summary and discussion are given in section 6.

3.2 Observational Evidence

The nature of air-sea interactions over the North Pacific is studied first by analyzing observed wintertime (December–February, DJF) SST and sea level pressure (SLP) anomalies using the Extended Reconstruction SST version 2 product (Smith et al., 2008) and the Extended Reconstruction SLP (Smith and Reynolds, 2004) data both covering 1909–1997. After linear detrending locally, regression patterns were computed with respect to an “El Niño/Southern Oscillation (ENSO)-removed” PDO index. The index has been obtained from empirical orthogonal function (EOF) analysis of winter mean North Pacific SST anomalies (120°E–80°W, 20°N–60°N) and is defined as the principal component of the leading EOF. ENSO (Philander, 1989) effects on the PDO index were strongly damped by previously removing SST variability associated with the leading two EOFs of tropical Pacific SST anomalies (120°E–80°W, 30°S–20°N).

The resulting SST anomaly pattern (positive phase shown by Fig. 3.1a) is very similar to the PDO pattern, i.e., the leading EOF, with a band of cold SST anomalies along the Kuroshio/Oyashio Extension that is surrounded by warm SST anomalies. When the regression analysis is repeated with a time lag of 1 year, the cold SST anomaly reappears with reduced size and strength (Fig. 3.1c). The SLP anomaly pattern associated with the PDO index at lag 0 depicts anomalously low pressure over the Aleutian Low region downstream and slightly to the north of the cold SST anomaly (Fig. 3.1b), which also persists into the next winter but with weaker amplitude (Fig. 3.1d). These features are statistically significant at the 99% level. Our results also suggest multiyear persistence of the SST and SLP anomalies (Figs. 3.S1 and 3.S2 in Section 3.A). The persistence of SST can be explained by the thermal inertia of the ocean mixed layer and by the reemergence mechanism (Alexander et al., 1999; Czaja and Frankignoul, 1999, 2002), in which the temperature perturbations are

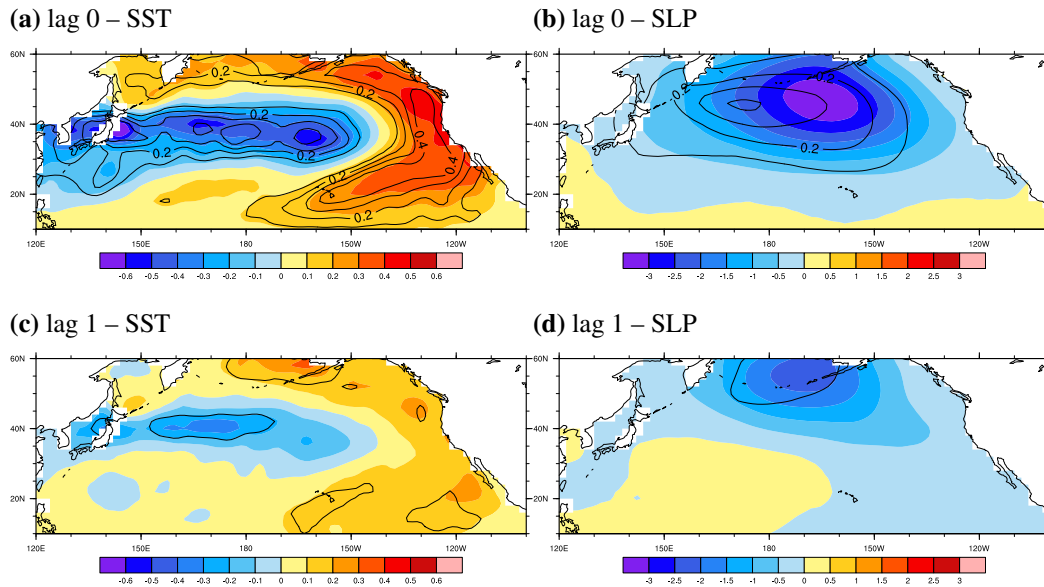


Fig. 3.1: Regression patterns of (a, c) observed SST [$^{\circ}\text{C}$], (b, d) SLP [hPa] anomalies on the ENSO-removed PDO index. Figs. 3.1a and 3.1b show simultaneous regressions (lag 0). Figs. 3.1c and 3.1d show regressions when the PDO index leads by one year (lag 1 year). Long-term linear trends are removed before computing regression. Color shading indicates the amplitudes (regression coefficients), while contours show the explained variances (contour interval 0.1). According to an F test, the 0.1 contour in Figs. 3.1b and 3.1d is significant at the 99% significance level.

stored in the deep oceanic mixed layer and brought up to the surface repeatedly for several winters by wind mixing. Bearing in mind the exclusion of most ENSO forcing and the short atmospheric adjustment time (Ferreira and Frankignoul, 2005), the long persistence of the linkage between SLP and SST presumably stems from the persistence of SST (Kushnir et al., 2002). This view is in general accordance with Frankignoul et al. (1998), Frankignoul and Sennéchael (2007), and the temporal “oceanic bridge” proposed by Rodwell and Folland (2002) except that our results the oceanic bridge acts for multiple years rather than months. Our findings agree well with the recent observational and modeling studies of, e.g., Liu et al. (2007), Wen et al. (2010), and Liu et al. (2012b).

3.3 Experimental Design

In order to investigate the dynamics of the atmospheric response to North Pacific SST variability, the European Centre/Hamburg version 5 atmospheric general circulation model (Roeckner et al., 2003) was integrated on a T213 ($\sim 0.56^{\circ}$ grid with 31 levels up to 10 hPa.

The daily observational data set NOAA-OI-SST Reynolds et al. (2007) covering 1981–2010 is used to derive the SST anomaly patterns in the North Pacific used to force the model. To do so, the multiyear time series of SST averaged over each respective calendar month are regressed against the ENSO-removed wintertime PDO index using the same data set, producing 12 anomaly patterns. We then position the 12 patterns at the middle of each month and linearly interpolate the time series to create a daily time series. Fig. 3.S3 shows the winter mean pattern of the daily varying SST anomaly. This daily SST anomaly time series was superimposed, with both positive and negative polarity, onto the observed high-resolution daily SST and used to drive the model. The model was integrated for each of the 10 winters during 1981–1990, where each experiment starts from a different 1 November initial condition taken 1 year apart from a continuous run forced by daily observed SST during 1981–1990. The background SST variability is substantial and associated with both small-scale perturbations which affect the structure of oceanic fronts and significant inter-annual variability. Thus, our configuration using observed daily SST considerably differs in comparison to previous studies where SST anomalies have been added to the monthly SST climatology (e.g., Ting and Peng, 1995). We name the ensemble of the 10 winter runs “DAGL” (meaning daily globally) and depict the atmospheric response in terms of the 10 year mean winter differences between cases with positive and negative SST forcing polarity. Vertical sections show zonal means across the North Pacific (120°E–100°W). Statistical significance of the 10 year mean differences is assessed by a one-sample *t* test using 9 degrees of freedom. Storm track is defined as the standard deviation of band-pass (2–8 days) filtered geopotential heights.

Four sensitivity experiments with the same SST anomalies as above are conducted for the 10 winters during 1981–1990 to investigate the importance of background SST variability. We first compute the daily SST climatology for the period 1981–1990, which basically eliminates variability superimposing the annual cycle as well as small-scale spatial variability (Figs. 3.S4–3.S6). In the first sensitivity experiment (DANP), the daily climatological SST is used as background SST outside the North Pacific, while the SST is unchanged over the North Pacific. A 10° linear transition zone (10°N–20°N) is applied to the southern boundary of the North Pacific to ensure smooth merging of the two background SSTs. In the second experiment (CLIM), daily climatological SST is used everywhere over the global oceans. In the third experiment (FILT), the same setup is used as that in DANP except that an 11 day running average is applied to the background SST over the North Pacific. For the fourth sensitivity experiment (HFCL), we extract from the winter 1984/1985 the high-frequency component of North Pacific SST by deducting the 11 day running averaged SST from the original data and add it to the daily SST climatology. The winter of 1984/1985 has the

largest daily SST standard deviation of all 10 winters. This setup eliminates the interannual variability from the background SST while keeping the high-frequency daily variability and also strongly damps small-scale SST structures (Figs. 3.S4 and 3.S6).

3.4 Response Characteristics

A statistically significant reduction in SLP is simulated over the North Pacific in DAGL (Fig. 3.2a), which is generally consistent with observations (Figs. 3.1b and 3.1d) in that large parts of the North Pacific north of 40°N depict lower pressure; regional details, however, differ. The anomalously low pressure at sea level is the surface expression of an equivalent barotropic response centered at around 250 hPa over the latitude belt 35°N–50°N (Figs. 3.2b and 3.3a). Zonal velocity at 500 hPa depicts a positive anomaly across the North Pacific which is strongest near 150°W and 30°N (Fig. 3.2c), suggesting an eastward extension of the jet stream. Our model results agree with previous observational (e.g., Liu et al., 2012b; Wen et al., 2010) and modeling (e.g., Latif and Barnett, 1994, 1996; Liu and Wu, 2004) studies with regard to the pressure response. However, the surface latent heat flux response (Fig. 3.2d) differs from many previous modeling and observational studies (e.g., Frankignoul and Kestenare, 2002; Okajima et al., 2014) in that over the western half of the North Pacific, there is no clear damping of the SST anomalies. This discrepancy must be attributed to the inclusion of daily background SST in this study, as discussed below.

Two types of model response to midlatitude SST anomalies have been noted in the literature, a shallow linear response and a deep response supported by eddy fluxes (Kushnir et al., 2002). The former has been shown to act at the very initial stage of the response (Ferreira and Frankignoul, 2005), while the latter dominantly operates in our high-resolution model. In particular, the mean flow response over the eastern North Pacific is associated with a significant northeast-southwest shift in the storm track (Fig. 3.2e). This change results from the anomalous baroclinic deformation caused by the increased zonal velocity gradient (Chang et al., 2002) and also contributes to the mean flow response. According to the quasi-geostrophic vorticity equation (Hoskins, 1983), the eddy vorticity flux convergence in the upper troposphere near 40°N (Fig. 3.3b) is partly balanced by divergence of the mean flow, resulting in ascending motion at low and middle levels (Figs. 3.2f and 3.3c) and near-surface convergence. Convergence of eddy-induced zonal momentum flux (Fig. 3.3d), on the other hand, directly accelerates the zonal flow aloft (Fig. 3.3e). All these features are statistically significant at the 90% level.

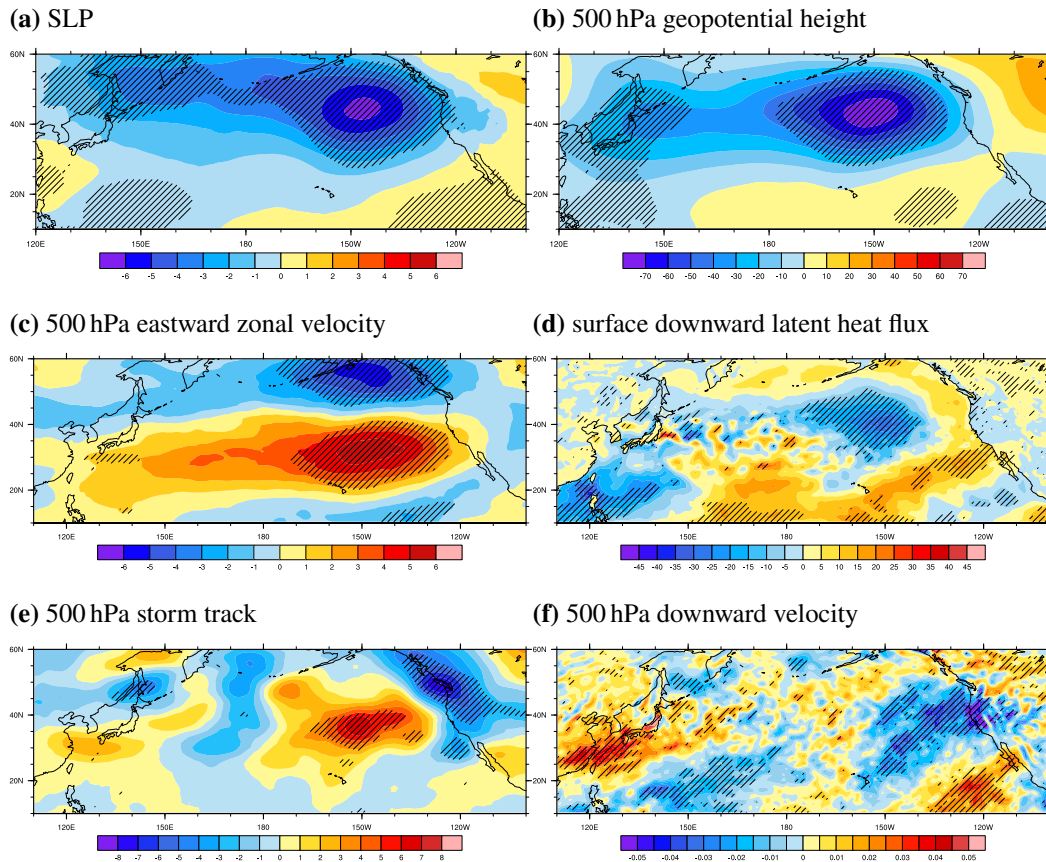


Fig. 3.2: Ten year mean winter (DJF) response of (a) sea level pressure [hPa], (b) 500 hPa geopotential height [m], (c) 500 hPa eastward zonal velocity [m s^{-1}], (d) surface latent heat flux (downward positive) [W m^{-2}], (e) 500 hPa storm track defined as the standard deviation of band-pass (2–8 days) filtered geopotential heights [m], (f) vertical velocity (downward positive) [Pa s^{-1}] simulated by the experiment DAGL. Statistical significance at the 90% level is indicated by hatching.

3.5 Importance of Daily SST Variability

Our experimental setup preserves both spatially small scale and temporally high frequency SST fluctuations and thus resolves local and transient variations in SST. To further investigate the impact of background SST variability on the atmospheric response, we performed a number of sensitivity experiments. In DANP in which daily SST variability is restricted to the North Pacific, the response is similar to that discussed above (Fig. 3.3a) in that there is a reduction in geopotential height of similar amplitude throughout the troposphere over the midlatitude North Pacific (Fig. 3.4a). No statistically significant response is simulated in CLIM in which climatological SST is used everywhere (Fig. 3.4b). These experiments demonstrate that variability in the background SST other than the seasonally varying clima-

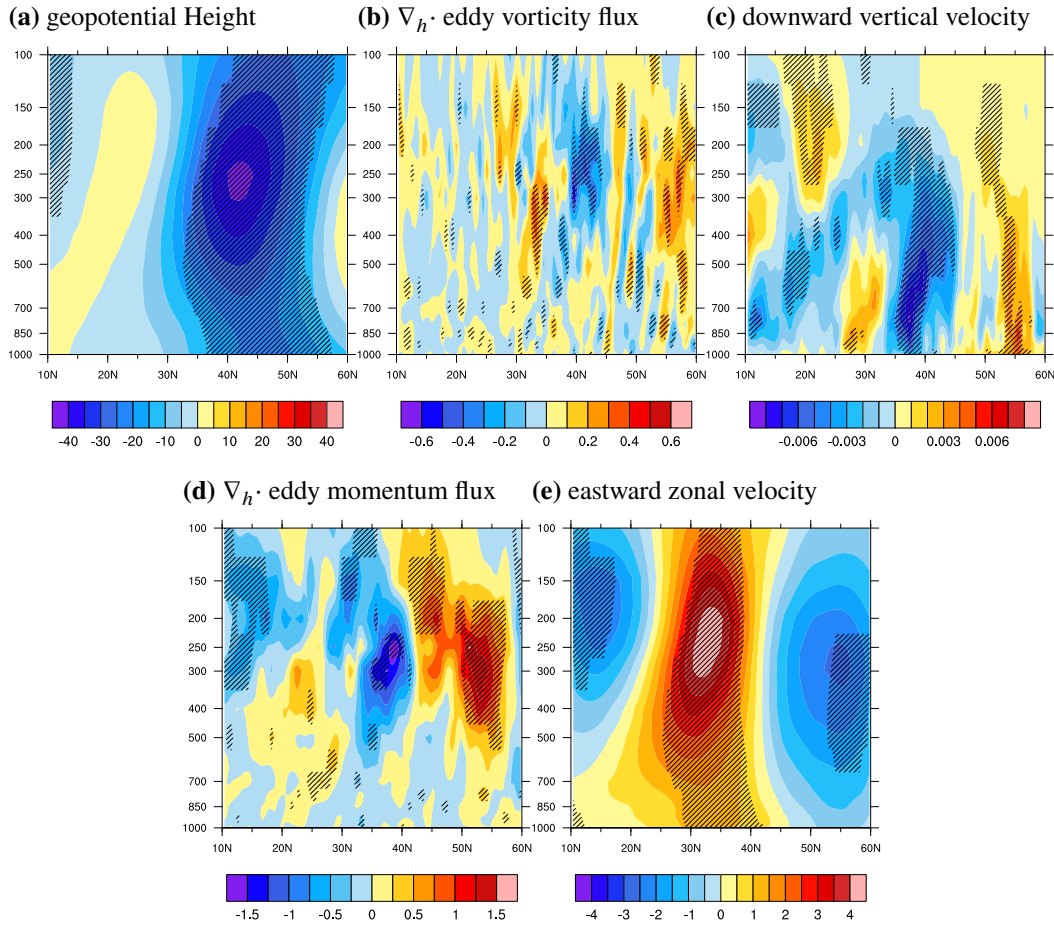


Fig. 3.3: Vertical sections of the 10 year mean winter (DJF) response simulated by the experiment DAGL, zonally averaged over the Pacific sector for (a) geopotential height [m], (b) divergence of eddy vorticity flux [d^{-2}], (c) downward vertical velocity [Pa s^{-1}], (d) divergence of eddy momentum flux [$\text{m s}^{-1} \text{d}^{-1}$], (e) zonal wind velocity [m s^{-1}]. Statistical significance at the 90% level is indicated by hatching.

tology in the region where the SST anomalies are superimposed is essential to drive a significant large-scale response. The FILT experiment fails to reproduce a statistically significant response (Fig. 3.4c), indicating sufficiently strong daily variability in the background North Pacific SST is crucial in establishing the response in DAGL. The HFCL experiment, which eliminates the effects of interannual variability, yields a very similar response (Fig. 3.4d) to that shown in Fig. 3.3a. Thus, our results suggest that retaining interannual variability in the background SST is of minor importance to the large-scale atmospheric response. Previous studies have used rather strong SST anomalies (Kushnir et al., 2002; Liu and Wu, 2004; Peng and Robinson, 2001; Peng et al., 1997). We employed SST anomalies of realistic strength to drive the model. This too may suggest that daily SST variability in the background SST is

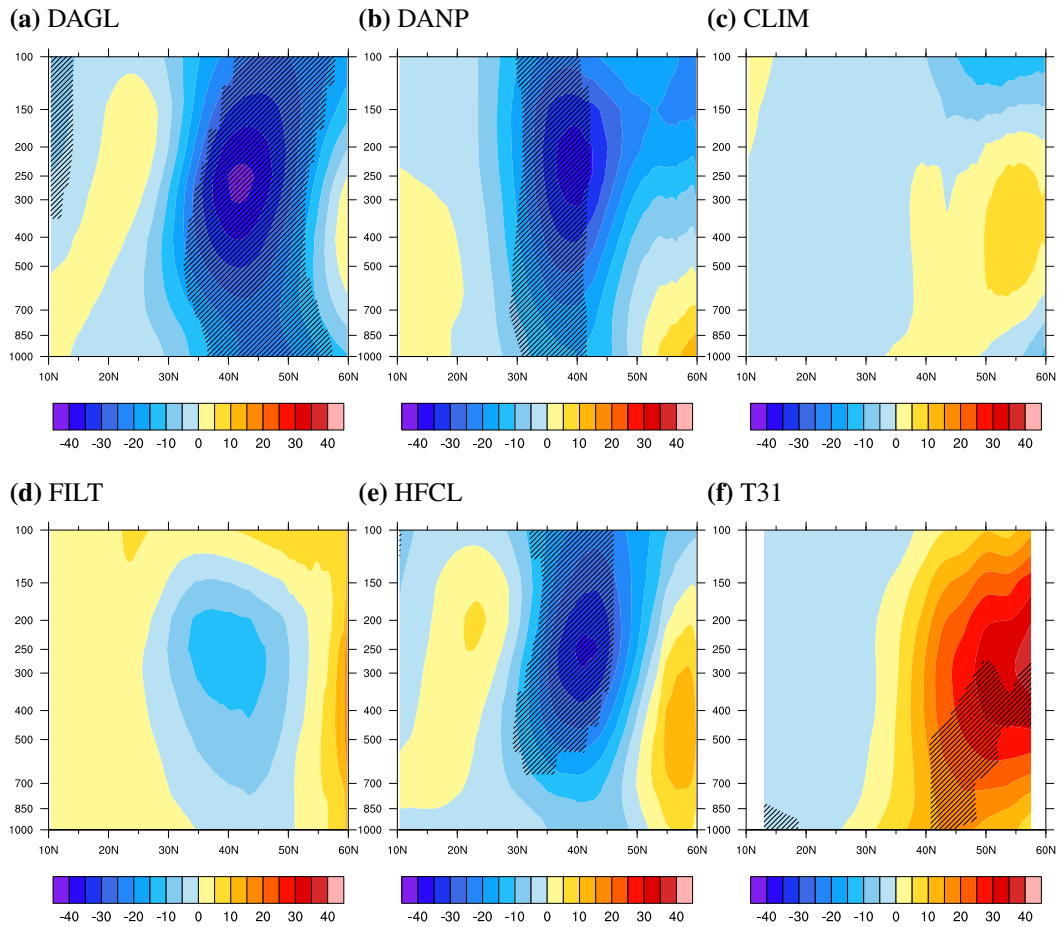


Fig. 3.4: Vertical sections of the 10 year mean winter (DJF) response zonally averaged over the Pacific sector for geopotential height [m] simulated in the experiments (a) DAGL, (b) DANP, (c) CLIM, (d) FILT, (e) HFCL, (f) the T31-experiment. Statistical significance at the 90% level is indicated by hatching.

important for driving a large-scale atmospheric circulation response to midlatitudinal SST anomalies, as it can enhance the atmospheric response to an extent that would otherwise only be achieved by a much stronger SST anomaly.

The reason why daily SST variability is so important in the background SST, on which the SST anomaly is superimposed, remains unclear to us. As the atmospheric response itself is maintained by baroclinic eddies, a plausible pathway is through the modulation of the atmospheric storm track. The storm track response exhibits a common pattern over the eastern North Pacific in all experiments (Figs. 3.2d and 3.57). However, the response in FILT and CLIM is reduced compared to that in DAGL, DANP, and HFCL (Fig. 3.5). One may assume that sharp local SST gradients are one energy source for midlatitudinal storms and that the probability of occurrence of such gradients is enhanced when the background

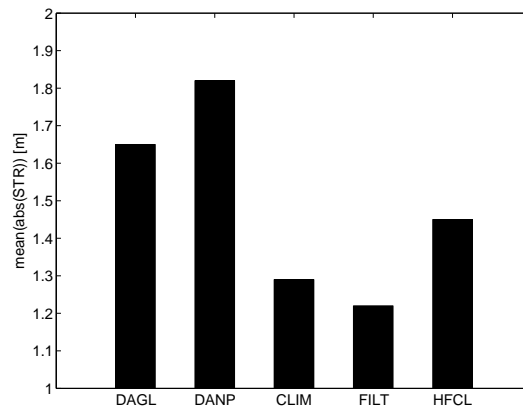


Fig. 3.5: Bar chart showing the mean absolute value of the storm track [m] response at 500 hPa spatially averaged over the eastern North Pacific (180°E – 100°W , 10°N – 60°N). Storm track is defined as the standard deviation of band-pass (2–8 days) filtered geopotential heights.

SST varies on daily timescales. However, the corresponding probabilities are inconclusive (Fig. 3.S8b), indicating that other energizing factors should also be considered.

We computed the Eady growth rate (Fig. 3.S9a, computed over the region of the cold SST anomaly in the western half of the basin and following Hoskins and Valdes (1990)). The Eady growth rate is an indicator of baroclinicity. In the experiments with daily background SST variability (DAGL, DANP, and HFCL), the Eady growth rate response is generally positive, while in the other two experiments (CLIM and FILT), it is basically negative. Moreover, the patterns of surface latent heat flux (Figs. 3.2d and 3.S10) also differ markedly between the experiments with and without daily background SST variability: in CLIM and FILT, the response tends to damp the SST anomaly over the western North Pacific, while in the others the picture is less clear. Due to the atmospheric heat loss in CLIM and FILT, the lower atmosphere is more stably stratified (Fig. 3.S9b), which tends to reduce the Eady growth rate (Fig. 3.S9a) and thus weakens the storm track downstream (Fig. 3.S7). The effect of the vertical wind shear is negligible (Fig. 3.S9c). Finally, eddy heat flux convergence in the critical height range of 900 hPa–700 hPa is found in DAGL, DANP, and HFCL (Fig. 3.S9d), which opposes the thermal damping of the cold SST anomaly, leading to a patchy latent heat flux pattern (Fig. 3.S10).

We note that a coarse-resolution ($T31$, $\sim 3.75^{\circ}$) version of the AGCM with exactly the same setup as DAGL does not reproduce the above results (Figs. 3.4f and 3.S10e). As the coarse-resolution model also resolves daily SST variability, its failure is likely due to its inadequate spatial resolution which inhibits realistic representation of eddy activity.

3.6 Summary and Discussion

We have shown by high-resolution atmosphere model experiments that the daily component of the background sea surface temperature (SST) variability is important in driving a statistically significant large-scale atmospheric response to Pacific Decadal Oscillation (PDO)-like SST anomalies. The mechanism is most likely through modulation of atmospheric storm activity. Daily SST fluctuations have largely been regarded as noise and were often ignored in previous modeling studies on the atmospheric response to midlatitudinal SST anomalies. Climate variability in the extratropics may be underestimated, if daily SST variability is not realistically simulated by the ocean and not resolved by the atmospheric components of climate models. Moreover, seasonal to decadal prediction (e.g., [Scaife et al., 2014](#)) may be enhanced when climate models realistically represent the effects of daily SST variability on large-scale air-sea interactions. The exact mechanism why the daily SST variability matters, however, needs further investigation.

Appendix 3.A Supplementary Figures

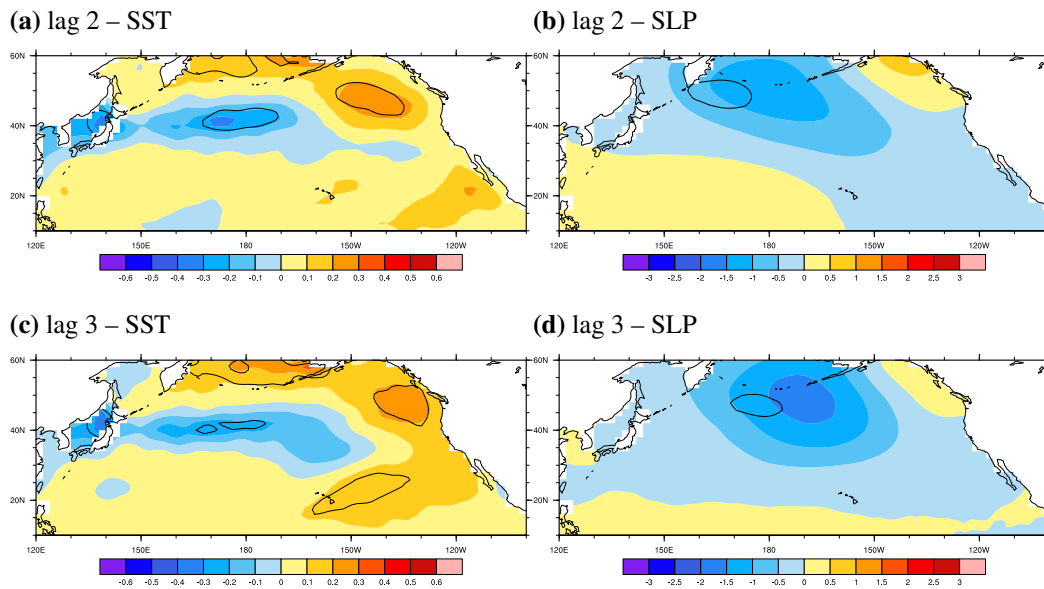


Fig. 3.S1: Same as Fig. 3.1 but for further lags at (a, b) 2, (c, d) 3 years.

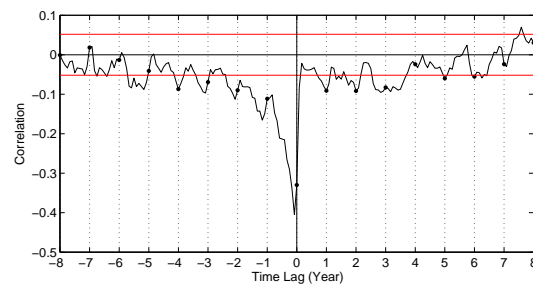


Fig. 3.S2: Cross-correlation between the leading PC of North Pacific SLP and the ENSO-removed PDO index. Positive lag means the PDO index leads. The PCs and correlations are based on monthly data. Time lags being multiples of 12 months are denoted by dots. The 95% significance level is shown by the red horizontal lines.

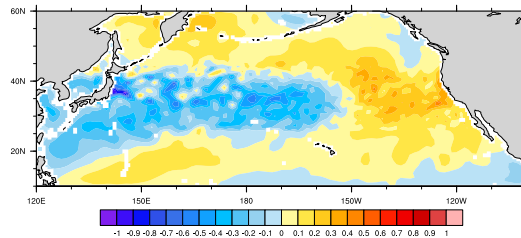


Fig. 3.S3: Positive phase of the winter (DJF) mean pattern of the daily SST anomaly forcing in the North Pacific [$^{\circ}\text{C}$]. No SST anomaly is present in other basins.

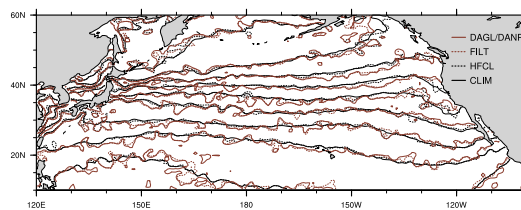


Fig. 3.S4: NOAA-OI-SST observation at 1 January, 1984 (red solid contours; DAGL/DANP), the 11-day filtered SST (red dashed contours; FILT), the “high-frequency-plus-climatological” SST (black dashed contours; HFCL), and the 1981–1990 daily climatology (black solid contours; CLIM) for the same calendar day [$^{\circ}\text{C}$].

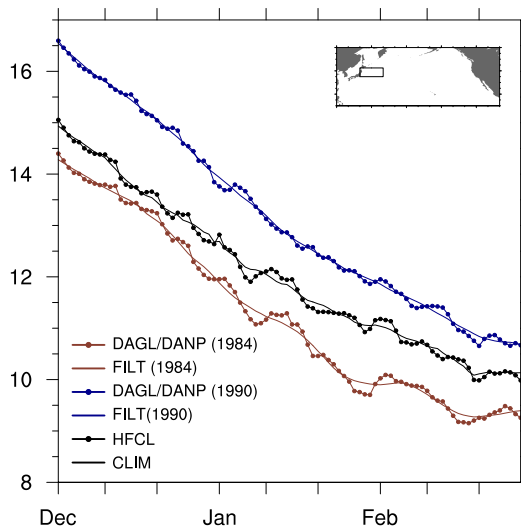


Fig. 3.S5: Time series of wintertime (DJF) SST [$^{\circ}\text{C}$] averaged over 145°E – 150°E , 35°N – 42.5°N (indicated by the box in the inset) from the NOAA-OI-SST daily observations. The red and blue dotted curves represent the 1984–85 and 1990–91 winters (DAGL/DANP) respectively, whereas the smooth red and blue curves are the 11-day running means of the same winters (FILT). The black dotted curve shows the “high-frequency-plus-climatological” SST (HFCL), and the smooth black curve is the 10-year daily climatology (CLIM).

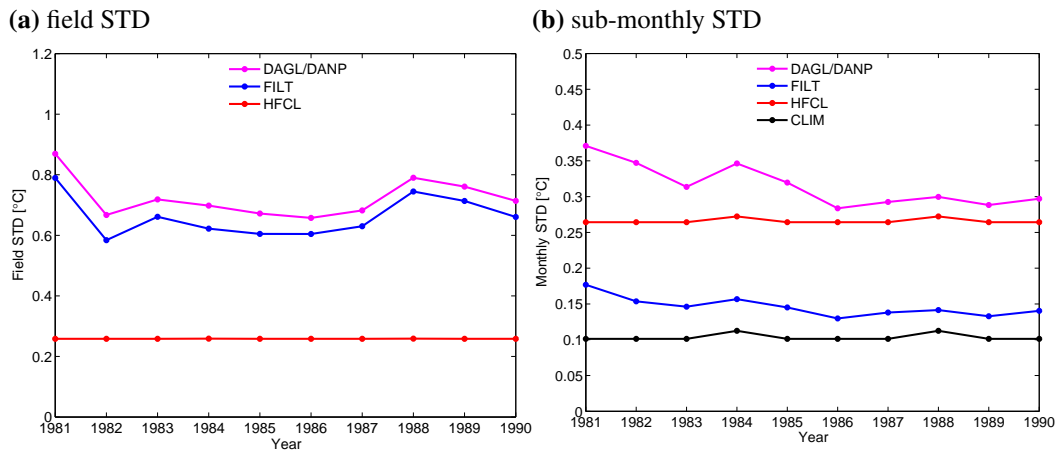


Fig. 3.S6: 10-year time series of (a) winter mean field STD [$^{\circ}\text{C}$] indicating the level of spatially small-scale variability. It is the spatial STD of SST difference from the 10-year daily climatology computed using every ocean grid point in the North Pacific (120°E – 100°W , 10°N – 60°N). (b) winter-mean sub-monthly STD [$^{\circ}\text{C}$] indicating the level of temporally high-frequency variability computed after subtracting the linear trend within each month. The variability in CLIM and HFCL is due to leap years.

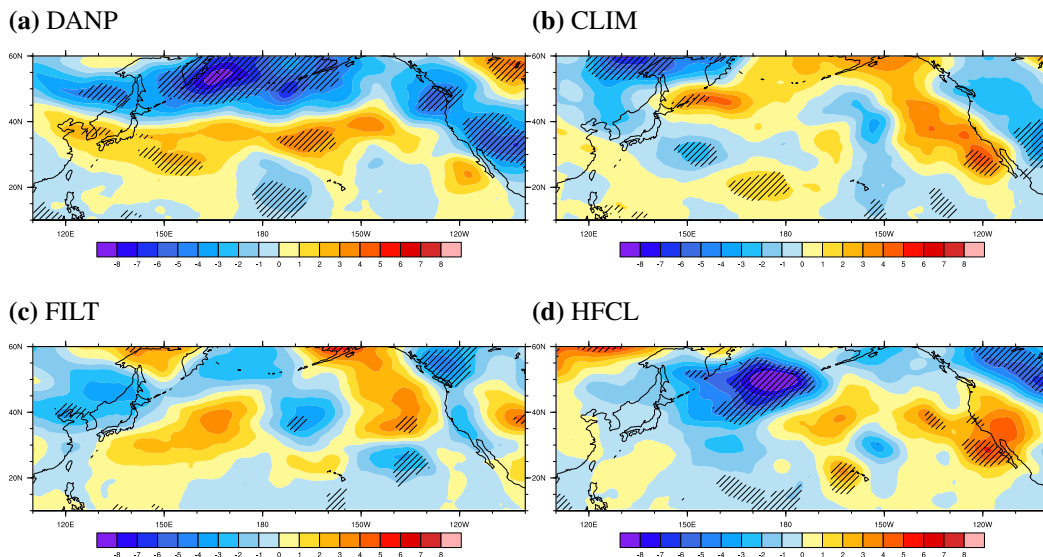


Fig. 3.S7: Ten year mean winter (DJF) storm track [m] response at 500 hPa simulated in (a) DANP, (b) CLIM, (c) FILT, (d) HFCL. Storm track is defined as the standard deviation of band-pass (2–8 days) filtered geopotential heights. Statistical significance at the 90% level is indicated by hatching.

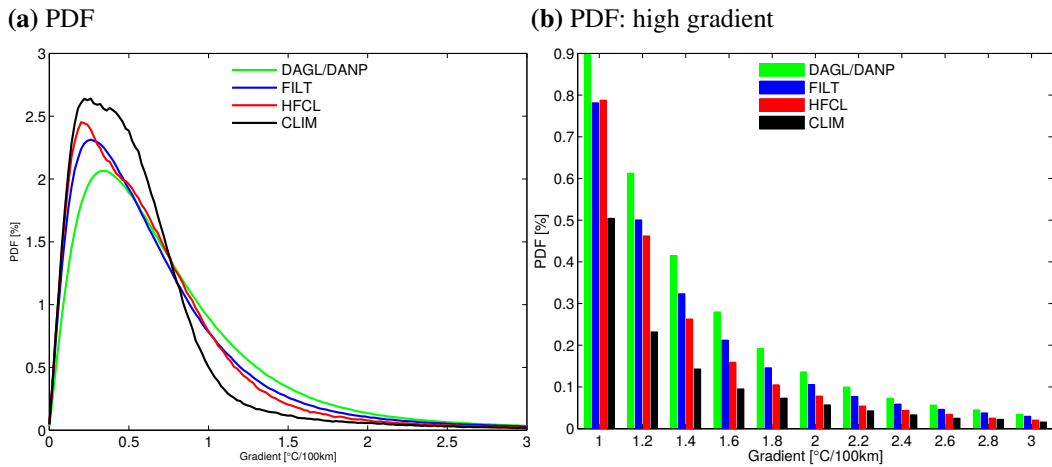


Fig. 3.S8: Probability density function (PDF) of the magnitude of 2-dimensional SST gradients over (a) the whole gradient range, (b) the high gradient range ($\geq 1 \text{ }^\circ\text{C } 100 \text{ km}^{-1}$). Note that in (b), bars within each group have the same gradient value. Gradients are computed by comparing adjacent grid points. The PDF is computed over all grid points in the North Pacific and at all time steps during the 10 winters.

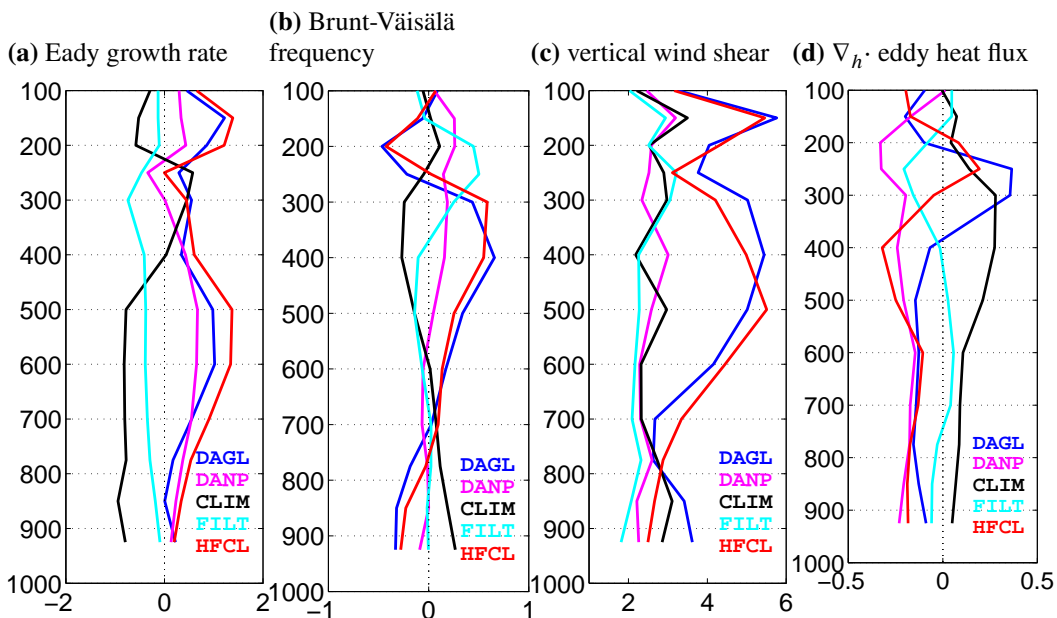


Fig. 3.S9: Vertical profiles of the 10 year mean winter (DJF) response of (a) Eady growth rate [10^6 s^{-1}], (b) Brunt-Väisälä frequency [10^3 s^{-1}], (c) vertical wind shear [10^4 s^{-1}], (d) divergence of eddy heat flux [$^\circ\text{C d}^{-1}$] averaged over the area 30°N – 40°N , 120°E – 180°E .

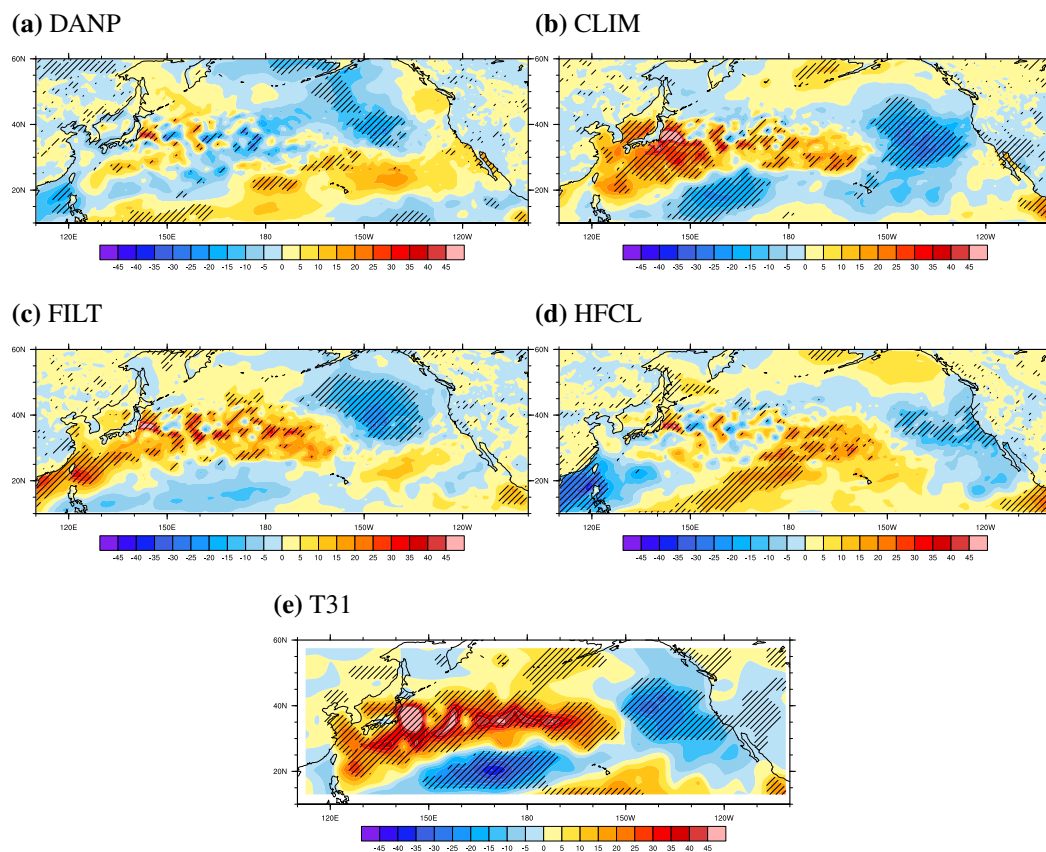


Fig. 3.S10: Ten year mean winter (DJF) surface latent heat flux [W m^{-2}] response (downward positive) simulated in (a) DANP, (b) CLIM, (c) FILT, (d) HFCL, (e) the T31-experiment. Statistical significance at the 90% level is indicated by hatching.

Chapter 4

State-Dependence of Atmospheric Response to Extratropical North Pacific SST Anomalies¹

Abstract

By performing two sets of high-resolution atmospheric general circulation model (AGCM) experiments, we find that the atmospheric response to a sea surface temperature (SST) anomaly in the extratropical North Pacific is sensitive to decadal variations of the background SST on which the SST anomaly is superimposed. The response in the first set of experiments, in which the SST anomaly is superimposed on the observed daily SSTs of 1981–1990, strongly differs from the response in the second experiment, in which the same SST anomaly is superimposed on the observed daily SSTs of 1991–2000. The atmospheric response is characterized by an equivalent barotropic, circum-global Rossby wave train which exhibits a significant decadal trend and can even reverse sign. The primary wave source switches from baroclinic eddy vorticity forcing over the eastern North Pacific in 1981–1990 to mean flow divergence over the western North Pacific in 1991–2000. The wave source changes are linked to the decadal reduction of daily SST variability over the eastern North Pacific and strengthening of the Oyashio Extension front over the western North Pacific. Thus, the daily *and* frontal aspects of the background SST variability in determining the atmospheric response to extratropical North Pacific SST anomalies are emphasized by our AGCM experiments.

¹Reformatted based on [Zhou et al. \(2016\)](#).

4.1 Introduction

It is universally believed that extratropical sea surface temperature (SST) anomalies are largely forced by the atmosphere on interannual to decadal time scales, as put forward by the pioneering work of Bjerknes (1964) and confirmed by many succeeding studies (e.g., Cayan, 1992a,b,c). On the other hand, Bjerknes (1964) also proposed that on longer time scales, the ocean significantly contributes to the extratropical SST variability, an argument supported subsequently by e.g. Deser and Blackmon (1993), Kushnir (1994), Nakamura et al. (1997), and Gulev et al. (2013). However, there is a controversy about whether extratropical SST anomalies significantly affect the large-scale atmospheric circulation, and if so, how. Unlike in the tropics where a pronounced locally-driven, thermally direct and far-reaching atmospheric response to SST changes is found, owing to deep convection (Neelin et al., 1998), the extratropical response to SST anomalies is in most cases smaller than the intrinsic atmospheric variability (Kushnir et al., 2002). Thus, more effort is required to tackle the low signal-to-noise ratio problem.

Over the last three decades or so, considerable effort has been applied to this problem by means of observational analyses (Frankignoul and Sennéchael, 2007; Liu et al., 2006, 2012a,b; Wen et al., 2010), theoretical studies (e.g., Frankignoul, 1985), forced atmospheric general circulation model experiments (Kushnir and Held, 1996; Latif and Barnett, 1994; Liu and Wu, 2004; Palmer and Sun, 1985; Peng et al., 1997) and coupled climate model simulations (Kwon and Deser, 2007; Latif and Barnett, 1994, 1996; Lee et al., 2008; Liu et al., 2007; Liu and Wu, 2004; Saravanan, 1998; Zhong and Liu, 2008). Until now the results about the atmospheric response to extratropical SST anomalies are still controversial and sometimes perplexing, yet a set of common conclusions have been widely accepted (see Kushnir et al., 2002). Among other things, the response can be modulated by baroclinic eddy feedback, and it depends on the atmospheric basic state. However, the current understanding of the state-dependence of the atmospheric response to extratropical SST anomalies is far from satisfactory. For example, the role of the background SST variability, on which an SST anomaly is superimposed, has received little attention. Observational studies have been devoted to detecting the response and describing its characteristics, whereas model experiments usually employed climatologically varying background SST, which is unrealistic given the large daily and interannual SST variability in the extratropics. Recently, Zhou et al. (2015) show that daily variability in the background SST is important for determining the atmospheric response to midlatitudinal North Pacific SST anomalies.

Here, we follow up the work of Zhou et al. (2015). We investigate the state dependence of the atmospheric response to midlatitudinal North Pacific SST anomalies by superimpos-

ing them on the observed daily SST during 1981–2000 which exhibits significant decadal variability. Section 4.2 briefly introduces the model and experimental setup, and the forcing SSTs. In Section 4.3, we examine the decadal evolution of the response. Finally, we discuss in Section 4.4 the difference in the decadal-mean response in terms of the decadal background SST changes. Summary and discussion are presented in Section 4.5.

4.2 Model, Experimental Setup, Data

We carry out a series of SST-forced simulations with the ECHAM5 atmospheric general circulation model (AGCM; Roeckner et al., 2003) on a T213 grid ($\sim 60 \text{ km} \times \sim 60 \text{ km}$) with 31 vertical levels extending up to 10 hPa, resolving only the lower part of the stratosphere. Li (2006, Table 4.3) showed that a 20-year AMIP-type (Atmospheric Model Intercomparison Project; Gates et al., 1999) run with the same model simulates the planetary wave climatology reasonably well, in some aspects even better than a high-top (0.01 hPa) version of the model.

The SST data used in this study cover the period 1981–2000 and are from the daily NOAA OI-SST dataset (Reynolds et al., 2007), and have been linearly interpolated from the original quarter-degree resolution to the T213-resolution of the AGCM. To examine the atmospheric response to large-scale decadal North Pacific SST anomalies, we first compute the Pacific Decadal Oscillation (PDO Mantua et al., 1997) index as the leading principal component (PC) of North Pacific (120°E – 100°W , 20°N – 60°N) SSTs, and reduce the ENSO signature by removing the variability associated with the leading two PCs of tropical Pacific (120°E – 100°W , 30°S – 20°N) SSTs by means of linear regression. The SSTs in each calendar month are then regressed onto the “ENSO-removed” PDO index, producing 12 patterns which are positioned at the middle of the corresponding months and then interpolated into a daily record to create an annual cycle. This record is used as the SST anomaly forcing in the AGCM simulations described below. No SST anomaly forcing is used outside the North Pacific. Fig. 4.1a depicts the SST anomaly pattern averaged over boreal winter (December–February, DJF).

In contrast to many previous studies using climatological SST as background SST, we superimpose the SST anomalies on the observed daily SSTs during 1981–2000. Our approach appears to be more realistic, as it retains significant daily and interannual variability in the background SST (Zhou et al., 2015)).

The model is integrated for each of the 20 winters (November–February) during 1981–2000, with November considered as the “spin-up” period and omitted in the subsequent

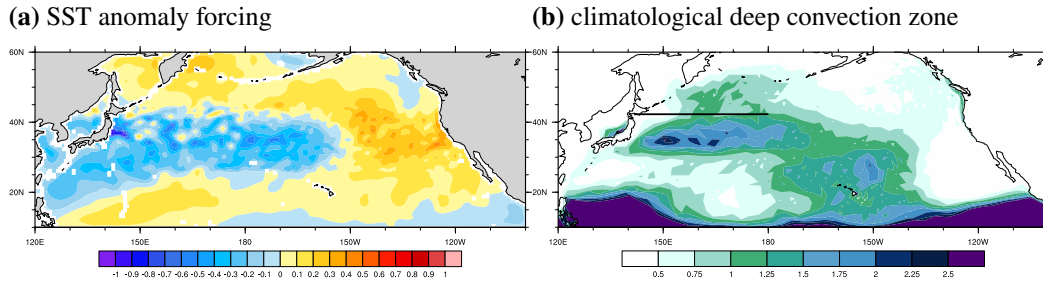


Fig. 4.1: (a) Positive phase of the winter-mean (DJF) SST anomaly forcing in the North Pacific [$^{\circ}\text{C}$]. No SST anomaly is present in other basins. (b) 1981–2000 mean winter (DJF) convective precipitation [mm d^{-1}] from the control run showing the climatological deep convection zone south the Oyashio Extension front, whose climatological mean position is indicated by the black line.

analyses. Experiments are performed with both the positive and negative polarity of the SST anomalies separately. The winter-mean (DJF) atmospheric response is then defined as the difference between the cases with positive and negative polarity. For the decade 1981–1990 (hereafter Dec8190), the model setup is exactly the same as in Zhou et al. (2015), with one integration per winter, each initialized with the 1 November conditions of the corresponding year taken from a control run forced by observed daily SSTs of 1981–2000 but with no SST anomaly applied. For the decade 1991–2000 (hereafter Dec9100), two integrations are performed for each winter, using the 1 November and 1 December conditions from the control run to initialize the integrations on 1 November. The average of the two integrations is used in the subsequent analyses.

Although the number of realizations for each winter is small, when analyzing decadal averages, the sample size is increased to 10 (20) for Dec8190 (Dec9100). The robustness of the decadal-mean Dec8190 results is further supported by additional sensitivity experiments presented in Zhou et al. (2015). Statistical significance of the decadal averages is estimated using a one-sample t test with 9 (19) degrees of freedom for Dec8190 (Dec9100). We note that for Dec9100, the results don't significantly change if only one of the two integrations is used to compute the decadal mean response. Additionally, the linear trends during 1981–2000 provide useful information about decadal variability and are also tested for statistical significance with a t test using 18 degrees of freedom. More details can be found in Section 4.A.

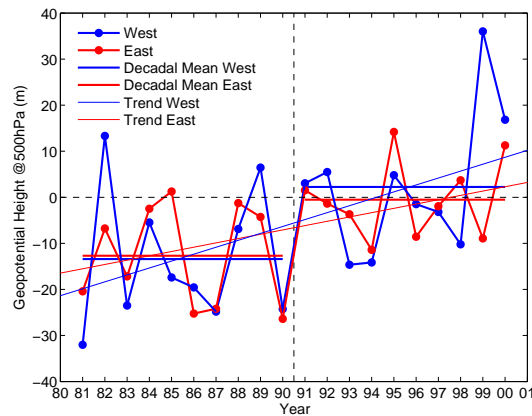


Fig. 4.2: Time series of 500 hPa geopotential height [m] responses during winter (DJF) averaged over the western (120°E – 180°E , blue dotted curves) and eastern (180°W – 100°W , red dotted curves) North Pacific (10°N – 60°N). The thick horizontal lines denote the two separate decadal means, and the thin lines are the decadal trends for the two decades. The trends for the western and eastern North Pacific are both statistically significant at the 90% level.

4.3 Response

4.3.1 Linear Trend

We examine the 500 hPa geopotential height response over the North Pacific (10°N – 60°N) in the western (120°E – 180°E , hereafter WNP) and eastern (180°W – 100°W , hereafter ENP) parts separately (Fig. 4.2), because the dynamics in the storm track entrance and exit regions are different (Chang et al., 2002). The model simulates an ascending trend which is statistically significant at the 95% level over both regions: the two decadal means are negative during Dec8190, while during Dec9100, the WNP response is positive and the ENP response wobbles around zero. This is indicative of a decadal transition between two different response regimes. In the following, the two decadal-mean responses are investigated separately to obtain further insight into the role of the background SSTs in the decadal transition.

4.3.2 Decadal-Mean Response 1981–1990

The decadal-mean air pressure response during Dec8190 (Fig. 4.3) is equivalent barotropic in the extratropics, as indicated by the sea level pressure (Fig. 4.3a) and 500 hPa geopotential height (Fig. 4.3b) responses. A significant zonal wavenumber-2 structure is simulated in the midlatitudes, with anomalously low pressure over the Pacific and Atlantic, and anomalously

high pressure over North America and Eurasia. The strongest response is found over the ENP and appears to be the origin of the wave train. Correspondingly, in the positive compared to the negative polarity case (Fig. 4.3c), the westerly jets at 500 hPa are more zonally elongated over the oceans and terminate more abruptly over the continents. Similarly, the 500 hPa storm track response exhibits a NW–SE shift over the ENP, which in turn makes the storm track more zonally confined (Fig. 4.3d). The ENP trough is associated with enhanced vertical motion at its eastern side that goes along with enhanced convective precipitation (Figs. 4.3e and 4.3f), related to the anomalous storm track. Over the WNP, the storm track response is weak and insignificant. However, a region of significantly reduced vertical motion and convective rainfall over the East China Sea, compensated by upward motion to the south, is found (Figs. 4.3e and 4.3f), which largely follows the regional SST anomaly pattern, suggesting a linear response to the SST anomaly in this region.

The response (i.e. the winter-mean difference between the two SST polarity cases) in the ENP conforms to an eddy-mediated response (Zhou et al., 2015). First, the SST forcing drives an anomalous eddy vorticity flux convergence near 40°N in the upper troposphere. This leads to enhanced vorticity, decreased geopotential height and an accelerated jet stream, consistent with the quasi-geostrophic vorticity equation (Hoskins et al., 1983). Second, the rather abrupt termination of the jet stream in the east causes increased barotropic deformation of individual propagating eddies near the storm track exit region, feeding back positively onto the storm track (Chang et al., 2002). Anomalous convergence of eddy momentum flux directly accelerates the jet. The eddy vorticity flux convergence is the primary source for changing the mean-flow vorticity and generating Rossby waves (Sardeshmukh and Hoskins, 1988) which propagate along the Rossby wave guide (Branstator, 2002; Hoskins and Ambrizzi, 1993). The strongest pressure (Figs. 4.3a and 4.3b) and vorticity (not shown) changes appear at the beginning of the wave train and not at a noticeable distance downstream of the Rossby wave source, which may be attributed to the relatively slow climatological zonal flow over the ENP (Fig. 4.3c).

Over the WNP, where the storm track response is weak and insignificant, the mechanism must be different. Although it may sound plausible that the low-pressure response over Japan is just the third trough of the eastward propagating wave train forced in the ENP region, the significant changes in vertical velocity and convective precipitation over the East China Sea and south of it (Figs. 4.3e and 4.3f) suggests another Rossby wave source: the upper level convergence over southeast China and the East China Sea driving a positive vorticity anomaly over Japan. Advection by the well-developed jet stream in this region (Fig. 4.3c) moves the vorticity and pressure response downstream of the wave source (Sardeshmukh and Hoskins, 1988).

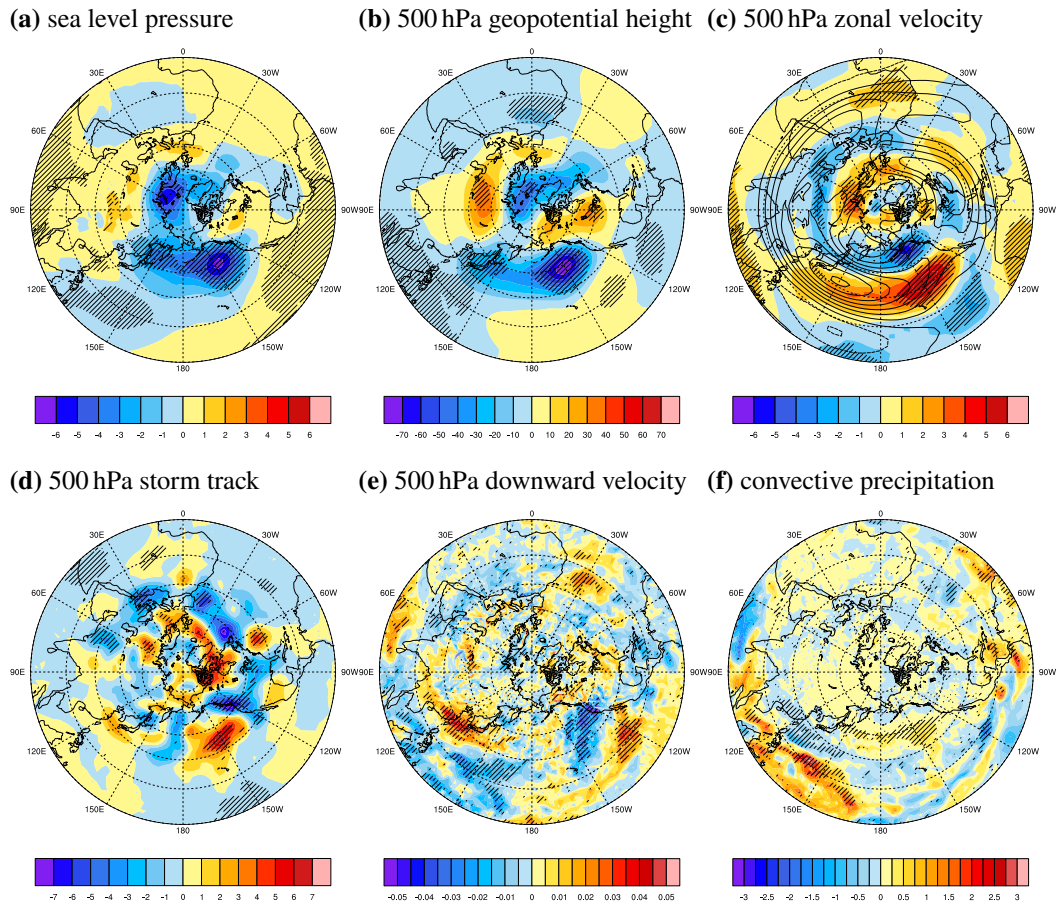


Fig. 4.3: 1981–1990 decadal-mean winter (DJF) responses of (a) sea level pressure [hPa], (b) 500 hPa geopotential height [m], (c) 500 hPa zonal wind velocity [m s^{-1}]. In (c), contours show the decadal mean zonal velocity from the negative SST anomaly polarity case, where solid and dashed contours indicate positive and negative values, and the zero contours are highlighted by bold lines. Contour interval is 5 m s^{-1} . (d) Response of winter (DJF) 500 hPa storm track [m] defined as the standard deviation of 2–8 day filtered geopotential height. (e) Winter (DJF) responses of 500 hPa downward velocity [Pa s^{-1}] and (f) convective precipitation [mm d^{-1}]. Statistical significance at the 90% level is indicated by hatching.

4.3.3 Decadal-Mean Response 1991–2000

The decadal-mean winter atmospheric response to the PDO-like SST anomaly (Fig. 4.1a) during Dec9100 is remarkably different to that in Dec8190. Particularly, the ENP low-pressure response is very weak and statistically insignificant (Figs. 4.4a and 4.4b), while the corresponding zonal velocity exhibits little change in that region (Fig. 4.4c). The storm track response over the ENP becomes much weaker (Fig. 4.4d) and is associated with reduced vertical velocity and convective precipitation anomalies (Figs. 4.4e and 4.4f). Hence

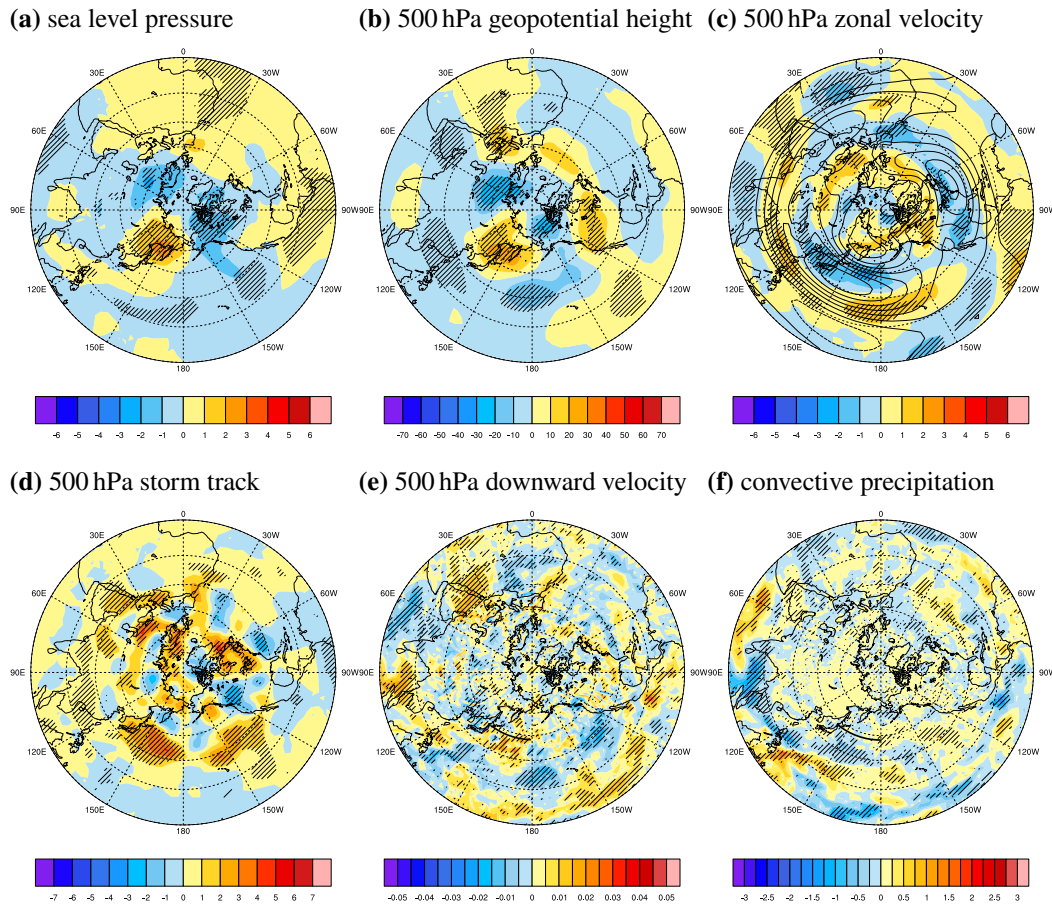


Fig. 4.4: 1991–2000 decadal-mean winter (DJF) responses of (a) sea level pressure [hPa], (b) 500 hPa geopotential height [m], (c) 500 hPa zonal wind velocity [m s^{-1}]. In (c), contours show the decadal mean zonal velocity from the negative SST anomaly polarity case, where solid and dashed contours indicate positive and negative values, and the zero contours are highlighted by bold lines. Contour interval is 5 m s^{-1} . (d) Response of winter (DJF) 500 hPa storm track [m] defined as the standard deviation of 2–8 day filtered geopotential height. (e) Winter (DJF) responses of 500 hPa downward velocity [Pa s^{-1}] and (f) convective precipitation [mm d^{-1}]. Statistical significance at the 90% level is indicated by hatching.

the ENP response in Dec9100 generally exhibits a similar pattern but much reduced amplitude in comparison to that during Dec8190.

More interestingly, the WNP low-pressure anomaly is replaced by an equivalent barotropic high-pressure anomaly which also marks the beginning of a wave train (Figs. 4.4a and 4.4b). Due to pressure adjustment, the jet stream is locally weakened over the WNP (Fig. 4.4c). Further, a significant increase of the storm track response is observed over the WNP (Fig. 4.4d). The vertical velocity and convective precipitation (Figs. 4.4e and 4.4f) both show a region of significantly reduced response on the south flank of the Oyashio Ex-

tension front (hereafter OEF; [Frankignoul et al., 2011b](#); [Smirnov et al., 2015](#)), a sharp SST front (Fig. 4.5c). Upstream, a region with downward motion over northeast China and the Japan Sea is observed.

In contrast to the dominating eddy-mediated Rossby wave source in Dec8190, the Dec9100 response over the WNP is not primarily established by eddy forcing. In particular, the increased storm track response induces only little eddy vorticity and momentum flux convergence (not shown). In looking for the potential Rossby wave source, one should keep in mind that the WNP is characterized by strong mean westerly winds (Fig. 4.4c, contours) driving noticeable downstream vorticity advection. According to the quasi-geostrophic vorticity equation ([Hoskins, 1983](#)) and in the absence of eddy forcing, the high pressure and thus negative vorticity anomalies must be generated by upper level divergence. As a result, the upward vertical velocity response (Fig. 4.4e) and associated upper level divergence over northeast China and the Japan Sea appears to be the most likely wave source ([Sardeshmukh and Hoskins, 1988](#)). The mechanism driving the upward motion is likely to be the compensation of the descending motion south of the OEF.

In summary, a clear decadal regime shift can be inferred from the two experiments: the primary Rossby wave source is due to eddy vorticity flux forcing over the ENP during Dec8190, while it is caused by mean flow divergence over the WNP during Dec9100. The regime shift in the response must be related to decadal background SST variability, as the SST anomaly forcing is identical during the two decades.

4.4 Relation to Background SST Changes

4.4.1 Deep Convection Associated with Sharp SST Fronts

In order to understand the impact of the decadal SST changes on the atmospheric response to the North Pacific SST anomaly, we first notice a region of deep convection south of the OEF, as indicated by the convective rainfall climatology derived from our control run (Fig. 4.1b). In the North Atlantic south of the Gulf Stream front, [Minobe et al. \(2008\)](#) found such a deep convection zone and associated heavy rainfall, high clouds, and upper level divergence. Regarding the mechanism, they proposed that the deep convection zone is maintained by the SST front through pressure adjustment. [Taguchi et al. \(2009\)](#) presented similar findings for the North Pacific in the Kuroshio/Oyashio Extension region.

4.4.2 Decadal SST Changes in the North Pacific

During 1981–2000, the North Pacific SST has experienced substantial decadal changes. Figs. 4.5a and 4.5b depict that on the one hand, the SST is characterized by warming in many regions of the North Pacific, especially over the WNP (see also Wu et al., 2012). On the other hand, important spatial features and high-frequency SST variability have undergone remarkable decadal changes as well. Figs. 4.5c and 4.5d indicate that the OEF strengthened, which is consistent with being part of a longer-time-scale variation recently reported by Smirnov et al. (2015). Moreover, the level of high-frequency, i.e. daily SST variability dropped dramatically over both the western and eastern parts of the basin, with the region off the west coast of North America being one of the most noticeable regions (Figs. 4.5e and 4.5f). These decadal changes modify the background SST on which the SST anomaly is applied. However, though interesting, understanding the dynamics behind the decadal SST changes is beyond the scope of this paper.

4.4.3 The WNP Divergence-Driven Wave Source

The boundary between the positive and negative SST anomalies (Fig. 4.1a) is roughly aligned with the OEF. The positive polarity of the SST anomaly forcing, as well as the difference (positive minus negative) between the polarities, thus reduces the strength of the front. This perturbation to the frontal strength, by definition, acts in both decades, yet with rather different effects. In Dec8190, no significant response in vertical velocity and convective precipitation is simulated over the deep convection zone (Fig. 4.1b). The anomalies in the two variables rather closely follow the SST anomaly pattern in the East China Sea and east of the Philippines (Figs. 4.3e and 4.3f), suggesting a direct connection. In Dec9100, on the other hand, the response in vertical velocity and convective precipitation primarily takes place over the deep convection zone (Fig. 4.1b) and shows little pattern correlation with the SST anomaly (Figs. 4.4e and 4.4f). We hypothesize that the atmosphere is more sensitive to OEF perturbations in the context of a stronger OEF. In particular, when the OEF is relatively weak, as in Dec8190, OEF perturbations are not very effective in driving a significant atmospheric response.

4.4.4 The ENP Eddy-Driven Wave Source

Zhou et al. (2015) recently showed by analyzing the model results in Dec8190 that retaining daily variability in the background SST played a key role in the eddy-driven atmospheric response, especially over the ENP. The primary Rossby wave source in Dec8190 is the eddy

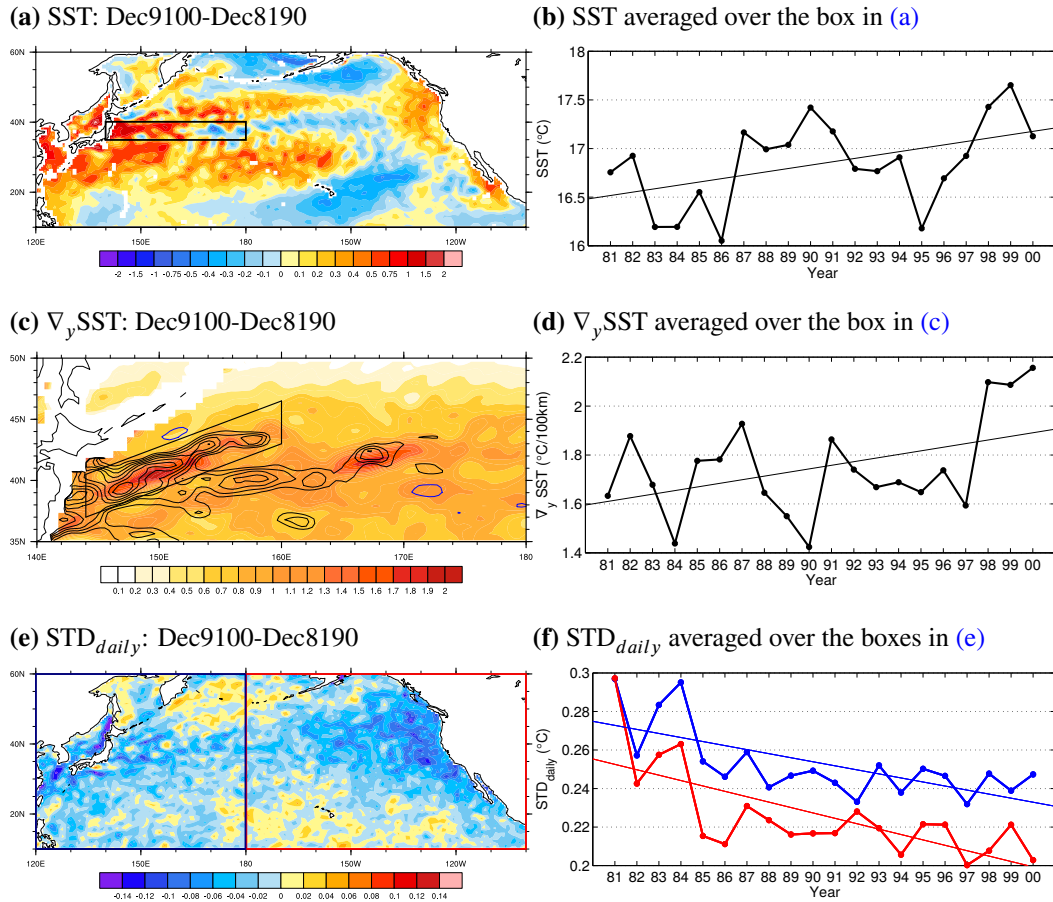


Fig. 4.5: (left) Difference (Dec9100-Dec8190) of decadal-mean (a) SST [$^{\circ}\text{C}$], (c) (contours) Meridional SST gradient [$^{\circ}\text{C } 100 \text{ km}^{-1}$] with black and blue respectively stand for positive and negative values. Contours start at ± 0.4 with interval 0.2. Color coding shows Dec8190 mean. (e) standard deviation of daily SST variability [$^{\circ}\text{C}$]. (right) Time series averaged over the boxes indicated in the respective left panels. Solid lines show the linear trends. All trends pass the t test at the 95% level.

vorticity divergence over the ENP (Figs. 4.3a and 4.3b), which is sensitive to daily background SST variability. The decadal downward trend in the level of daily SST variability (Figs. 4.5e and 4.5f) is then indicative of a reduction of the eddy-driven wave source, thus explaining the difference of the ENP response to identical SST anomalies during the two decades. In summary, in our experiments, it is the relative importance of the Rossby wave sources in the WNP and ENP that eventually determines the atmospheric response to identical extratropical SST anomalies.

4.5 Summary and Discussion

Using a global high-resolution atmospheric general circulation model (AGCM), we have investigated the wintertime (December–February, DJF) atmospheric response to identical extratropical North Pacific sea surface temperature (SST) anomalies superimposed on daily-varying background SST for the two adjacent decades 1981–2000. The response is characterized by a Rossby wave train in both decades, but the primary mechanism and location of the wave source are rather different. In the first decade, the response is dominated by eddy vorticity flux forcing over the eastern North Pacific (ENP) together with a secondary wave source over the western North Pacific (WNP) directly related to the SST anomaly. In the second decade, mean-flow divergence over the WNP becomes the primary wave source, whereas the eddy-driven wave source over the ENP substantially decays. The model results can be understood as a regime shift in the response between the two decades, with significant changes in the character of the decadal-mean geopotential height response. The origin of the regime shift in the response can be traced back to decadal background SST changes, specifically the strength of the Oyashio Extension front (OEF). It is proposed that the strengthening of the front during the second decade makes the atmosphere more sensitive to modifications to the front by SST anomalies, producing a more significant response in the deep convection zone south of the OEF, overriding the secondary wave source noted in the previous decade. On the other hand, the decay of the eddy vorticity flux-driven wave source in the ENP is proposed to be a result of the decadal reduction of daily SST variability in that region.

Our AGCM results shed some light on the long-standing problem of the state-dependence of the atmospheric response to extratropical SST anomalies. We propose a novel perspective and interpret the atmospheric response as a Rossby wave train, and have analyzed the results in terms of the Rossby wave source. The decadal regime shift in the atmospheric response under identical SST anomaly forcing is of particular importance to the fields of large-scale atmosphere-ocean interactions and climate modeling, as well as decadal climate variability and predictability. Both frontal and high-frequency SST perturbations appear to be important and must be resolved to understand and simulate decadal variability of the atmosphere in the extratropics.

Appendix 4.A Significance Tests

4.A.1 Decadal Means

To test the statistical significance of the decadal-mean winter atmospheric response, i.e., the winter-mean difference between the positive (P) and negative (N) SST anomaly cases, we use a one-sample t test against the null hypothesis that the mean of the difference is zero. The two decades are treated separately, using 9 degrees of freedom for Dec8190 and 19 for Dec9100. This approach is appropriate because of the following considerations. For more fundamentals of the t test consult section 6.6 of [von Storch and Zwiers \(1999\)](#).

1. The two-sample t test tests the equality of population means, assuming that the two populations are independent of each other (also known as the population independence assumption). Here the individual integrations for one winter (forced by the P and N cases, i.e. the populations) are started from the same initial condition and thus potentially correlated, in case the “spin-up” period is not long enough. This may violate the population independence assumption. The one-sample t test of the mean difference avoids that.
2. The one-sample t test assumes that the individual realizations come from the same population with a certain distribution (also known as the identical distribution assumption). In our experimental setup, although the SST anomaly is kept the same every winter, the background SST forcing varies from winter to winter. Therefore the individual winters are not realizations of the same population. However, by taking the difference between the P and N cases of each winter, in which the background SST is the same and thus cancels out, the assumption of identical distribution can be roughly met.

Since the background SST can have rectified impacts on the atmosphere in the P and N cases, their difference (i.e., the atmospheric response) may still carry varying residual forcing from the varying background SSTs, also possibly violating the identical distribution assumption. In fact, such forcing from the varying background SSTs on the atmospheric response is exactly what we have found and examined in this study, which, as shown in [Fig. 4.2](#), is on a time-scale longer than a decade. Hence within one decade the varying residual forcing can be neglected, and the individual winters can be considered as realizations of approximately the same population. In this way, using a one-sample t test to test the significance of decadal means remains applicable.

3. The one-sample t test assumes that the individual realizations are independent of each other (also known as the realization independence assumption). In our setup, each winter simulations are started from initial conditions taken one-year apart each other from the control run. Assuming that any atmospheric state with a time lag as long as one year is independent, this assumption can also be met.
4. Furthermore, for Dec9100, there are two realizations for each winter and for each of the two SST anomaly polarities, starting from the 1 November and 1 December conditions of the same year taken from the control run. As required by the realization independence assumption, these two realizations have to be independent of each other too. However, the one-month distance between the initial conditions might be too short to meet this requirement. Therefore we computed the correlation coefficient between the multi-year series of the realizations initialized with the different initial conditions. The correlation computed from geopotential height at 500 hPa is generally smaller than 0.2 in the hatched regions of Fig. 4.4b, indicating that the requirement can be approximately met. As such the statistical significance estimated using the t test is justified.

4.A.2 Linear Trends

The linear trends of the multi-year time series of the winter-mean atmospheric response are estimated using the least squares estimator, which requires that the individual winter means are independent realizations of the same population with a normal distribution. Under these assumptions, the linear trends can be tested with a one-sample t test using 18 degrees of freedom against the null hypothesis that the trend is zero, following section 8.3.8 of [von Storch and Zwiers \(1999\)](#). As discussed above for the decadal means, the application of the one-sample t test is justified.

Chapter 5

Summary and Discussion

5.1 Summary

In Chapter 2, it has been suggested from observations that extratropical North Pacific sea surface temperature (SST) anomalies associated with the Pacific Decadal Oscillation (PDO) significantly impact the overlying atmosphere and cause large-scale atmospheric circulation changes. This is supported by dedicated high-resolution atmospheric general circulation model (AGCM) experiments which indicate the existence of a basin-scale pressure response to PDO-like SST anomalies that is consistent with observations. A coarse-resolution coupled ocean-atmospheric general circulation model (CGCM) previously failed to produce the response, emphasizing the need of high model resolution.

Regarding the mechanism of the atmospheric response, the results of forced high-resolution AGCM simulations presented in Chapter 3 confirm the importance of the eddy-feedback: the atmospheric eddies in the storm track region exert substantial vorticity and momentum forcing on the mean flow, which in turn modifies the storm track, thus forming a two-way interaction. The eddy vorticity forcing is in fact the source of the vorticity perturbation that triggers the Rossby wave train propagating eastwards along the Rossby wave guide. As the response depends on the SST basic state in the uncoupled experimental setup, the roles of various temporal and spatial components of the background SSTs are examined. Results of a series of sensitivity experiments reveal that high-frequency North Pacific SST variability on daily timescales plays the most important role in shaping the response and thus must be resolved and retained in the experimental setup. Other components, e.g. interannual variability, small-scale spatial structures and background SSTs in other basins only have minor effects on the atmospheric response. The reason why high-frequency background SST

variability is important is proposed to stem from the modulation of individual eddies that form the storm track.

SSTs also exhibit substantial decadal variability not only with regard to large-scale pattern but also the level of small-scale (e.g., frontal) and high-frequency (e.g., daily) features. In Chapter 4, another set of AGCM experiments is described showing that the atmospheric response to identical extratropical North Pacific SST anomalies varies on decadal timescales. This is shown by superimposing the SST anomalies on the observed SSTs of two adjacent decades. The atmospheric response experiences a significant regime transition from an eddy-driven Rossby wave train originating over the eastern North Pacific, which is described in Chapter 3, to a Rossby wave train driven by mean-flow divergence originating over the western North Pacific and producing pressure anomalies of opposite sign, as discussed in Chapter 4. The decayed eddy-driven response is attributed to the decadal reduction of daily SST variability, the mean-flow divergence to the enhanced Oyashio Extension front (OEF). Based on the results of Chapters 3 and 4, a novel perspective is proposed: the climatological deep convection zone controlled by the OEF is more sensitive to perturbations to the front when the front itself is stronger.

To summarize, this thesis makes contributions to the long-standing problem of extratropical large-scale ocean-atmosphere interactions by linking the large-scale atmospheric response to extratropical North Pacific SST anomalies to small spatial and temporal scales of the background SSTs on which the SST anomalies are superimposed. In the following section, a few remaining questions regarding the research presented in this thesis are discussed.

5.2 Discussion

5.2.1 Role of Model Resolution

As shown in Chapter 2, the coarse-resolution CGCM, the Kiel Climate Model (KCM), does not reproduce a statistically significant response consistent with observations. The horizontal resolution of the AGCM (ECHAM5) used in the KCM is T31 ($\sim 3.75^\circ$) with 19 vertical levels reaching up to 10 hPa. It has been argued here that such a relatively coarse resolution may be inadequate to properly resolve atmospheric eddies and sharp SST fronts (Section 2.6). By contrast, the forced ECHAM5 simulations have been conducted with the much higher resolution of T213 ($\sim 0.56^\circ$) with 31 levels again reaching up to 10 hPa. The importance of model resolution has long been appreciated (Manabe et al., 1970; Welck et al.,

1971). Boville (1991) compared dynamical quantities (e.g. winds, eddy fluxes) simulated by an AGCM at various resolutions ranging from T21 ($\sim 5.6^\circ$) to T63 ($\sim 1.9^\circ$). His results showed that the simulations of the troposphere significantly benefits from increased model resolution. Jung et al. (2006) compared cyclone statistics from three ECMWF model integrations at T95 ($\sim 1.88^\circ$), T195 ($\sim 1.13^\circ$), and T255 ($\sim 0.7^\circ$) resolution and found that higher resolution generally represents intense extratropical cyclones more realistically. Recently, simulations of extreme precipitation simulation has been shown to also benefit from high model resolution (Volosciuk et al., 2015). Regarding the ECHAM5 model, Roeckner et al. (2006) and Hagemann et al. (2006) reported similar findings.

To further investigate the role of model resolution in the atmospheric response to extratropical North Pacific SST anomalies, we performed a series of ECHAM5 simulations at T31-resolution for the 20 winters (December–February, DJF) during 1981–2000 forced by NOAA OI-SST observations. The results of the first decade (1981–1990) of this simulation have already been briefly presented in Chapter 3. It has been shown that the T31-experiment failed to reproduce the atmospheric response simulated by the high-resolution model. Here additional material for the decades 1981–1990 and 1991–2000 are presented (Fig. 5.1). It can be inferred that except for being barotropic, the T31-response markedly differs from its high-resolution counterpart in both decades, in terms of pressure and surface latent heat flux. The T31-response nevertheless shows some similarities. First, a high pressure response over the North Pacific is present in both decades, despite discrepancies regarding the shape of the high pressure and the response in other regions (Figs. 5.1a–5.1d). This high pressure response is presumably a direct consequence of the cold SST anomaly. As shown in Chapters 3 and 4, the baroclinic eddy feedback and the mean-flow divergence associated with the OEF are the dominant mechanisms of the response in the first and second decade, respectively. The difference between the T31-response and the T213-response is understandable from the inadequate representation of both baroclinic eddies and sharp SST fronts at T31-resolution. Moreover, the T31-heat flux response also agrees in both decades but significantly differs from the T213-counterpart, suggesting a direct thermal response that damps the SST anomalies (Figs. 5.1e and 5.1f). Such a damping has been previously reported by observational and modeling studies (Frankignoul and Kestenare, 2002; Okajima et al., 2014) and is also seen in the sensitivity experiments presented in Chapter 3, in which daily background SST variability is absent. The 1991–2000 mean latent heat flux response exhibits a similar pattern, which can be attributed to the level of daily background SST variability which is significantly reduced during this decade (Section 4.4). The fact that the T31-simulation *does* retain daily SST variability indicates that an adequate spatial resolution of the AGCM and properly resolved daily background SST variability are equally important.

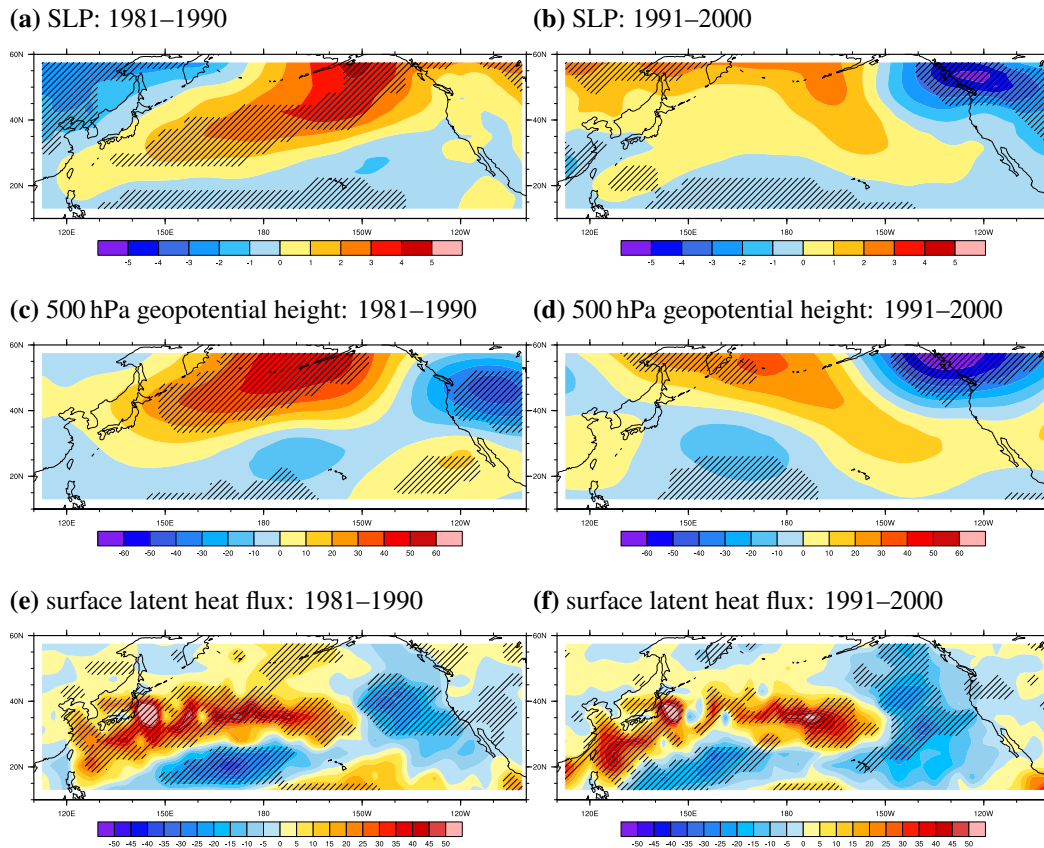


Fig. 5.1: 10-year mean winter (DJF) response simulated by the T31-experiment averaged over the (left) 1981–1990 and (right) 1991–2000 decade for (a, b) sea level pressure [hPa], (c, d) 500 hPa geopotential height [m], (e, f) surface latent heat flux (downward positive) [W m^{-2}]. Statistical significance at the 90% level is indicated by hatching.

5.2.2 Role of the Arch of Warm SST Anomaly

This study has been focusing on the atmospheric response to a “PDO-like” extratropical SST anomaly which features both positive and negative SST anomalies (Figs. 3.S3 and 4.1a). An experiment with exactly the same setup as the DAGL (daily background SST variability retained globally, decade 1981–1990) experiment discussed in Chapter 3 is performed, except that only the SST anomaly depicted in blue in Figs. 3.S3 and 4.1a is used. As in Chapters 3 and 4, both the positive and negative polarity of the SST anomaly is used to force the model, and the response is defined as the winter mean difference between the two polarity cases. The results are displayed in Fig. 5.2. The response is still barotropic, although at the surface, it lacks statistical significance (Figs. 5.2a and 5.2b). Compared to the DAGL results (Fig. 3.2), the response exhibits both similarities and discrepancies. The secondary center of action with anomalously low pressure over the extratropical western North Pacific (WNP)

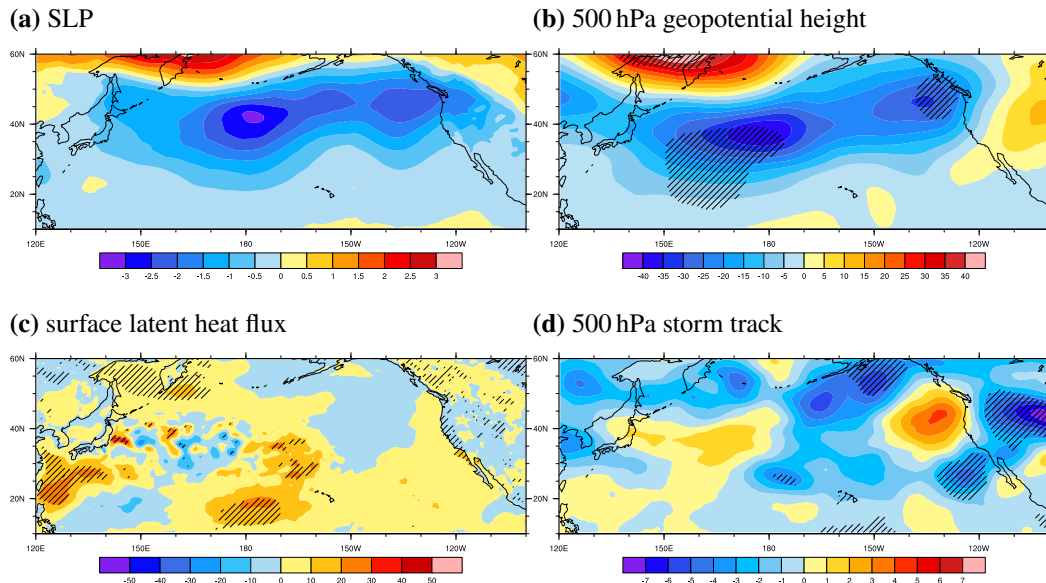


Fig. 5.2: 1981–1990 mean winter (DJF) response simulated by the “PDO-cold”-experiment in which only the cold SST anomaly shown in Figs. 3.S3 and 4.1a drives the AGCM for (a) sea level pressure [hPa], (b) 500 hPa geopotential height [m], (c) surface latent heat flux (downward positive) [W m^{-2}], (d) 500 hPa storm track [m]. Statistical significance at the 90% level is indicated by hatching.

is largely kept, while anomalously high pressure is simulated further poleward. The eastern North Pacific (ENP) low-pressure anomaly dominating in DAGL is reproduced but with smaller amplitude. Concerning the surface latent heat flux, the response resembles that in DAGL over large areas of the WNP, especially in the Kuroshio/Oyashio-Extension region where the pattern is very patchy, hindering damping of the SST anomaly by the atmosphere (Fig. 5.2c). Over the ENP, no significant heat flux response is simulated. Surprisingly, the heat flux response over the East China Sea and south of Japan is reversed, although the SST anomaly there is unchanged. This indicates that the upward heat flux in DAGL, feeding back positively on the SST anomaly, is caused by the warm SST anomaly further to the east, suggesting an upstream influence which is not examined here. Moreover, the storm track response over the ENP has large similarities with that in DAGL, but lacks statistical significance (Fig. 5.2d). To summarize, the center, i.e. negative part of the PDO-like SST anomaly which drives the AGCM appears to be the main forcing of the atmospheric response.

5.3 Outlook

This thesis addresses the problem of the atmospheric response to extratropical large-scale SST anomaly associated with the PDO from various aspects. It presents observational evidence of the atmospheric response as well as the results of dedicated AGCM experiments providing further insights into the mechanism and decadal variability of the response. The findings deepen the understanding concerning the nature of extratropical atmosphere-ocean interactions and also shed light on the seasonal to decadal predictability potential in the North Pacific sector. The importance of high-frequency, i.e. daily SST variability and small-scale SST structures in large-scale atmosphere-ocean interactions revealed by this study draws attention to processes that have so far been generally regarded as “noise” which can be ignored in climate variability and predictability studies. The climate research community is starting to realize that better resolving sub-grid scale processes such as mesoscale ocean eddies (e.g., [Frenger et al., 2013](#)), sharp SST fronts (e.g., [Minobe et al., 2008](#); [Smirnov et al., 2015](#); [Taguchi et al., 2009](#)), atmospheric gravity waves (e.g., [Lott et al., 2014](#); [Manzini et al., 2014](#)), and moist convection and cloud formation (e.g., [Bony et al., 2015](#); [Jakob, 2014](#); [Stevens and Bony, 2013](#)) are becoming the keystone of further progresses. This study adds another piece to the puzzle of large-scale atmosphere-ocean interactions.

Throughout this study, we did not pay attention to the role of the stratosphere in establishing the atmospheric response to extratropical North Pacific SST anomalies. Although, as discussed in [Li \(2006\)](#), low-top AGCMs are able to reasonably simulate vertically propagating planetary waves, other aspects of troposphere-stratosphere coupling may still play a role. In fact, recent studies do show that the stratosphere can modulate the atmospheric signal arising from surface forcing in the North Atlantic sector and that the use of stratosphere resolving models may improve the simulation, prediction, and projection of extratropical climate ([Omrani et al., 2014](#)). We also showed in Chapter 2 a hint of the QBO, a stratospheric phenomenon, impacting the surface atmosphere in the Pacific sector. This hence opens an interesting path to revisit the analyses carried out in this study in a stratosphere-resolving model. Furthermore, deep convection ([Fritts and Alexander, 2003](#)), including that induced by storms ([Wu et al., 2015](#)), has been recognized as being important for the generation of atmospheric gravity waves. In our results, both the prominent eddy-driven response during 1981–1990 and the upper-level divergence-forced response associated with deep convection anomalies during 1991–2000 have the potential to impact gravity wave statistics. Therefore including a better-resolved stratosphere and investigating the gravity wave response to the PDO-like SST anomaly should provide further insight into the problem of long-term modulation of gravity waves due to SST variability.

References

- Alexander, M. A. and Deser, C. (1995). A mechanism for the recurrence of wintertime midlatitude SST anomalies. *J. Phys. Oceanogr.*, 25(1):122–137.
- Alexander, M. A., Deser, C., and Timlin, M. S. (1999). The reemergence of SST anomalies in the North Pacific Ocean. *J. Clim.*, 12:2419–2433.
- Alexander, M. A. and Penland, C. (1996). Variability in a mixed layer model of the upper ocean driven by stochastic atmospheric surface fluxes. *J. Clim.*, 9(10):2424–2442.
- Angell, J. K. (2000). Tropospheric temperature variations adjusted for El Nino, 1958–1998. *J. Geophys. Res.*, 105(D8):11841–11849.
- Baldwin, M. P., Gray, L. J., Dunkerton, T. J., Hamilton, K., Haynes, P. H., Randel, W. J., Holton, J. R., Alexander, M. J., Hirota, I., Horinouchi, T., Jones, D. B. A., Kinnerson, J. S., Marquardt, C., Sato, K., and Takahashi, M. (2001). The quasi-biennial oscillation. *Rev. Geophys.*, 39(2):179–229.
- Baquero-Bernal, A., Latif, M., and Legutke, S. (2002). On Dipolelike Variability of Sea Surface Temperature in the Tropical Indian Ocean. *J. Clim.*, 15(11):1358–1368.
- Bell, T. L. (1980). Climate sensitivity from fluctuation dissipation - Some simple model tests. *J. Atmos. Sci.*, 37(8):1700–1707.
- Bhatt, U. S., Alexander, M. A., Battisti, D. S., Houghton, D. D., and Keller, L. M. (1998). Atmosphere–ocean interaction in the North Atlantic: Near-surface climate variability. *J. Clim.*, 11:1615–1632.
- Bjerknes, J. (1959). The recent warming of the North Atlantic. In Bolin, B., editor, *Atmos. Sea Motion*, pages 65–73. Rockefeller Institute Press and Oxford University Press.
- Bjerknes, J. (1964). Atlantic air-sea interaction. *Adv. Geophys.*, 10(1):1–82.
- Bony, S., Stevens, B., Frierson, D. M. W., Jakob, C., Kageyama, M., Pincus, R., Shepherd, T. G., Sherwood, S. C., Siebesma, A. P., Sobel, A. H., Watanabe, M., and Webb, M. J. (2015). Clouds, circulation and climate sensitivity. *Nat. Geosci.*, 8(4):261–268.
- Boville, B. A. (1991). Sensitivity of Simulated Climate to Model Resolution. *J. Clim.*, 4(5):469–485.
- Branstator, G. (2002). Circumglobal teleconnections, the jet stream waveguide, and the North Atlantic Oscillation. *J. Clim.*, 15(14):1893–1910.

- Bretherton, C. S., Smith, C., and Wallace, J. M. (1992). An Intercomparison of Methods for Finding Coupled Patterns in Climate Data. *J. Clim.*, 5(6):541–560.
- Carton, J. A., Chepurin, G., and Cao, X. (2000a). A Simple Ocean Data Assimilation Analysis of the Global Upper Ocean 1950–95. Part II: Results. *J. Phys. Oceanogr.*, 30:311–326.
- Carton, J. A., Chepurin, G., Cao, X., and Giese, B. (2000b). A Simple Ocean Data Assimilation Analysis of the Global Upper Ocean 1950–95. Part I: Methodology. *J. Phys. Oceanogr.*, 30:294–309.
- Cayan, D. R. (1992a). Latent and sensible heat flux anomalies over the northern oceans: Driving the sea surface temperature. *J. Phys. Oceanogr.*, 22(8):859–881.
- Cayan, D. R. (1992b). Latent and sensible heat-flux anomalies over the northern oceans: The connection to monthly atmospheric circulation. *J. Clim.*, 5(4):354–369.
- Cayan, D. R. (1992c). Variability of latent and sensible heat fluxes estimated using bulk formulas. *Atmosphere-Ocean*, 30(1):1–42.
- Chalikov, D. and Rainchik, S. (2011). Coupled Numerical Modelling of Wind and Waves and the Theory of the Wave Boundary Layer. *Boundary-Layer Meteorol.*, 138(1):1–41.
- Chang, E. K. M., Lee, S., and Swanson, K. L. (2002). Storm track dynamics. *J. Clim.*, 15(16):2163–2183.
- Chen, S. (2008). The Kuroshio extension front from satellite sea surface temperature measurements. *J. Oceanogr.*, 64(6):891–897.
- Collins, W. D., Bitz, C. M., Blackmon, M. L., Bonan, G. B., Bretherton, C. S., Carton, J. A., Chang, P., Doney, S. C., Hack, J. J., Henderson, T. B., Kiehl, J. T., Large, W. G., McKenna, D. S., Santer, B. D., and Smith, R. D. (2006). The Community Climate System Model version 3 (CCSM3). *J. Clim.*, 19(11):2122–2143.
- Compo, G. P. and Sardeshmukh, P. D. (2010). Removing ENSO-Related Variations from the Climate Record. *J. Clim.*, 23(8):1957–1978.
- Czaja, A. and Frankignoul, C. (1999). Influence of the North Atlantic SST on the Atmospheric Circulation. *Geophys. Res. Lett.*, 26(19):2969–2972.
- Czaja, A. and Frankignoul, C. (2002). Observed impact of Atlantic SST anomalies on the North Atlantic Oscillation. *J. Clim.*, 15:606–623.
- Davis, R. E. (1976). Predictability of sea surface temperature and sea level pressure anomalies over the North Pacific Ocean. *J. Phys. Oceanogr.*, 6(3):249–266.
- Davis, R. E. (1978). Predictability of Sea Level Pressure Anomalies Over the North Pacific Ocean. *J. Phys. Oceanogr.*, 8(2):233–246.
- de Boyer Montégut, C., Madec, G., Fischer, A. S., Lazar, A., and Iudicone, D. (2004). Mixed layer depth over the global ocean: An examination of profile data and a profile-based climatology. *J. Geophys. Res.*, 109(C12003):1–20.

- Deser, C. and Blackmon, M. L. (1993). Surface climate variations over the North Atlantic Ocean during winter: 1900–1989. *J. Clim.*, 6(9):1743–1753.
- Deser, C., Phillips, A. S., and Hurrell, J. W. (2004). Pacific Interdecadal Climate Variability: Linkages between the Tropics and the North Pacific during Boreal Winter since 1900. *J. Clim.*, 17:3109–3124.
- Deser, C. and Timlin, M. S. (1997). Atmosphere-ocean interaction on weekly timescales in the North Atlantic and Pacific. *J. Clim.*, 10(3):393–408.
- Diaz, H. F. and Markgraf, V. (2000). *El Niño and the Southern Oscillation: Multiscale Variability and Global and Regional Impacts*, volume 9. Cambridge University Press, Cambridge.
- Ferranti, L., Molteni, F., and Palmer, T. N. (1994). Impact of localized tropical and extra-tropical SST anomalies in ensembles of seasonal GCM integrations. *Q. J. R. Meteorol. Soc.*, 120(520):1613–1645.
- Ferreira, D. and Frankignoul, C. (2005). The Transient Atmospheric Response to Midlatitude SST Anomalies. *J. Clim.*, 18(7):1049–1067.
- Frankignoul, C. (1985). Sea surface temperature anomalies, planetary waves, and air-sea feedback in the middle latitudes. *Rev. Geophys.*, 23(4):357–390.
- Frankignoul, C., Chouaib, N., and Liu, Z. (2011a). Estimating the observed atmospheric response to SST anomalies: Maximum covariance analysis, generalized equilibrium feedback assessment, and maximum response estimation. *J. Clim.*, 24(10):2523–2539.
- Frankignoul, C., Czaja, A., and L’Heveder, B. (1998). Air-sea feedback in the North Atlantic and surface boundary conditions for ocean models. *J. Clim.*, 11(9):2310–2324.
- Frankignoul, C. and Kestenare, E. (2002). The surface heat flux feedback. Part I: estimates from observations in the Atlantic and the North Pacific. *Clim. Dyn.*, 19(8):633–647.
- Frankignoul, C., Kestenare, E., Botzet, M., Carril, A. F., Drange, H., Pardaens, A., Terray, L., and Sutton, R. (2004). An intercomparison between the surface heat flux feedback in five coupled models, COADS and the NCEP reanalysis. *Clim. Dyn.*, 22(4):373–388.
- Frankignoul, C. and Sennéchaël, N. (2007). Observed influence of North Pacific SST anomalies on the atmospheric circulation. *J. Clim.*, 20(3):592–606.
- Frankignoul, C., Sennéchaël, N., Kwon, Y. O., and Alexander, M. A. (2011b). Influence of the meridional shifts of the Kuroshio and the Oyashio Extensions on the atmospheric circulation. *J. Clim.*, 24(3):762–777.
- Frenger, I., Gruber, N., Knutti, R., and Münnich, M. (2013). Imprint of Southern Ocean eddies on winds, clouds and rainfall. *Nat. Geosci.*, 6(8):608–612.
- Friederichs, P. and Hense, A. (2003). Statistical inference in canonical correlation analyses exemplified by the influence of North Atlantic SST on European climate. *J. Clim.*, 16(3):522–534.

- Fritts, D. C. and Alexander, M. J. (2003). Gravity wave dynamics and effects in the middle atmosphere. *Rev. Geophys.*, 41(1):1003.
- Gan, B. and Wu, L. (2013). Seasonal and Long-Term Coupling between Wintertime Storm Tracks and Sea Surface Temperature in the North Pacific. *J. Clim.*, 26(16):6123–6136.
- Gastineau, G. and Frankignoul, C. (2012). Cold-season atmospheric response to the natural variability of the Atlantic meridional overturning circulation. *Clim. Dyn.*, 39(1-2):37–57.
- Gastineau, G. and Frankignoul, C. (2015). Influence of the North Atlantic SST Variability on the Atmospheric Circulation during the Twentieth Century. *J. Clim.*, 28(4):1396–1416.
- Gates, W. L., Boyle, J. S., Covey, C., Dease, C. G., Doutriaux, C. M., Drach, R. S., Fiorino, M., Gleckler, P. J., Hnilo, J. J., Marlais, S. M., Phillips, T. J., Potter, G. L., Santer, B. D., Sperber, K. R., Taylor, K. E., and Williams, D. N. (1999). An Overview of the Results of the Atmospheric Model Intercomparison Project (AMIP I). *Bull. Am. Meteorol. Soc.*, 80(1):29–55.
- Gislason, S. R., Oelkers, E. H., Eiriksdottir, E. S., Kardjilov, M. I., Gisladottir, G., Sigfusson, B., Snorrason, A., Elefsen, S., Hardardottir, J., Torssander, P., and Oskarsson, N. (2009). Direct evidence of the feedback between climate and weathering. *Earth Planet. Sci. Lett.*, 277(1-2):213–222.
- Gulev, S. K., Latif, M., Keenlyside, N. S., Park, W., and Koltermann, K. P. (2013). North Atlantic Ocean control on surface heat flux on multidecadal timescales. *Nature*, 499(7459):464–467.
- Hagemann, S., Arpe, K., and Roeckner, E. (2006). Evaluation of the hydrological cycle in the ECHAM5 model. *J. Clim.*, 19(16):3810–3827.
- Hara, T. and Belcher, S. E. (2004). Wind Profile and Drag Coefficient over Mature Ocean Surface Wave Spectra. *J. Phys. Oceanogr.*, 34(11):2345–2358.
- Harzallah, A. and Sadourny, R. (1995). Internal versus SST-forced atmospheric variability as simulated by an atmospheric general circulation model. *J. Clim.*, 8(3):474–495.
- Hasselmann, K. (1988). PIPs and POPs: The Reduction of Complex Dynamical Systems Using Principal Interaction and Oscillation Patterns. *J. Geophys. Res.*, 93(D9):11015–11021.
- Honda, M., Kushnir, Y., Nakamura, H., Yamane, S., and Zebiak, S. E. (2005). Formation, mechanisms, and predictability of the Aleutian-Icelandic low seesaw in ensemble AGCM simulations. *J. Clim.*, 18(9):1423–1434.
- Honda, M. and Nakamura, H. (2001). Interannual seesaw between the Aleutian and Icelandic lows. Part II: Its significance in the interannual variability over the wintertime Northern Hemisphere. *J. Clim.*, 14(24):4512–4529.
- Hoskins, B. J. (1983). Modelling of the transient eddies and their feedback on the mean flow. In Hoskins, B. J. and Pearce, R. P., editors, *Large-scale Dyn. Process. Atmos.*, pages 169–199. Academic Press, New York.

- Hoskins, B. J. and Ambrizzi, T. (1993). Rossby Wave Propagation on a Realistic Longitudinally Varying Flow. *J. Atmos. Sci.*, 50(12):1661–1671.
- Hoskins, B. J., James, I. N., and White, G. H. (1983). The shape, propagation and mean-flow interaction of large-scale weather systems. *J. Atmos. Sci.*, 40(7):1595–1612.
- Hoskins, B. J. and Valdes, P. J. (1990). On the existence of storm-tracks. *J. Atmos. Sci.*, 47(15):1854–1864.
- Iizumi, T., Luo, J.-J., Challinor, A. J., Sakurai, G., Yokozawa, M., Sakuma, H., Brown, M. E., and Yamagata, T. (2014). Impacts of El Niño Southern Oscillation on the global yields of major crops. *Nat. Commun.*, 5:3712.
- Jakob, C. (2014). Going back to basics. *Nat. Clim. Chang.*, 4(12):1042–1045.
- Jung, T., Gulev, S. K., Rudeva, I., and Soloviev, V. (2006). Sensitivity of extratropical cyclone characteristics to horizontal resolution in the ECMWF model. *Q. J. R. Meteorol. Soc.*, 132(619):1839–1857.
- Kelly, K. A., Small, R. J., Samelson, R. M., Qiu, B., Joyce, T. M., Kwon, Y.-O., and Cronin, M. F. (2010). Western Boundary Currents and Frontal Air–Sea Interaction: Gulf Stream and Kuroshio Extension. *J. Clim.*, 23(21):5644–5667.
- Kiehl, J. T. and Gent, P. R. (2004). The Community Climate System Model, version 2. *J. Clim.*, 17(19):3666–3682.
- Kihara, N. and Hirakuchi, H. (2008). A Model for Air–Sea Interaction Bulk Coefficient over a Warm Mature Sea under Strong Wind. *J. Phys. Oceanogr.*, 38(6):1313–1326.
- Kushnir, Y. (1994). Interdecadal Variations in North Atlantic Sea Surface Temperature and Associated Atmospheric Conditions. *J. Clim.*, 7(1):141–157.
- Kushnir, Y. and Held, I. M. (1996). Equilibrium atmospheric response to North Atlantic SST anomalies. *J. Clim.*, 9(6):1208–1220.
- Kushnir, Y., Robinson, W. A., Bladé, I., Hall, N. M. J., Peng, S., and Sutton, R. (2002). Atmospheric GCM Response to Extratropical SST Anomalies: Synthesis and Evaluation. *J. Clim.*, 15(16):2233–2256.
- Kwon, Y.-O., Alexander, M. A., Bond, N. A., Frankignoul, C., Nakamura, H., Qiu, B., and Thompson, L. A. (2010). Role of the Gulf Stream and Kuroshio–Oyashio Systems in Large-Scale Atmosphere–Ocean Interaction: A Review. *J. Clim.*, 23(12):3249–3281.
- Kwon, Y.-O. and Deser, C. (2007). North Pacific Decadal Variability in the Community Climate System Model Version 2. *J. Clim.*, 20(11):2416–2433.
- Latif, M. (2009). *Climate change: the point of no return*. Haus Publishing Ltd, London.
- Latif, M. and Barnett, T. P. (1994). Causes of Decadal Climate Variability over the North Pacific and North America. *Science (80-.)*, 266(5185):634–637.
- Latif, M. and Barnett, T. P. (1996). Decadal climate variability over the North Pacific and North America: Dynamics and predictability. *J. Clim.*, 9(10):2407–2423.

- Lau, K.-M., Kim, K.-M., and Shen, S. S. P. (2002). Potential predictability of seasonal precipitation over the United States from canonical ensemble correlation predictions. *Geophys. Res. Lett.*, 29(7):1097.
- Lee, D. E., Liu, Z., and Liu, Y. (2008). Beyond thermal interaction between ocean and atmosphere: On the extratropical climate variability due to the wind-induced SST. *J. Clim.*, 21(10):2001–2018.
- Leith, C. E. (1975). Climate Response and Fluctuation Dissipation. *J. Atmos. Sci.*, 32(10):2022–2026.
- Levitus, S., Boyer, T. P., Conkright, M. E., O'Brien, T., Antonov, J., Stephens, C., Stathopoulos, L., Johnson, D., and Gelfeld, R. (1998). World Ocean Database 1998. *NOAA Atlas NESDIS 40*, 18:346.
- Li, Q. (2006). Climatological analysis of planetary wave propagation in Northern Hemisphere winter. Technical report, Max Planck Institute for Meteorology, Hamburg, Germany.
- Liu, Q., Wen, N., and Liu, Z. (2006). An observational study of the impact of the North Pacific SST on the atmosphere. *Geophys. Res. Lett.*, 33(18):L18611.
- Liu, Z., Fan, L., Shin, S. I., and Liu, Q. (2012a). Assessing atmospheric response to surface forcing in the observations. Part II: Cross validation of seasonal response using GEFA and LIM. *J. Clim.*, 25(19):6817–6834.
- Liu, Z., Liu, Y., Wu, L., and Jacob, R. (2007). Seasonal and long-term atmospheric responses to reemerging North Pacific Ocean variability: A combined dynamical and statistical assessment. *J. Clim.*, 20(6):955–980.
- Liu, Z. and Wen, N. (2008). On the assessment of nonlocal climate feedback. Part II: EFA-SVD and optimal feedback modes. *J. Clim.*, 21(20):5402–5416.
- Liu, Z., Wen, N., and Fan, L. (2012b). Assessing Atmospheric Response to Surface Forcing in the Observations. Part I: Cross Validation of Annual Response Using GEFA, LIM, and FDT. *J. Clim.*, 25(19):6796–6816.
- Liu, Z., Wen, N., and Liu, Y. (2008). On the assessment of nonlocal climate feedback. Part I: The generalized equilibrium feedback assessment. *J. Clim.*, 21(1):134–148.
- Liu, Z. and Wu, L. (2004). Atmospheric Response to North Pacific SST: The Role of Ocean-Atmosphere Coupling. *J. Clim.*, 17(9):1859–1882.
- Lott, F., Denvil, S., Butchart, N., Cagnazzo, C., Giorgetta, M. A., Hardiman, S. C., Manzini, E., Krismer, T., Duvel, J. P., Maury, P., Scinocca, J. F., Watanabe, S., and Yukimoto, S. (2014). Kelvin and Rossby-gravity wave packets in the lower stratosphere of some high-top CMIP5 models. *J. Geophys. Res. Atmos.*, 119(5):2156–2173.
- Lyon, B. and Barnston, A. G. (2005). ENSO and the Spatial Extent of Interannual Precipitation Extremes in Tropical Land Areas. *J. Clim.*, 18(23):5095–5109.

- Madec, G. (2008). NEMO ocean engine. *Note du Pôle modélisation l'Institut Pierre-Simon Laplace*, 27.
- Madec, G., Delecluse, P., Imbard, M., and Lévy, C. (1998). OPA 8.1 ocean general circulation model reference manual. *Note du Pôle modélisation l'Institut Pierre-Simon Laplace*, 11:91.
- Manabe, S., Smagorinsky, J., Holloway, J. Leith, J., and Stone, H. M. (1970). Simulated Climatology of A General Circulation Model with a Hydrologic Cycle III. Effect of Increased Horizontal Computational Resolution. *Mon. Weather Rev.*, 98(3):175–212.
- Mantua, N. J. and Hare, S. R. (2002). The Pacific decadal oscillation. *J. Oceanogr.*, 58:35–44.
- Mantua, N. J., Hare, S. R., Zhang, Y., Wallace, J. M., and Francis, R. C. (1997). A Pacific interdecadal climate oscillation with impacts on salmon production. *Bull. Am. Meteorol. Soc.*, 78(6):1069–1079.
- Manzini, E., Karpechko, A. Y., Anstey, J., Baldwin, M. P., Black, R. X., Cagnazzo, C., Calvo, N., Charlton-Perez, A., Christiansen, B., Davini, P., Gerber, E., Giorgetta, M. A., Gray, L., Hardiman, S. C., Lee, Y.-Y., Marsh, D. R., McDaniel, B. A., Purich, A., Scaife, A. A., Shindell, D., Son, S.-W., Watanabe, S., and Zappa, G. (2014). Northern winter climate change: Assessment of uncertainty in CMIP5 projections related to stratosphere-troposphere coupling. *J. Geophys. Res. Atmos.*, 119:7979–7998.
- Marotzke, J. and Pierce, D. W. (1997). On spatial scales and lifetimes of SST anomalies beneath a diffusive atmosphere. *J. Phys. Oceanogr.*, 27:133–139.
- Marshall, J. and Plumb, R. A. (2008). *Atmosphere, Ocean and Climate Dynamics: An Introductory Text*. Elsevier Academic Press, London.
- Minobe, S. (2000). Spatio-temporal structure of the pentadecadal variability over the North Pacific. *Prog. Oceanogr.*, 47(2-4):381–408.
- Minobe, S., Kuwano-Yoshida, A., Komori, N., Xie, S.-P., and Small, R. J. (2008). Influence of the Gulf Stream on the troposphere. *Nature*, 452(7184):206–209.
- Nakamura, H., Lin, G., and Yamagata, T. (1997). Decadal climate variability in the North Pacific during the recent decades. *Bull. Am. Meteorol. Soc.*, 78(10):2215–2225.
- Nakamura, H., Sampe, T., Goto, A., Ohfuchi, W., and Xie, S.-P. (2008). On the importance of midlatitude oceanic frontal zones for the mean state and dominant variability in the tropospheric circulation. *Geophys. Res. Lett.*, 35(15):L15709.
- Nakamura, H., Sampe, T., Tanimoto, Y., and Shimpo, A. (2004). Observed associations among storm tracks, jet streams and midlatitude oceanic fronts. In Wang, C., Xie, S.-P., and Carton, J. A., editors, *Earth's Clim.* American Geophysical Union, Washington, D. C.
- Namias, J. (1959). Recent seasonal interactions between north Pacific waters and the overlying atmospheric circulation. *J. Geophys. Res.*, 64(6):631–646.

- Namias, J. and Born, R. M. (1970). Temporal coherence in North Pacific sea-surface temperature patterns. *J. Geophys. Res.*, 75(30):5952–5955.
- Namias, J. and Born, R. M. (1974). Further studies of temporal coherence in North Pacific sea surface temperatures. *J. Geophys. Res.*, 79(6):797–798.
- Neelin, J. D., Battisti, D. S., Hirst, A. C., Jin, F.-F., Wakata, Y., Yamagata, T., and Zebiak, S. E. (1998). ENSO Theory. *J. Geophys. Res.*, 103(C7):14261–14290.
- Newman, M., Gilbert P. Compo, and Alexander, M. A. (2003). ENSO-Forced Variability of the Pacific Decadal Oscillation. *J. Clim.*, 16(23):3853–3857.
- Newman, M., Sardeshmukh, P. D., and Penland, C. (2009). How important is air-sea coupling in ENSO and MJO evolution? *J. Clim.*, 22(11):2958–2977.
- Nonaka, M. and Xie, S.-P. (2003). Covariations of sea surface temperature and wind over the Kuroshio and its extension: Evidence for ocean-to-atmosphere feedback. *J. Clim.*, 16(9):1404–1413.
- Ogawa, F., Nakamura, H., Nishii, K., Miyaska, T., and Kuwano-Yoshida, A. (2012). Climatological dependence of the tropospheric zonal-mean circulation and transient eddy activity on the latitude of a midlatitude oceanic front. *Geophys. Res. Lett.*, 39(5):L05804.
- Okajima, S., Nakamura, H., Nishii, K., Miyasaka, T., and Kuwano-Yoshida, A. (2014). Assessing the importance of prominent warm SST anomalies over the midlatitude north pacific in forcing large-scale atmospheric anomalies during 2011 summer and autumn. *J. Clim.*, 27(11):3889–3903.
- Omrani, N.-E., Keenlyside, N. S., Bader, J., and Manzini, E. (2014). Stratosphere key for wintertime atmospheric response to warm Atlantic decadal conditions. *Clim. Dyn.*, 42(3):649–663.
- Overland, J. E., Adams, J. M., and Bond, N. a. (1999). Decadal variability of the Aleutian low and its relation to high-latitude circulation. *J. Clim.*, 12(5 II):1542–1548.
- Palmer, T. N. and Sun, Z. (1985). A modelling and observational study of the relationship between sea surface temperature in the north-west Atlantic and the atmospheric general circulation. *Q. J. R. Meteorol. Soc.*, 111(470):947–975.
- Park, W., Keenlyside, N. S., Latif, M., Ströh, A., Redler, R., Roeckner, E., and Madec, G. (2009). Tropical Pacific Climate and Its Response to Global Warming in the Kiel Climate Model. *J. Clim.*, 22(1):71–92.
- Park, W. and Latif, M. (2005). Ocean Dynamics and the Nature of Air– Sea Interactions over the North Atlantic at Decadal Time Scales. *J. Clim.*, 18:982–995.
- Peng, S. and Robinson, W. A. (2001). Relationships between atmospheric internal variability and the responses to an extratropical SST anomaly. *J. Clim.*, 14(1994):2943–2959.
- Peng, S., Robinson, W. A., and Hoerling, M. P. (1997). The modeled atmospheric response to midlatitude SST anomalies and its dependence on background circulation states. *J. Clim.*, 10(5):971–987.

- Peng, S. and Whitaker, J. S. (1999). Mechanisms determining the atmospheric response to midlatitude SST anomalies. *J. Clim.*, 12:1393–1408.
- Penland, C. and Sardeshmukh, P. D. (1995a). Error and sensitivity analysis of geophysical eigensystems. *J. Clim.*, 8(8):1988–1998.
- Penland, C. and Sardeshmukh, P. D. (1995b). The optimal growth of tropical sea surface temperature anomalies. *J. Clim.*, 8:1999–2024.
- Philander, S. G. (1989). *El Niño, La Niña, and the southern oscillation*. Academic Press, San Diego.
- Pickart, R. S., Macdonald, A. M., Moore, G. W. K., Renfrew, I. A., Walsh, J. E., and Kessler, W. S. (2009). Seasonal Evolution of Aleutian Low Pressure Systems: Implications for the North Pacific Subpolar Circulation. *J. Phys. Oceanogr.*, 39(6):1317–1339.
- Pitcher, E. J., Blackmon, M. L., Bates, G. T., and Muñoz, S. (1988). The effect of North Pacific sea surface temperature anomalies on the January climate of a general circulation model. *J. Atmos. Sci.*, 45(2):173–188.
- Qiu, B. and Chen, S. (2005). Variability of the Kuroshio Extension Jet, Recirculation Gyre, and Mesoscale Eddies on Decadal Time Scales. *J. Phys. Oceanogr.*, 35(11):2090–2103.
- Ratcliffe, R. A. S. and Murray, R. (1970). New lag associations between North Atlantic sea temperature and European pressure applied to long-range weather forecasting. *Q. J. R. Meteorol. Soc.*, 96(408):226–246.
- Reynolds, R. W., Smith, T. M., Liu, C., Chelton, D. B., Casey, K. S., and Schlax, M. G. (2007). Daily High-Resolution-Blended Analyses for Sea Surface Temperature. *J. Clim.*, 20(22):5473–5496.
- Robock, A. and Mao, J. (1995). The volcanic signal in surface temperature observations. *J. Clim.*, 8(5):1086–1103.
- Rodionov, S. N., Bond, N. A., and Overland, J. E. (2007). The Aleutian Low, storm tracks, and winter climate variability in the Bering Sea. *Deep. Res. Part II Top. Stud. Oceanogr.*, 54(23-26):2560–2577.
- Rodwell, M. J. and Folland, C. K. (2002). Atlantic air–sea interaction and seasonal predictability. *Q. J. R. Meteorol. Soc.*, 128:1413–1443.
- Roeckner, E., Bäuml, G., Bonaventura, L., Brokopf, R., Esch, M., Giorgetta, M., Hagemann, S., Kirchner, I., Kornblueh, L., Manzini, E., Rhodin, A., Schlese, U., Schulzweida, U., and Tompkins, A. (2003). The atmospheric general circulation model ECHAM5: Part 1: Model description. Technical Report 349, Max Planck Institute for Meteorology, Hamburg, Germany.
- Roeckner, E., Brokopf, R., Esch, M., Giorgetta, M. A., Hagemann, S., Kornblueh, L., Manzini, E., Schlese, U., and Schulzweida, U. (2006). Sensitivity of simulated climate to horizontal and vertical resolution in the ECHAM5 atmosphere model. *J. Clim.*, 19(16):3771–3791.

- Rowntree, P. R. (1972). The influence of tropical east Pacific Ocean temperatures on the atmosphere. *Q. J. R. Meteorol. Soc.*, 98(416):290–321.
- Saravanan, R. (1998). Atmospheric low-frequency variability and its relationship to midlatitude SST variability: studies using the NCAR climate system model. *J. Clim.*, 11(6):1386–1404.
- Sardeshmukh, P. D. and Hoskins, B. J. (1988). The Generation of Global Rotational Flow by Steady Idealized Tropical Divergence. *J. Atmos. Sci.*, 45(7):1228–1251.
- Scaife, A. A., Athanassiadou, M., Andrews, M., Arribas, A., Baldwin, M., Dunstone, N., Knight, J., Maclachlan, C., Manzini, E., Müller, W. A., Pohlmann, H., Smith, D., Stockdale, T., and Williams, A. (2014). Predictability of the quasi-biennial oscillation and its northern winter teleconnection on seasonal to decadal timescales. *Geophys. Res. Lett.*, 41(5):1752–1758.
- Seager, R., Kushnir, Y., Visbeck, M., Naik, N., Miller, J., Krahnmann, G., and Cullen, H. (2000). Causes of Atlantic Ocean climate variability between 1958 and 1998. *J. Clim.*, 13(16):2845–2862.
- Small, R. J., Tomas, R. A., and Bryan, F. O. (2014). Storm track response to ocean fronts in a global high-resolution climate model. *Clim. Dyn.*, 43:805–828.
- Smirnov, D., Newman, M., Alexander, M. A., Kwon, Y.-O., and Frankignoul, C. (2015). Investigating the local atmospheric response to a realistic shift in the Oyashio sea surface temperature front. *J. Clim.*, 28(3):1126–1147.
- Smith, T. M. and Reynolds, R. W. (2004). Reconstruction of monthly mean oceanic sea level pressure based on COADS and station data (1854–1997). *J. Atmos. Ocean. Technol.*, 21:1272–1282.
- Smith, T. M., Reynolds, R. W., Peterson, T. C., and Lawrimore, J. (2008). Improvements to NOAA’s Historical Merged Land–Ocean Surface Temperature Analysis (1880–2006). *J. Clim.*, 21(10):2283–2296.
- Stevens, B. and Bony, S. (2013). What are climate models missing? *Science*, 340(6136):1053–1054.
- Taguchi, B., Nakamura, H., Nonaka, M., and Xie, S.-P. (2009). Influences of the Kuroshio/Oyashio Extensions on Air–Sea Heat Exchanges and Storm-Track Activity as Revealed in Regional Atmospheric Model Simulations for the 2003/04 Cold Season. *J. Clim.*, 22(24):6536–6560.
- Taylor, K. E., Stouffer, R. J., and Meehl, G. a. (2012). An Overview of CMIP5 and the Experiment Design. *Bull. Am. Meteorol. Soc.*, 93(4):485–498.
- Thompson, D. W. J., Kennedy, J. J., Wallace, J. M., and Jones, P. D. (2008). A large discontinuity in the mid-twentieth century in observed global-mean surface temperature. *Nature*, 453(7195):646–649.
- Ting, M. and Peng, S. (1995). Dynamics of the early and middle winter atmospheric responses to the northwest Atlantic SST anomalies. *J. Clim.*, 8:2239–2254.

- Toth, Z. and Kalnay, E. (1993). Ensemble Forecasting at NMC: The Generation of Perturbations. *Bull. Am. Meteorol. Soc.*, 74(12):2317–2330.
- Valcke, S. (2013). The OASIS3 coupler: a European climate modelling community software. *Geosci. Model Dev.*, 6:373–388.
- Volosciuk, C., Maraun, D., Semenov, V. A., and Park, W. (2015). Extreme Precipitation in an Atmosphere General Circulation Model: Impact of Horizontal and Vertical Model Resolutions. *J. Clim.*, 28(3):1184–1205.
- von Storch, H., Bruns, T., Fischer-Bruns, I., and Hasselmann, K. (1988). Principal Oscillation Pattern Analysis of the 30- to 60-Day Oscillation in General Circulation Model Equatorial Troposphere. *J. Geophys. Res.*, 93(D9):11022–11036.
- von Storch, H. and Zwiers, F. W. (1999). *Statistical Analysis in Climate Research*. Cambridge University Press, New York.
- Wallace, J. M. and Jiang, Q. (1987). On the observed structure of the interannual variability of the atmosphere/ocean climate system. *Atmos. Ocean. Var.*, pages 17–43.
- Wang, F., Liu, Z., and Notaro, M. (2013). Extracting the dominant SST modes impacting North America’s observed climate. *J. Clim.*, 26(15):5434–5452.
- Welck, R. E., Kasahara, A., Washington, W. M., and de Santo, G. (1971). Effect of horizontal resolution in a finite-difference model of the general circulation. *Mon. Weather Rev.*, 99(9):673–683.
- Wen, N., Liu, Z., and Liu, Q. (2013). Observational assessment of nonlocal heat flux feedback in the North Atlantic by GEFA. *J. Appl. Meteorol. Climatol.*, 52(3):645–653.
- Wen, N., Liu, Z., Liu, Q., and Frankignoul, C. (2010). Observed atmospheric responses to global SST variability modes: A unified assessment using GEFA. *J. Clim.*, 23(7):1739–1759.
- Wilkinson, C., Lindén, O., Cesar, H., Hodgson, G., Rubens, J., and Strong, A. E. (1999). Ecological and socioeconomic impacts of 1998 coral mortality in the Indian Ocean: an ENSO impact and a warning of future change? *Ambio*, 28(2):188–196.
- Wu, J. F., Xue, X. H., Hoffmann, L., Dou, X. K., Li, H. M., and Chen, T. D. (2015). A case study of typhoon-induced gravity waves and the orographic impacts related to Typhoon Mindulle (2004) over Taiwan. *J. Geophys. Res. Atmos.*, Accepted:DOI:10.1002/2015JD023517.
- Wu, L., Cai, W., Zhang, L., Nakamura, H., Timmermann, A., Joyce, T., McPhaden, M. J., Alexander, M. A., Qiu, B., Visbeck, M., Chang, P., and Giese, B. (2012). Enhanced warming over the global subtropical western boundary currents. *Nat. Clim. Chang.*, 2(1):161–166.
- Wu, L., Liu, Z., Gallimore, R. G., and Jacob, R. (2003). Pacific Decadal Variability: The Tropical Pacific Mode and the North Pacific Mode. *J. Clim.*, 16(8):1101–1120.

- Wu, L., Liu, Z., Liu, Y., Liu, Q., and Liu, X. (2005). Potential global climatic impacts of the North Pacific Ocean. *Geophys. Res. Lett.*, 32(24):L24710.
- Xu, H., Xu, M., Xie, S.-P., and Wang, Y. (2011). Deep Atmospheric Response to the Spring Kuroshio over the East China Sea. *J. Clim.*, 24(18):4959–4972.
- Yim, B. Y., Kwon, M., Min, H. S., and Kug, S. (2015). Pacific Decadal Oscillation and its relation to the extratropical atmospheric variation in CMIP5. *Clim. Dyn.*, 44(5-6):1521–1540.
- Yu, L. and Weller, R. A. (2007). Objectively analyzed air-sea heat fluxes for the global ice-free oceans (1981-2005). *Bull. Am. Meteorol. Soc.*, 88(4):527–539.
- Zhang, L., Sielmann, F., Fraedrich, K., Zhu, X., and Zhi, X. (2015). Variability of winter extreme precipitation in Southeast China: contributions of SST anomalies. *Clim. Dyn.*
- Zhao, X. and Li, J. (2010). Winter-to-winter recurrence of sea surface temperature anomalies in the Northern Hemisphere. *J. Clim.*, 23(14):3835–3854.
- Zhao, X. and Li, J. (2012a). Winter-to-winter recurrence and non-winter-to-winter recurrence of SST anomalies in the central North Pacific. *J. Geophys. Res.*, 117(C05):C050.
- Zhao, X. and Li, J. (2012b). Winter-to-winter recurrence of atmospheric circulation anomalies in the central North Pacific. *J. Geophys. Res.*, 117(C12):C12023.
- Zhong, Y. and Liu, Z. (2008). A joint statistical and dynamical assessment of atmospheric response to North Pacific Oceanic variability in CCSM3. *J. Clim.*, 21(22):6044–6051.
- Zhong, Y., Liu, Z., and Notaro, M. (2011). A GEFA assessment of observed global ocean influence on U.S. precipitation variability: Attribution to regional SST variability modes. *J. Clim.*, 24(3):693–707.
- Zhou, G., Latif, M., Greatbatch, R. J., and Park, W. (2015). Atmospheric response to the North Pacific enabled by daily sea surface temperature variability. *Geophys. Res. Lett.*, 42(18):7732–7739.
- Zhou, G., Latif, M., Greatbatch, R. J., and Park, W. (2016). State-Dependence of Atmospheric Response to Extratropical North Pacific SST Anomalies. *J. Clim.*, submitted.

Acknowledgments

First, I would like to express my deepest thanks to my supervisor, Prof. Dr. Mojib Latif, for his excellent guidance and continuous support for my PhD study. I will never forget the hours of inspiring but also delightful discussions, and the manuscripts full of changes made by Mojib. Over the years I have learned so much from him, not only about how to perform good scientific research, but also how to present the results in easily understandable ways. His gentle personality, always being patient, generous, nice, and funny, greatly eased my difficult years as a foreign student. He is my best role model of a scientist, mentor, and adviser.

I also owe my sincere gratitude to my co-supervisor, Prof. Dr. Richard Greatbatch. His immense knowledge and penetrating insight brilliantly guided my study, and his encouragement was sometimes all that kept me going. In the many discussions we had either in person or by email, I learned from him both knowledge and the way of thinking. He also spent a lot of effort improving my papers and this thesis. I could not have imagined accomplishing this thesis without Richard's help.

My sincere thanks also goes to Dr. Wonsun Park for his extensive help and advice, which ensured my smooth entrance to the field in the initial stage of my PhD and kept me on the right track ever since. His great ideas have always been stimulating my research. Being also an Asian scientist, he often selflessly passed on his valuable academic experience which benefited me to a great extent.

Moreover, the excellent general courses and soft skill training provided by the Integrated School of Ocean Sciences (ISOS) of the Kiel University, headed by PD. Dr. Avan Antia, are deeply acknowledged. Avan has always cared about me and supported me, which I sincerely appreciate.

I am also grateful to Prof. Dr. Claus Böning (GEOMAR), Prof. Dr. Shoshiro Minobe (Hokkaido University), and Prof. Dr. Fei-Fei Jin (University of Hawaii), for the very insightful discussions.

I would like to acknowledge Reverend and Mrs Samuel Ng of the Chinesische Christliche Gemeinde Hamburg (CCG-Ham), who, ever since my early days in Germany, have been taking care of me, teaching me principles, passing on their wisdom, and listening to me in the hard times. Although they are not scientists, their support made it easy for me to continue. In addition, I thank the members of the Chinesische Bibelkreis Kiel (CBK-Kiel) and the CCG-Ham. Special thanks goes to Dr. Bin Wu (Max-Planck Institute for Evolutionary Biology), member of the CBK-Kiel, a dear friend who helped building up my confidence in science and always offered to help without being asked to.

Last but not least, none of this would have been possible without the endless love and patience of my family. Over all these years, every member of my family, namely my parents, my parents-in-law, and my siblings-in-law have supported me with their understanding, concern and encouragement. They have always believed in me, and always been there for me. Most importantly, I am greatly indebted to my beloved wife Zhuhua, who walked this wonderful journey hand by hand with me, always standing by me through the good times and the bad. We shared every moment of excitement and depression, success and failure. Her love, care and tenderness never let me feel alone. She is indeed the most precious gift.

Finally, I appreciate the financial support from the Chinese Scholarship Council (CSC).

Curriculum Vitae

Personal Information

Surname: Zhou
Given name: Guidi
Date of birth: 12.10.1985
Place of birth: Qingdao, Shandong, China PR
Nationality: China, PR
Marital status: Married

Education

2011–present **Doctor of Philosophy, Meteorology**
Department of Ocean Circulation and Climate Dynamics,
GEOMAR Helmholtz Centre for Ocean Research Kiel, Kiel, Germany
Supervisor: Prof. Dr. Mojib Latif

2008–2011 **Master of Science, Physical Oceanography**
College of Physical and Environmental Oceanography,
Ocean University of China, Qingdao, China
Supervisor: Prof. Dr. Liangming Zhou

2004–2008 **Bachelor of Science, Marine Sciences**
College of Physical and Environmental Oceanography,
Ocean University of China, Qingdao, China

Declaration

I hereby declare that this work is my own work apart from my supervisors' guidance and acknowledged assistance. This thesis has not been submitted for the award of doctoral degree in any other examining body and was prepared according to the Rules of Good Scientific Practice of the German Research Foundation.

Guidi Zhou
19.01.2016